



1 **European tectosphere and slabs beneath the greater Alpine area - Interpretation of mantle**
2 **structure in the Alps-Apennines-Pannonian region from teleseismic V_p studies**

3

4 Mark R. Handy¹, Stefan M. Schmid², Marcel Paffrath³, Wolfgang Friederich³ and the AlpArray
5 Working Group*

6

7 ¹ Institut für Geologische Wissenschaften, Freie Universität Berlin, Malteserstr. 74-100, 12249

8 Berlin, Germany; Institut für Geologie, ETH-Zürich, Sonneggstr. 5, 8092 Zürich

9 ² Institut für Geophysik, ETH-Zürich, Sonneggstr. 5, 8092 Zürich

10 ³ Institut für Geologie, Mineralogie, Geophysik, Ruhr-Universität Bochum, 44780 Bochum, Germany

11 *For the complete team list visit the link which appears at the end of the paper

12

13

14



15 **Abstract**

16 Based on recent results of AlpArray, we propose a new model of Alpine collision that involves
17 subduction and detachment of thick (180-200 km) European tectosphere. Our approach combines
18 teleseismic P-wave tomography and existing Local Earthquake Tomography (LET) allowing us to
19 image the Alpine slabs and their connections with the overlying orogenic crust at an unprecedented
20 resolution. The images call into question the conventional notion that slabs comprise only
21 seismically fast lithosphere and suggest that the mantle of the downgoing European Plate is
22 heterogeneous, containing both positive and negative V_p anomalies of up to 5-6%. We interpret
23 these as compositional rather than thermal anomalies, inherited from the Variscan and pre-Variscan
24 orogenic cycles. They make up a kinematic entity referred to as tectosphere, which presently dips
25 beneath the Alpine orogenic front. In contrast to the European Plate, the tectosphere of the Adriatic
26 Plate is thinner (100-120 km) and has a lower boundary approximately at the interface between
27 positive and negative V_p anomalies.

28 Horizontal and vertical tomographic slices reveal that beneath the Central and Western Alps, the
29 downgoing European tectospheric slab dips steeply to the S and SE and is only locally still attached
30 to the Alpine crust. However, in the Eastern Alps and Carpathians, the European slab is completely
31 detached from the orogenic crust and dips steeply to the N-NE. This along-strike change in
32 attachment coincides with an abrupt decrease in Moho depth below the Tauern Window, the Moho
33 being underlain by a pronounced negative V_p anomaly that reaches eastward into the Pannonian
34 Basin area. This negative V_p anomaly is interpreted to represent hot upwelling asthenosphere that
35 was instrumental in accommodating Neogene orogen-parallel lateral extrusion of the ALCAPA
36 tectonic unit (upper plate crustal edifice of Alps and Carpathians) to the east. A European origin of
37 the northward-dipping, detached slab segment beneath the Eastern Alps is likely since its imaged
38 down-dip length (300-500 km) matches estimated Tertiary shortening in the Eastern Alps
39 accommodated by south-dipping subduction of European tectosphere.

40 A slab anomaly beneath the Dinarides is of Adriatic origin and dips to the northeast. There is no
41 evidence that this slab dips beneath the Alps. The slab anomaly beneath the northern Apennines,
42 also of Adriatic origin, hangs subvertically and is detached from the Apenninic orogenic crust and
43 foreland. Except for its northernmost segment where it locally overlies the southern end of the
44 European slab of the Alps, this slab is clearly separated from the latter by a broad zone of low V_p
45 velocities located south of the Alpine slab beneath the Po Basin. Considered as a whole, the slabs of
46 the Alpine chain are interpreted as attenuated, largely detached sheets of continental margin and
47 Alpine Tethyan lithosphere that locally reach down to a slab graveyard in the Mantle Transition
48 Zone (MTZ).

49

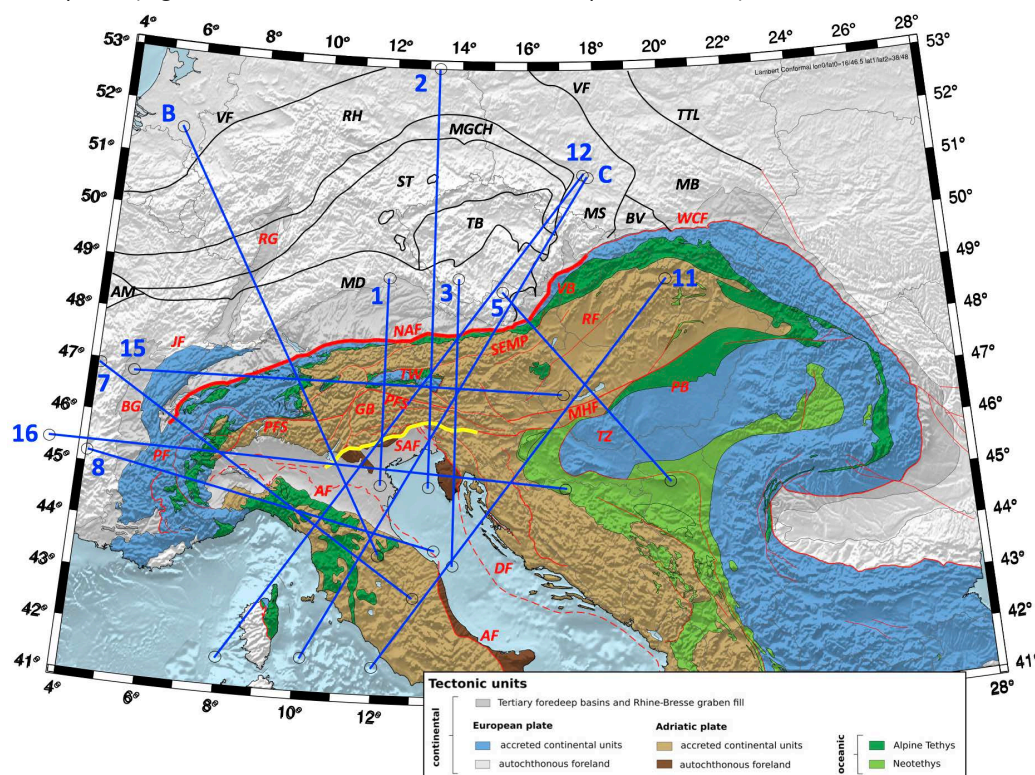
50

51 **1 Introduction**

52 The prevailing paradigm of mountain building in the greater Alpine area (Fig. 1) involves subduction
53 of European continental lithosphere that is some 100-120 km thick beneath the upper Adriatic
54 Plate, lithosphere thickness being based largely on seismological criteria (Jones et al., 2010; Geissler
55 et al., 2010, Kissling et al., 2006). We refer to this as the *classical lithosphere model* of continental
56 subduction to distinguish it from a new model here involving the subduction and partial
57 delamination of much thicker, compositionally heterogeneous European mantle, referred to as
58 *tectosphere* (Jordan, 1975, 1981) based on recent P-wave images of the AlpArray seismological
59 campaign (Paffrath et al., 2021b) presented below. Jordan (1975) introduced this term, in his words,
60 “to avoid the misuse of the term lithosphere” and to “denote the region occupied by kinematic
61 entities (plates) which remain coherent in the course of large-scale lateral motions”. As pointed out



62 by Artemieva (2011) different geophysical techniques have given rise to a multitude of definitions of
 63 the lithosphere based on seismic, thermal, electrical, rheological, and petrological properties.
 64 Therefore, in this paper, we use the terms *plate* and *tectosphere* in a strictly kinematic sense to
 65 refer to bodies of compositionally heterogeneous mantle and crust that have moved coherently
 66 with respect to markers in both the mantle and at the surface. This differs somewhat from current
 67 seismological definitions, which treat plates as entities comprising only seismically fast mantle
 68 lithosphere (e.g., Piromallo & Morelli, 2003; Wortel & Spakman, 2000).



69
 70 **Figure 1:** Tectonic map of the Alpine chain and its foreland, including Variscan units. Thin red lines – main Tertiary
 71 tectonic faults after Schmid et al. (2004) and (2008); Thin black lines – tectonic lineaments separating Variscan
 72 tectonometamorphic domains after Franke (2017, 2000), Mazur et al. (2020), and Schulmann et al. (2014). Blue
 73 lines are traces of vertical tomographic profiles in Figs. 3-7. The numbers of the traces are in accordance with their
 74 appearance in Appendix A. Thick red line along the NAF marks the Oligo-Miocene plate boundary in the Alps;
 75 Yellow line along the SAF marks the presently active plate boundary in the Alps; Green units are the Adria-Europe
 76 suture marking the Late Cretaceous-to-late Eocene plate boundary.

77 **Alpine faults and related structures:** NAF - North Alpine Front, SAF – Southern Alps Front; PFS - Periadriatic Fault
 78 System, GB – Giudicarie Belt, JF – Jura Front, PF – Penninic Front, RG – Rheine Graben, BG – Bresse Graben, TW –
 79 Tauern Window, SEMP – Salzach-Ennstal –Mariazell-Puch Fault, MHF – Mid-Hungarian Fault Zone, VB – Vienna
 80 Basin, PB – Pannonian Basin, RF – Raba Fault, WCF – Western Carpathian Front, DF – Dinaric Front

81 **Variscan tectonic domains and faults:** VF – Variscan orogenic front, RH – Rheno-Hercynian, MGCH – Mid-German
 82 Crystalline High, ST – Saxo-Thuringian, MD – Moldanubian, TB – Tepla-Barrandian, AM – Armorican Massif, BV –
 83 Bruno-Vistulian, MB – Malopolska Block, MS – Moravo-Silesian. Other faults: TTL - Teyseyre-Thornquist Line

84

85 As in other orogenic belts, the classical model of lithospheric subduction in the Alps was initially
 86 supported by teleseismic body-wave studies showing fast seismic velocity anomalies dipping



87 beneath the Alpine-Mediterranean mountain belts (Wortel and Spakman, 2000). They are often
88 inclined in the same direction as the dipping Moho's that define the base of the orogenic crust
89 (Waldhauser et al., 2002; Lippitsch et al., 2003; Spada et al., 2013). These seismically fast domains
90 are inferred to reflect negative temperature anomalies that mark descending slabs of cold
91 subcontinental lithospheric mantle, whereas positive anomalies at the base of, and surrounding,
92 these seismically fast domains are often interpreted as warm asthenospheric mantle (e.g. Spakman
93 and Wortel, 2004). In the Alps, the base of the subducting European Plate has thus been taken to be
94 the boundary between seismically fast and slow domains (respectively, blue and red domains in
95 most tomographic slices), whereas its top is the interface with the upper Adriatic Plate.
96 Seismological studies in the Western Alps have shown that this interface includes subducted crust
97 down to depths of > 90 km (Lippitsch et al., 2003; Zhao et al., 2016), corroborating geological
98 evidence of deeply subducted and exhumed fragments of oceanic and continental crust (e.g.,
99 Chopin, 1984; Schertl et al., 1991) and mantle (Brenker and Brey, 1997) preserved in the Alps (Agard
100 and Handy, 2021).

101 When assessing the geometry of subduction and plate boundaries in the Alps, it is important
102 to distinguish the Late Cretaceous-Paleogene Adria-Europe subduction plate boundary represented
103 by the Tethyan ophiolite belt along the Alps (Fig. 1) from the Oligo-Miocene collisional boundary
104 exposed along the northern Alpine orogenic front (labeled NAF in Fig. 1). Both of these boundaries
105 differ from the Pliocene-to-active plate boundary along the Southern Alpine Front (SAF in Fig. 1). In
106 the analysis below, these differently aged boundaries provide important kinematic and time
107 constraints for the tectonic interpretation of mantle anomalies. None of these geological
108 boundaries coincide at the surface, nor do they necessarily merge at depth given that the Alps have
109 experience changes in the amount and direction of shortening with time (Schmid et al., 2004; Handy
110 et al., 2010). This is especially true of the eastern part of the Alps, where Paleogene N-S shortening
111 and subduction has given way to Mio-Pliocene eastward lateral extrusion of orogenic crust and
112 possibly upper mantle (e.g., Ratschbacher et al., 1991) that is still ongoing during continued Adria-
113 Europe N-S convergence (e.g., Grenerzcy et al., 2005; Serpelloni et al., 2016).

114 Controversy on Alpine subduction has arisen because the SE dip of the Alpine slab anomaly
115 in the Central and Western Alps (Lippitsch et al., 2003; Zhao et al., 2015) indicating "classical" SE-
116 directed subduction of the European slab (e.g., Argand, 1924; Pfiffner et al. eds., 1997; Schmid et
117 al., 1996) contrasts with a dip to the NE of a positive V_p slab anomaly in the eastern part of the
118 chain, i.e., east of 12-13°E in Fig. 1 (Lippitsch et al., 2003; Mitterbauer et al., 2011; Karousová et al.,
119 2013). This NE dip is inconsistent with SE-directed Alpine subduction inferred from the uniformly S-
120 dip and N- to NW-directed shear sense indicators of sutured oceanic lithosphere and crustal nappes
121 all along the Alps (e.g., Schmid et al., 2004), including the Eastern Alps (e.g., Handy et al., 2010 and
122 refs. therein). The plate tectonic affinity of this part of the slab beneath the Eastern Alps therefore
123 remains unclear and debated. Proponents of a European origin propose the existence of a very
124 steeply NE-dipping overturned to subvertically oriented slab that detached from the crust east of
125 the Tauern Window (Mitterbauer et al., 2011; Rosenberg et al., 2018). Proponents of an Adriatic
126 origin of this slab based their interpretation on the tomographic images of Lippitsch et al. (2013;
127 their Fig. 13c) that depict a moderately NE-dipping slab still attached to the still undeformed parts
128 of the Adriatic Plate. They therefore proposed a late-stage reversal of subduction polarity (Schmid
129 et al., 2004; Kissling et al., 2006; Handy et al., 2015). A recent review by Kästle et al. (2020) that also
130 takes surface wave tomography into consideration considers the possibility that this slab has a
131 combined European-Adriatic origin, as discussed in Handy et al. (2015).

132



133 In this paper, we interpret vertical and horizontal tomographic slices of the Alps generated by
134 integrating crustal and mantle tomographic P-wave models gleaned from the AlpArray seismological
135 network (Hetényi et al., 2018). This new method, described in the next section and in more detail in
136 Paffrath et al. (2021b), employs teleseismic tomography and integrates the crustal/uppermost
137 mantle models of Diehl et al. (2009) as a priori information into the teleseismic inversion, weighted
138 according to its reliability. This allows us to image the Alpine slabs and their potential connections
139 with the orogenic edifice as well as the fore- and hinterland lithospheres at an unprecedented
140 resolution. The images presented in sections 3 and 4 call into question the conventional notion
141 based on seismological criteria that slabs comprise only seismically fast mantle lithosphere that is
142 some 100-120 km thick. Instead, they suggest that the downgoing European Plate in the Alps is
143 much thicker and contains positive and negative seismic anomalies inherited from pre-Alpine
144 (Variscan) events that, given their age, are likely to be of compositional rather than thermal nature.
145 In section 5, we showcase evidence for large-scale delamination of the slabs in the Alps and
146 northern Apennines, with slabs that have been partly to entirely detached from their orogenic
147 edifices. The discussion in section 6 revisits the debate on subduction polarity in light of the new
148 data and touches on some implications of widespread delamination and slab detachment for crustal
149 seismicity and foreland basin evolution. We conclude with a conceptual 3-D visualization of mantle
150 structure beneath the Alps and Apennines that serves as a vehicle for assessing the interaction of
151 slabs and asthenosphere at depths down to the 410 km discontinuity at the top of the Mantle
152 Transition Zone (MTZ).

153
154

155 2. Methodology

156 The images of mantle structure in the following sections are derived from a 3D-model of P-wave
157 velocity in the crust and mantle below the greater Alpine region (Paffrath et al., 2021b) obtained by
158 tomographic inversion of teleseismic P-wave travel time residuals measured on records of the
159 AlpArray Seismic Network (Paffrath et al., 2021a). The travel time database comprises 162366
160 onsets of 331 teleseismic earthquakes of magnitude 5.5 or higher at epicentral distances between
161 35 and 135 degrees occurring between January 2015 and July 2019. Travel time residuals are
162 commonly defined as the difference between the observed and a theoretical travel time calculated
163 for a standard earth model. Here, in addition, we subtract the array average from these residuals on
164 an event-to-event basis to avoid errors in earthquake origin time and reduce influences of remote
165 heterogeneous earth structure outside the inversion domain. To obtain highly accurate travel time
166 residuals suitable for teleseismic inversion, we applied a specially designed procedure consisting of
167 automatic picking, beam forming and cross-correlation (Paffrath et al., 2021a).

168 The travel time residuals are inverted for P-wave velocity perturbations on a regular grid of
169 ca. 25 x 25 x 15 km (latitude, longitude, depth) relative to a purely depth-dependent reference
170 model using the inversion code FMTOMO (Rawlinson et al., 2006). The velocity perturbations are
171 found by minimizing an objective function calculated from the misfit between observations and
172 predictions plus two further terms that quantify the complexity of the velocity model by evaluating
173 its variance with respect to the initial model and its roughness. The variance is scaled to the
174 expected a priori standard deviations of P-wave velocity with deviations of P-wave velocity from the
175 initial model after inversion can be restricted. Roughness is calculated from the second derivative of
176 the velocity perturbations. The aim of the inversion is to find the least complex model able to
177 reduce the misfit to a certain threshold. Since the inversion is non-linear, the minimum of the
178 objective function is found in a linearized iterative way, beginning from an initial model constructed
179 from a standard earth model in the mantle and an a priori crustal model based on previous work (see



180 below). Iteration is stopped if either the observations fit within their uncertainties or if the misfit
181 reduction stagnates when executing further iterations.

182 Making predictions of travel time residuals involves solving the forward problem by
183 calculating travel times of P-waves propagating from a distant earthquake to the AlpArray seismic
184 stations. This is done in a hybrid way assuming a 1D standard earth model between earthquake and
185 inversion domain and a 3D model within the inversion domain. Rays propagated through the 1D
186 earth are injected at the boundary of the inversion domain and continued to the surface using the
187 3D eikonal solver FM3D (Rawlinson and Sambridge, 2005).

188 One major concern of teleseismic tomography is the influence of crustal and uppermost
189 mantle structure, which is not well resolved by teleseismic data owing to a lack of crossing rays.
190 Fortunately, crustal structure in the Alps has been studied very thoroughly using different methods,
191 including refraction seismics, reflection seismics, receiver functions, ambient noise studies and local
192 earthquake tomography. These studies provide models of crustal structure of varying resolution and
193 spatial coverage. The standard way of correcting for crustal structure is to compute travel time
194 residuals for the crustal model assuming vertical incidence, then subtract them from the observed
195 ones. However, this approach simplifies the true ray paths, which are refracted in the crust in
196 different ways depending on vertical and azimuthal incidence, and implies vanishing uncertainty of
197 the crustal model. The approach of Paffrath et al. (2021b) used here does not follow this standard
198 approach, but instead incorporates crustal models (see below) into the initial model. Varying spatial
199 reliability is accounted for by assigning corresponding a priori standard deviations to velocity values
200 in the crust, thus allowing the inversion to adjust the crustal model. Ray refraction is properly
201 considered automatically, as in each iteration the crustal model is always an integral part of the
202 entire model.

203 The crustal model used by Paffrath et al. (2021b) is composed of EuCRUST-07 (Tesauro et al.,
204 2008) and the fully three-dimensional, high resolution P-wave velocity model of the central Alpine
205 region created from local earthquake tomography by Diehl et al. (2009). In addition, information on
206 Moho depth in the Alpine region was refined using the study of Spada et al. (2013). The P-wave
207 velocity at a given point in the inversion domain is a weighted average of both models, with weights
208 depending on the reliability of Diehl's model measured via the values of the diagonal elements of
209 the resolution matrix (RDE) provided by T. Diehl (personal communication). For values of RDE above
210 0.15 the crustal model is dominated by Diehl's model, whereas for values below, the model of
211 Tesauro et al. (2008) takes over smoothly. In a similar way, a priori standard deviations are assigned
212 to P-wave velocity at a given point in the model domain using a mapping from RDE value to
213 standard deviation. Since outside of Diehl's model no RDE value is available we choose a uniform
214 standard deviation of 0.08 km/s for the upper crust (corresponding to a RDE value of 0.15) and 0.17
215 km/s for the sediments and the lower crust. Standard deviation decreases with increasing RDE
216 value.

217 Paffrath et al. (2021b) assessed the resolution of mantle structures imaged in this study by
218 employing different general tests, as well as very specific resolution tests that focus on crucial,
219 smaller scale structures in the Alps, e.g., gaps and bends in slabs. Among the general tests are two
220 checkerboard tests, which regularly alter the velocity of the mantle in a synthetic model by applying
221 a perturbation of +/- 10% in P-wave velocity on different cell sizes of 2 x 2 x 3 grid points and 3 x 3 x 4
222 grid points. Gaps in between the cells remain unperturbed in order to analyse smearing throughout
223 the irradiated model domain.

224 Analysis of the checkerboard tests shows that, due to the uneven event distribution,
225 smearing is more prominent in the NW-SE direction. Hence, velocity anomalies of slabs that trend in



226 this direction tend to be elongated in a downdip direction and lose amplitude, whereas structures
227 trending perpendicular to this direction tend to be broadened along strike of the slab.

228 Generally, vertical smearing is greater at shallow depths and horizontal smearing increases
229 with depth. Whereas the general recovery of the positions of the coarse checkerboard anomalies (75
230 x 75 x 60 km) is excellent down to the bottom of the model at 600 km, the amount of smearing
231 increases with depth, decreasing the resolution below ~400 km depth. Anomalies of the
232 checkerboard cell size below this depth are therefore smeared by several tens of kilometers.

233 For the finer checkerboard model, i.e., for smaller scale anomalies (50 x 50 x 45 km), recovery
234 of the pattern is impeded already below ~300 km depth, where smearing in the NW-SE direction as
235 well as with depth becomes more significant. Also, the amplitude of these smaller anomalies
236 decreases strongly at greater depths. Paffrath et al. (2021b) also state that, due to the hybrid
237 approach of their tomography which only accounts for three-dimensional velocity perturbations
238 down to the bottom depth of their regional domain, anomalies below this boundary may be appear
239 to be in the regional domain. Thus, this effect may generally alter the amplitude of structures that
240 appear close to the bottom boundary of the model and, more specifically, may amplify the amplitude
241 of anomalies below this boundary.

242 In a specific synthetic resolution test in the Eastern Alps, Paffrath et al. (2021b) found that
243 their setup can recover a detached slab modelled as a high velocity anomaly separated from the
244 lithosphere by a low velocity anomaly (see chapt 5.1). In a second test, they were also able to detect
245 the opposite geometry, i.e., a slab still attached to its orogenic lithosphere with a negative velocity
246 anomaly representing upwelling asthenosphere above the slab.

247 To conclude this section, Paffrath et al. (2021b) show that their source-receiver setup is able to
248 distinguish fundamental differences in the geometry of slabs on the scale of tens to hundreds of km,
249 thus aiding us in interpreting these structures. However, it is important to emphasize that the model
250 of the overlying crustal has a big impact on imaging the transition zone between the crust and the
251 uppermost part of the mantle.

252

253

254

255

256

257

258

259

260

261

262

263

264

265

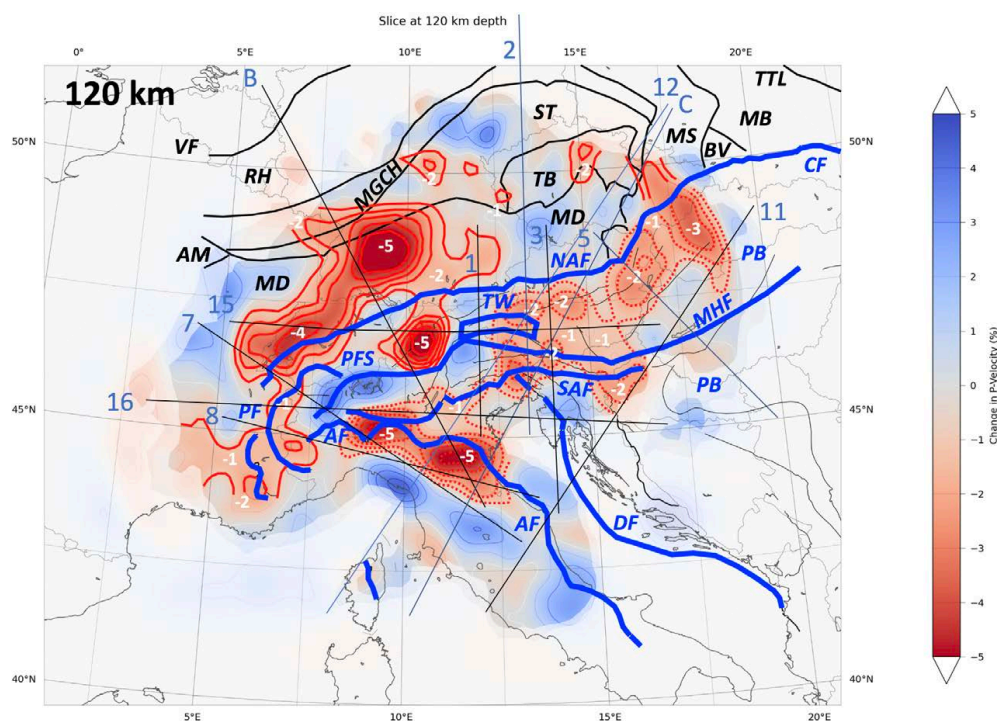
266

267

268

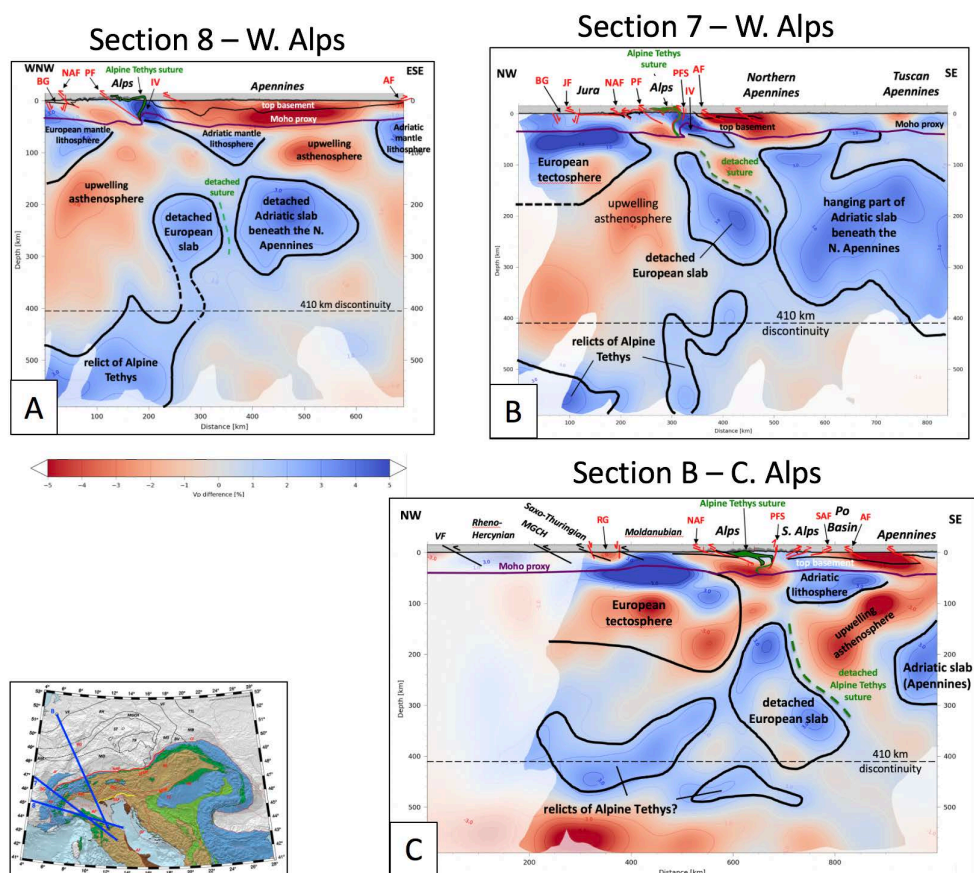
3. Mantle velocity structure

255 For highlighting and interpreting the major mantle structures, we found it useful to trace contours
256 of both positive and negative velocity anomalies in horizontal tomographic depth slices, then
257 superpose these traces on the tectonic map of the Alps (Fig. 2) and compare them with anomaly
258 contours in profiles across the orogen (Figs. 3-6). The surface location of the aforementioned plate
259 boundaries on these profiles are used as markers (e.g., Fig. 7). Also included in the profiles is the
260 trace of the 7.25 km/s iso-velocity contour from the P-wave local earthquake tomography images of
261 Diehl (2009). We use this contour as a proxy for the Moho in the entire Alps in lieu of other Moho
262 models which are either local in their coverage (e.g., Behm et al., 2007; Brückl et al., 2007 in the
263 Eastern Alps) or were found to provide inconsistent estimates of the Moho depth (Spada et al.,
264 2013, e.g., in the Apennines and Ligurian region). The reader is referred to Kind et al. (2021) for a re-
265 assessment of Moho depth. The crustal structure in the profiles is taken from Alpine cross sections
266 of Schmid et al. (2004, 2013, 2017) and Cassano et al. (1986), whereas schematic Variscan crustal
267 cross sections are from Franke et al. (2017), Franke (2020), Mazur et al. (2020) and Schulmann et al.
268 (2014).



269
270 **Figure 2:** Horizontal V_p tomographic slice at 120 km depth. Blue and red areas represent fast and slow teleseismic
271 p-wave anomalies, respectively. Contours of slow anomalies emphasized with thick red lines. Solid red contours -
272 negative velocity anomalies interpreted to correspond to pre-Alpine compositional domains in the mantle; dashed
273 red lines - negative velocity anomalies interpreted to correspond to positive thermal anomalies in the mantle (see
274 text for explanation). Thin black lines indicate the traces of all the profiles displayed in Figures 3 to 6. Thick blue
275 lines – main Alpine structures: NAF - North Alpine Front, SAF – Southern Alpine Front; Other Alpine structures and
276 related features: PFS - Periadriatic Fault System, PF – Penninic Front, TW – Tauern Window, PB – Pannonian Basin,
277 MHF – Mid-Hungarian Fault Zone, WCF – Western Carpathian Front. Thin black lines – Variscan boundaries: VF –
278 Variscan orogenic front, RH – Rheno-Hercynian, MGCH – Mid-German Crystalline High, ST – Saxo-Thuringian, MD –
279 Moldanubian, TB – Tepla-Barrandian, AM – Armorican Massif, BR – Bruno-Vistulian, MB – Malopolska Block, MS –
280 Moravo-Silesian. Other faults: TTL - Teyseyre-Thornquist Line.

281
282 A striking feature in horizontal slices at 100 to 220 km depth is the continuation of negative velocity
283 anomalies of up to 3-4% from the northern Alpine foreland across the Alpine orogenic front to
284 beneath the Western and Central Alps, as well as the westernmost part of the Eastern Alps (Fig. 2,
285 solid red contours). In three profiles crossing these parts (profiles 7, B, 1 of Figs. 3B, 3C, 4A), positive
286 and negative velocity anomalies in the 100-220 depth interval form coherent, inclined layers and
287 together outline a package that dips beneath the Alpine front to below the center of the orogen.
288 This layered structure, which we interpret as the European tectosphere (see next chapter below), is
289 interrupted down-dip to the SE and beneath the core of the orogen. The putative location of the
290 Alpine Tethys suture projected downward into the mantle (dashed green line) is a hypothetical
291 interpretation in order to show the affinity of the former Adria-Europe plate boundary to the
292 European slab (see chapter 5). Profile 8 across the foreland of the southernmost Western Alps (Fig.
293 3A), not a part of the Moldanubian core of the Variscan orogen (Franke et al., 2017), is different
294 from other profiles across the Alps in featuring only a high velocity layer dipping beneath the front
295 of the Alps.

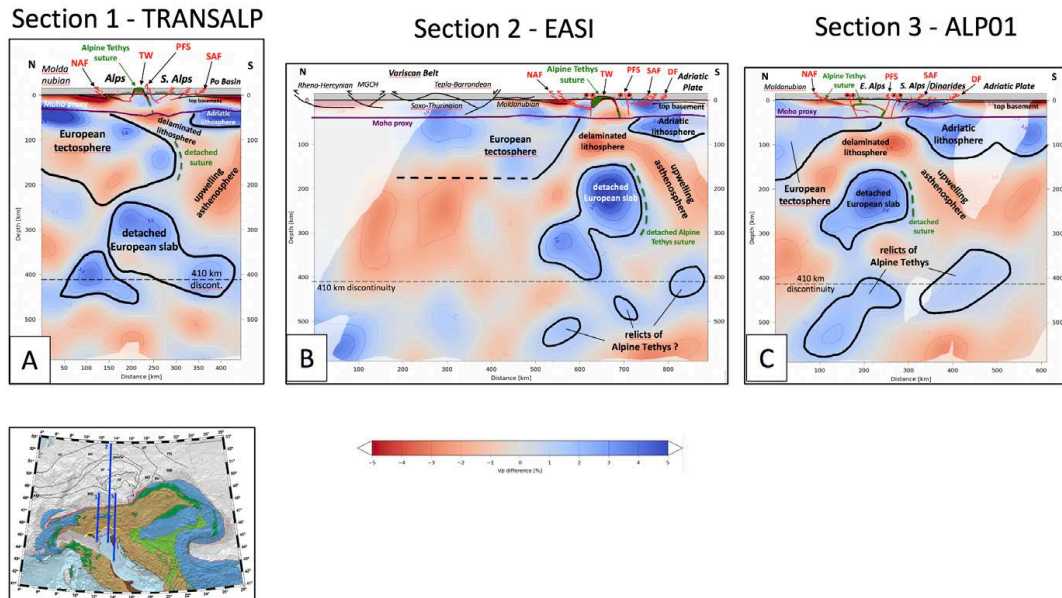


296
 297 **Figure 3:** Cross sections of the Western and Central Alps along traces of profiles 8, 7 and B shown in inset: (A)
 298 Western Alps; (B) Western Alps from the Bresse Graben to the Northern Apennines, parallel to profile B of
 299 Lippitsch et al. 2003; (C) Central Alps from the Variscan Belt to the Po Basin and Northern Apennines. Black solid
 300 lines: our interpretation of the contours of the European tectosphere, Adriatic lithosphere and detached to semi-
 301 detached slab material. Green dashed line – putative trace at depth of Alpine Tethys suture based on the location
 302 of this suture in the schematic crustal cross sections depicted above the Moho proxy. The Moho proxy follows the
 303 V_p velocity contour of 7.25 sec^{-1} obtained from the 3D crustal model of Diehl et al. (2009), where resolution is
 304 sufficient, a model that was directly injected into the tomographic model for obtaining crustal correction.
 305 Schematic Alpine cross sections largely after Schmid et al. (2004, 2013, 2017) and Cassano et al. (1986); schematic
 306 Variscan crustal cross sections after Franke (2017, 2000), Mazur et al. (2020), and Schulmann et al. (2014).
 307

308 Strong negative velocity anomalies of 3-5% (contoured solid red in Fig. 2) generally underlie
 309 the central and western parts of the Moldanubian domain in the Alpine foreland, and run
 310 somewhat oblique to the Variscan domain boundaries. They are not aligned with the Tertiary Bresse
 311 and Rhine Grabens of Oligocene age (Fig. 1). Further to the east, in the area traversed by profiles 2
 312 and 3 (Fig. 2), the subhorizontally oriented European tectosphere is characterized by dominantly
 313 positive velocity anomalies that cross beneath the front of the Alps and abut a low velocity area in
 314 the central part of the Alps (see Figs. 4B & 4C; stippled red contours in Fig. 2). A large 2% positive
 315 anomaly underlies the Moldanubian and Tepla-Barrandean domains beneath the foreland of the
 316 Eastern Alps, but does not extend beneath the orogenic front of the Eastern Alps (Fig. 2; profiles 2
 317 and 3 in Figs. 4B, 4C).



318
 319



320

321 **Figure 4:** Cross sections of the Eastern Alps along traces 1, 2 and 3 shown in inset: (A) profile 1 (TRANSALP profile)
 322 from the Variscan foreland to the Po Basin. The thick European tectosphere has the same structure as beneath the
 323 Central Alps (Fig. 3) and is partly detached; (B) Profile 2 (EASI profile) from the Variscan Belt to the Dinaric Front
 324 and Adriatic Plate. The base of the European tectosphere is poorly defined and the European slab is detached; (C)
 325 Profile 3 (ALP01 profile) from the Variscan Belt to the Adriatic Plate. See legend of Fig. 3 for further explanations.
 326 Alpine and related structures: NAF - North Alpine Front, SAF – Southern Alps Front; PFS - Periadriatic Fault System,
 327 TW – Tauern Window, DF – Dinaride Front

328

329

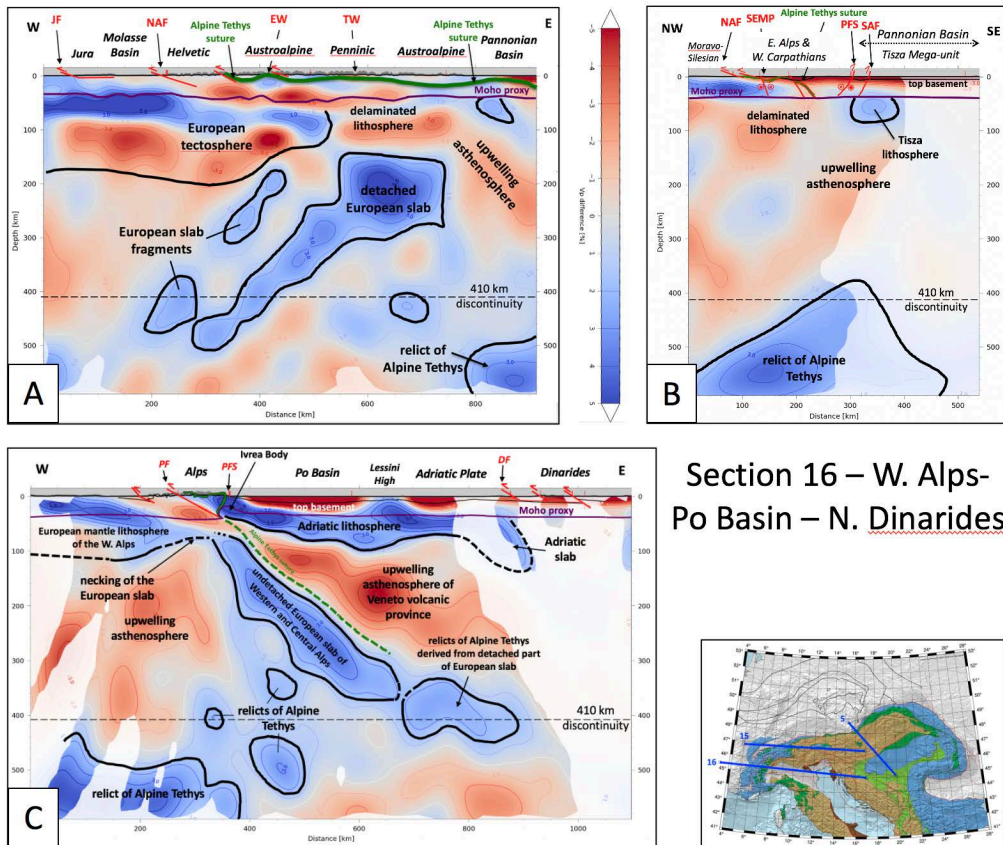
330 In the Eastern Alps, the negative anomaly contours at 120 km depth in Fig. 2 (dashed red
 331 contours) form a broad maximum of 2-5% in map view located between the Northern and Southern
 332 Alpine fronts, and extending eastward from beneath the middle of the Tauern Window to the
 333 Pannonian Basin. Beneath the Eastern Alpine foreland, the upper 80-100 km are characterized by a
 334 broad, moderately positive anomaly of 1-2%. This eastern area shows no horizontal layering of
 335 positive and negative anomalies (profiles 2 and 3 of Figs. 4B, 4C), in contrast to the layering seen
 336 beneath the foreland in the profile immediately to the west (profile 1, Fig. 4A). The mantle structure
 337 beneath the core of the Eastern Alps (profile 15, Fig. 5A) and beneath the transition to the
 338 Pannonian Basin (profiles 3 and 15, Figs. 4C, 5A) is marked by a shallow, strongly negative anomaly
 339 lid and, at depths between 150 and 400 km, by a strong, blob-like positive anomaly (5-6%)
 340 surrounded by a negative anomaly and unconnected to the Alpine-Carpathian foreland (profiles 2,
 341 3, 12 in Figs. 4B, 4C, 6A). The pronounced E-W change in anomaly structure below the core of the
 342 Alps is best seen in the orogen-parallel profiles (profile 15, Fig. 5A), where the 150-200 km thick
 343 positive-negative velocity layering characteristic of the Central and Western Alps gives way in the
 344 Eastern Alps, more precisely beneath the western Tauern Window, to a negative anomaly extending
 345 down to about 130 km underlain by the deep (130-300 km) positive anomalies mentioned above. In
 the next chapter, we interpret this orogen-parallel change to represent a first-order difference in
 the structure and composition of the subducted and delaminated slabs beneath the Alps.



347 The transitional area between Eastern Alps and Western Carpathians (profile 5, Fig. 5B) and
 348 the Pannonian Basin (profile 11, Fig. 6B) is characterized by widespread negative anomalies and by
 349 the almost complete absence of positive anomalies above the 410 km discontinuity marking the top
 350 of the Mantle Transition Zone. These negative anomalies extend to the shallow mantle and directly
 351 underlie the 7.25 km/s Moho proxy marking the base of thinned orogenic crust. Weak positive
 352 anomalies directly below the Moho are restricted to small parts of the Pannonian Basin (profile 11
 353 in Fig. 6B). However, stronger positive anomalies underlying the Moho are found beneath the
 354 Adriatic Sea (profiles 1, 2, 3 and 11, Figs. 4A-C, 6B), marking the still largely undeformed part of the
 355 plate of the same name.

Section 15 – C. Alps – E. Alps - Pannonian

Section 5 - Pannonian



357
 358 **Figure 5:** Cross sections of the Alps along traces 15, 5 and 16 shown in inset: (A) Orogen-parallel profile 15 from
 359 the Central Alps across the Eastern Alps to the Pannonian Basin; note the decrease in thickness of the European
 360 tectosphere before its delamination from the crust at and east of latitude 12°E crossing the area of the western
 361 part of the Tauern Window (TW); (B) Profile 5 from the Variscan Belt in the northwest to the Pannonian Basin in
 362 the southeast across the transition area between Eastern Alps and Western Carpathians. The European
 363 tectosphere has completely delaminated during Neogene stretching in the greater Pannonian area that formed a
 364 backarc basin in the upper plate consisting of the ALCAPA and Tisza Mega-units during Carpathian rollback
 365 subduction. See legend of Fig. 3 for further explanations; (C) Profile from the Western Alps across the Po Basin to
 366 the northern Dinarides (same as profile M1 in Paffrath et al. 2021); note the apparent dip of the still-attached

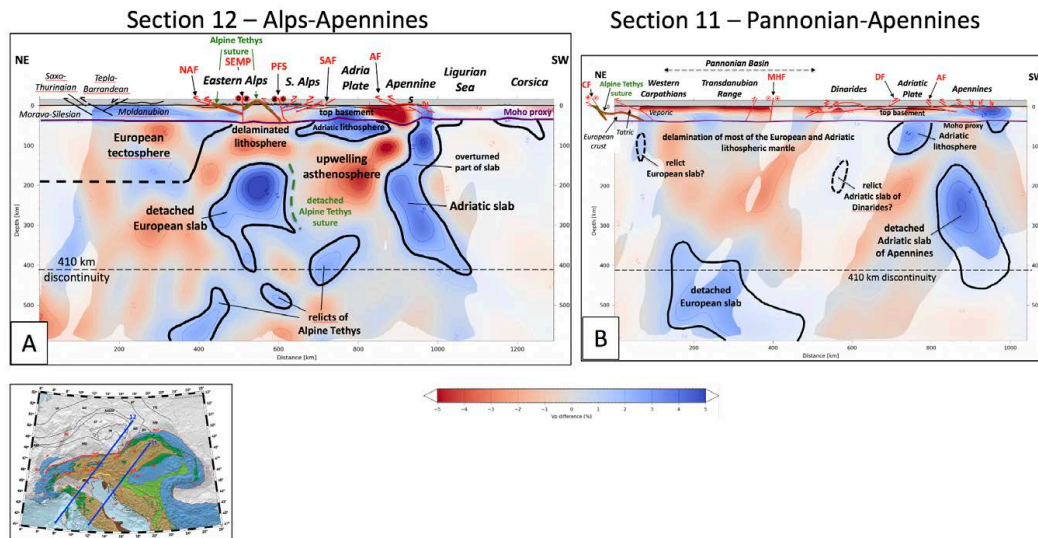


367 European slab beneath the Western and Central Alps, as well as the trace of a slab of Adriatic lithosphere under
368 the northern Dinarides.

369

370 Beneath the northern Dinarides (profile 11, Fig. 6B), no positive anomaly deeper than 100
371 km, except for a questionable small relict, is observed. The resolution is poor in this area, but the
372 interpretation is in line with previous teleseismic studies (e.g., Bijwaard & Spakmann, 2000; Wortel
373 & Spakmann, 2000; Piromallo and Morelli, 2003; Spakman and Wortel, 2004; Serretti and Morelli,
374 2011; Koulakov et al., 2009). However, somewhat further to the north, beneath the northernmost
375 Dinarides in Istria crossed by profile 16 (Fig. 5C), a generally northeast-dipping slab anomaly is fairly
376 well resolved beneath the Dinaride front, reaching a depth of about 140 km. Note that profile 16 is
377 the same as that presented as profile M1 in Paffrath et al. (2021b).

378



379

380 **Figure 6:** Profiles 12 and 11 along traces shown in Figs. 1 and 2 across the greater Alpine area, Adria and the
381 Apennines: (A) Profile from the Variscan Belt across the Eastern Alps to the northern Apennines and the Ligurian
382 Basin. The European slab beneath the Alps is detached, whereas the Adriatic slab beneath the Apennines hangs
383 subvertically and is partly overturned (see text); (B) Profile from the Central Western Carpathians across
384 Pannonian Basin, northern Dinarides, Adriatic plate, Central Apennines to the Tyrrhenian Sea. The European
385 lithosphere is completely delaminated, the Adriatic slab beneath the Dinarides is almost absent and the Adriatic
386 slab beneath the Apennines is detached from a remnant of the Adriatic lithosphere beneath the Adriatic Sea. See
387 legend of Fig. 3 for further explanations. Alpine faults and related structures (labeled red): NAF – North Alpine
388 Front, SAF – Southern Alps Front; PFS – Periadriatic Fault System, SEMP – Salzach-Ennstal-Mariazell-Puch Fault,
389 MHF – Mid-Hungarian Fault Zone, CF – Carpathian Front, DF – Dinaric Front, AF – Apennine Front.

390

391 A large, subvertically dipping positive anomaly directly below the Northern Apennines in profile
392 12 (Fig. 6A) is only connected to the crust near the Ligurian Sea and disconnected from the flat-lying
393 high V_p mantle below the undeformed part of the Adriatic Plate further to the NE. This Adria-
394 derived slab dips down to the 410 km discontinuity. Further to the southeast beneath the Tuscan
395 Apennines in profile 11 (Fig. 6B), this anomaly is completely disconnected from the orogenic crust
396 and dips steeply to the SW in a depth interval of 100-350 km. In a profile parallel to the Apennines
397 (profile 7, Fig. 3B), this positive anomaly is seen to lose its connection with the orogenic crust
398 between profiles 12 and 11 in Figs. 6A and 6B. Unfortunately, the resolution drops off to the SW



399 beneath the Ligurian and Tyrrhenian Seas, but the faint anomalies in the former region suggest that
400 the Moho proxy is directly underlain by a negative anomaly.

401

402 4. Choices in the interpretation of seismic structure

403 The tomographic profiles in Figs. 3-6 depict relative velocities as percentages of deviation from a
404 mean velocity model for crust and mantle (Paffrath et al. 2002b). There are two main challenges
405 when attempting to interpret the anomaly patterns down to a depth of around 600km: (1)
406 Distinguishing the effect of the present thermal state of the rocks from bulk composition on the
407 anomalies. This is difficult, if not impossible, in the absence of corroborative evidence from
408 independent approaches, e.g., heat flow, gravity, conductivity and/or other seismological methods;
409 (2) poor resolution of the tomographic images often precludes a unique determination of the
410 geometry of the anomalies. This is especially true of anomalies at great depth in the mantle, where
411 vertical smearing blurs the images (Foulger et al., 2013).

412 Further headway in interpretation can be made by invoking geological criteria and what we
413 broadly call “the geodynamic context” in order to weigh the consistency, and therefore the
414 plausibility, of some interpretations over others. We use this approach below too, while remaining
415 fully aware of the pitfalls of circular argumentation!

416 To illustrate this important point, we consider profile B across the Central Alps in Fig. 3C,
417 shown without interpretation in Fig. 7A and with two contrasting interpretations in Figs. 7B and 7C.
418 This profile is a good place to begin our interpretative foray, because the geology (i.e., the structure,
419 kinematics, metamorphism, thermal and stratigraphic ages) is well known along this classical
420 section of the Alps (e.g., Schmid et al., 1996, 2004) and previous active-source seismology provides
421 tight constraints on the crustal structure down to the Moho (Pfiffner and Hitz, 1997) and other
422 sources in NFP-20 volume (Pfiffner et al. 1997, eds).

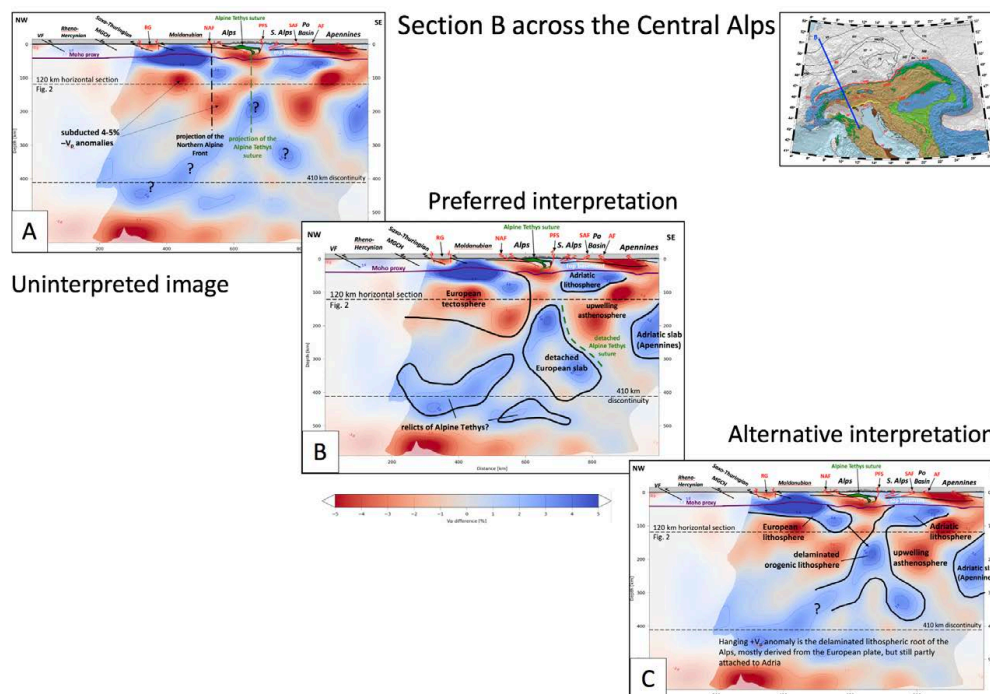
423 In the uninterpreted profile B of Fig. 7A shows two main features:(1) the positive-negative
424 anomaly layering extending down to about 200 km observed in the Alpine foreland and extending
425 to well south of the Northern Alps Front (see the negative anomaly part shown in the horizontal
426 depth slice at 120 km of Fig. 2) and (2) domains of deep-seated positive anomalies labeled with
427 question marks, one dipping northward from the Southern Alps down to the 410 km discontinuity
428 below the Alpine foreland, a second minor one dipping southward below the Po basin. In Fig. 7B,
429 the positive-negative anomaly layering is interpreted to make up a coherent kinematic entity that
430 moved as a unit with respect to the orogenic front and was subducted to the south beneath the
431 Adriatic Plate. As previously mentioned, it is this unit we refer to as *tectosphere* to distinguish it
432 from “ordinary” lithosphere and asthenosphere, which are usually used either according to
433 seismological criteria, or in a rheological sense for rigid-conductive and convecting parts of the
434 mantle, respectively (see review by Artemieva 2011). This distinction is relevant in our case because
435 *tectosphere* as first defined by Jordan (1975) is compositionally heterogeneous and thus can include
436 both positive and negative velocity anomalies that together form a tectonic plate. Tectosphere is a
437 kinematic entity similar to rheological lithosphere in the sense of a coherently moving plate
438 detached at its base from convecting mantle. We hasten to point out that not all plates in the
439 greater Alps area comprise such heterogeneous tectosphere in terms of V_p ; indeed, as shown in the
440 next section, the Adriatic Plate and the Adria-derived slab beneath the Apennines comprise
441 lithosphere in the classical sense of compositionally homogeneous, seismically “fast” kinematic
442 entities.

443 The slab of tectosphere descending beneath the Northern Alpine front in Fig. 7B is marked
444 as being slightly detached at a depth of 100- 300 km, with a possible continuation down to the 410
445 km discontinuity underneath the Po basin. Other positive anomalies beneath the Alps in the 300-



446 450 km depth interval may be subducted and detached relicts of the Alpine Tethyan Ocean. The
447 highly negative anomaly (up to 5-6%) in the downgoing plate is attributed to factors (e.g.
448 composition, anisotropy, anelasticity etc.) inherited from the late Paleozoic Variscan orogenic cycle
449 rather than a purely thermal anomaly that has persisted to the present day. The magnitude of this
450 anomaly for a given velocity anomaly depends on seismological attenuation, Q , which varies with
451 the age and tectonic setting of the lithosphere; active regions have lower Q values and therefore
452 lesser thermal anomalies for given velocity anomalies than shield regions (Mitchell 1995; Goes et al.
453 2000). In our case, the downgoing plate comprises Variscan and pre-Variscan lithosphere, such that
454 the thermal anomaly causing a 5-6% $-V_p$ anomaly is estimated to be somewhere between 300° and
455 600°C (using DV_p - T relations provided by Goes et al., 2000; Cammarano et al., 2003; Perry et al.,
456 2006) with the lower value including a poorly constrained compositional contribution. This range of
457 thermal anomalies seems unrealistically high for old, inactive mantle lithosphere in the downgoing
458 plate of a collisional orogen. Variscan crust in the foreland of the Alps underwent amphibolite- to
459 locally granulite-facies regional metamorphism some 340-360 Ma ago followed at 320-260 Ma by
460 calc-alkalic magmatism and thermal overprinting (e.g., Franke, 2000 and refs. therein). This Late
461 Carboniferous to Early Permian magmatic event is much older than the onset of Alpine collision at
462 40-32 Ma (Handy et al., 2010 and refs. therein). There is no known mechanism that could maintain
463 such a pronounced thermal anomaly for such a long time.

464 In the interpreted profile B (Fig. 7B) other negative V_p anomalies in the mantle occur
465 immediately beneath the Moho in the cores of the Alps and Apennines where the Moho lies at c. 50
466 km depth and where the lower crust is also characterized by low V_p . Finally, a deep seated negative
467 V_p anomaly is found below the Adriatic lithosphere, between the detached part of the European
468 slab and the Northern Apennines slab derived from Adriatic lithosphere (Fig. 7B). In the former case,
469 the negative anomaly in the mantle immediately below the Moho is interpreted to manifest a
470 depression of the absolute velocities by addition of wet and less-dense and therefore seismically
471 slower material in the subduction channel. In the case of the deep-seated negative anomaly labeled
472 “upwelling asthenosphere”, the negative anomalies of up 5-6% could possibly be caused by still hot,
473 upwelling asthenosphere. However, as argued above, this would need a ΔT of some 600-700°C
474 resulting in temperatures well above 1400°C. Following the suggestion by Giacomuzzi et al. (2011),
475 we envisage hydrated mantle in a backarc position behind the descending non-detached and
476 detached parts of the European tectosphere rather than still-existing, substantially elevated
477 temperatures as a suitable explanation for the low V_p in this area.
478



479
 480 **Figure 7:** Raw image of vertical tomographic profile B across the Central Alps and two alternative interpretations:
 481 (A) Raw image showing layered positive and negative V_p anomalies extending from the Variscan Belt to south of
 482 the Northern Alpine Front (NAF, see also Fig. 2); (B) Preferred interpretation shown in Fig. 3C, indicating
 483 coherence of layered positive and negative V_p anomalies that are interpreted as thick and old (Variscan or older?)
 484 European lithosphere (labeled tectosphere) dipping to the south beneath the Alps. The European slab is detached.
 485 In contrast, the Adriatic lithosphere beneath the Po Basin and Apennines is thin and underlain by a large negative
 486 anomaly interpreted as upwelling asthenosphere; (C) Alternative “classical” interpretation of lithosphere as
 487 comprising only positive V_p anomalies, thought to be old, cold lithosphere. The long N-dipping positive V_p
 488 anomaly is interpreted as delaminated lithospheric root of the Alps, mostly derived from the European Plate, but still partly
 489 attached to the Adriatic Plate (see text for discussion).

491 In the contrasting interpretation shown in Fig. 7C, all anomalies are considered primarily to
 492 reflect temperature anomalies, such that positive anomalies at depths below the Moho are
 493 interpreted as subducted lithosphere, whereas negative anomalies below the Moho are equated
 494 with hot asthenosphere and are not part of a subducted plate. This is in line with the classical
 495 rheological definition of a descending sheet of rigid and cold lithosphere. Thus, the long north-
 496 dipping, positive anomaly domain in this profile could be interpreted as subducted Adriatic
 497 lithosphere connected to Adriatic lithosphere beneath the Po Basin and the Adriatic Sea. If true,
 498 however, this would necessitate hundreds of kilometers of shortening within predominantly S-
 499 facing folds and thrusts in the Alps for which there is no geological evidence. Most folding and
 500 thrusting in the Alps is N-vergent, as documented by more than a century of detailed study. Within
 501 the Southern Alps where S-vergent thrusting is indeed observed, about ≤ 72 km of shortening was
 502 accommodated, mostly in Oligo-Miocene time (Schönborn, 1992; Schmid et al., 1996; Rosenberg
 503 and Kissling, 2013). This effectively precludes any scenario involving north-directed subduction of
 504 large amounts of Adriatic lithosphere beneath the Alps. This leaves Fig. 7B with its anomalously
 505 thick (180-200 km) subducting European tectosphere as the preferred interpretation. The total



506 length of subducted European slab according to the interpretation in Fig. 7B is roughly 400 km, as
507 measured between the Northern Alpine Front down to the 410 km discontinuity; this conforms with
508 the shorting estimates in the Alps since the European lithosphere entered the subduction zone in
509 the Alps in Eocene time (Schmid et al., 1997; Handy et al., 2010), which lends further support to our
510 interpretation. In the labeling of this figure and others that follow, we therefore used the term
511 “tectosphere” (Jordan, 1975) to refer to a kinematically coherent, yet compositionally
512 heterogeneous piece of mantle that forms a tectonic plate. We return to this point in the section 6
513 below.

514
515

516 **5. Regional tectonic interpretation**

517 In interpreting the images in Figs. 3-6 and all the additional profiles in Appendix A, we followed the
518 approach outlined above by marking the boundaries (thick black lines) around kinematically
519 coherent packages or tectonic plates whose geometry is consistent with available data on Moho
520 depth and with the kinematic history of the rocks exposed at the surface. Dashed solid black lines
521 delimit very poorly defined or even putative boundaries. We include two horizontal depth slices at
522 240 km and 90 km, respectively, in Figs. 8 and 9 to show the main structures outlined by velocity
523 anomalies in map view.

524

525 **5.1 Alps**

526 European tectosphere of Variscan or pre-Variscan origin originating in the Alpine foreland is evident
527 in all cross sections of the Alps (Figs. 3, 4), though its base in the Eastern Alps is undefined (e.g.
528 profile 2 in Fig. 4B). Beneath the Central Alps and westernmost Eastern Alps, this tectosphere dips
529 to the S to become the thick, subducted European slab (profiles B and 1 in Figs. 3C, 4A), whereas in
530 the Western Alps (profiles 8 and 7 in Figs. 3A, B) and in the Eastern Alps east of 12°E (profiles 2, 3
531 and 12 in Figs. 4B, C, 6A), the European slab is completely detached from its foreland. Only in the
532 transitional area between Western and Central Alps is the slab still tenuously connected to the
533 European tectosphere of the Alpine foreland (profile 16, Fig. 5C). The moderate dip and inordinate
534 length of the slab beneath the entire E-W extent of the Po Basin in this particular profile reflect the
535 fact that this W-E running profile obliquely slices the European slab at a considerable angle to the SE
536 dip of Alpine subduction in the Western and Central Alps. Moreover, the E-dipping positive anomaly
537 seen in Fig. 5C comprises different pieces, with the positive anomaly at the eastern end (below the
538 Adriatic plate east of the Lessini Mountains, at a depth of around 350-450 km) originating from a
539 south-dipping slab fragment below the Eastern Alps depicted in Fig. 4A. This easternmost part of
540 the positive anomaly in profile 16 of Fig. 5C also slices minor, discontinuous relics of Alpine Tethys
541 south of the main slab in the Eastern Alps (see lower righthand side of N-S trending profile 2 in Fig.
542 4B).

543 In the Western Alps, detachment of the European slab (Figs. 3A, 3B) was previously noted by
544 Lippitsch et al. (2003) and interpreted as a subhorizontal tear that is currently propagating from SW
545 to NE towards the still-attached part of the slab in the western Central Alps (Kissling et al., 2006).
546 The detachment of this part of the slab (profile A in Appendix A), possibly combined with unloading
547 due to glacial erosion and melting (Champagnac et al., 2007; Mey et al., 2016), have been deemed
548 responsible for rapid Plio-Pleistocene exhumation and surface uplift of the Western Alps (Fox et al.,
549 2015, 2016) which have the highest peaks (≤ 5000 m) and greatest relief (< 3000 m) of the entire
550 Alpine chain.

551 In the Eastern Alps, the detached European slab hangs subvertically to steeply N-dipping in a
552 depth interval ranging from 150 to 350-400 km. We note that the pronounced along-strike change



553 in mantle structure between nearby profiles 1 and 2 (Figs. 4A and 4B) does not coincide with the
554 classical Austroalpine-Penninic boundary marking the Alpine Tethys suture between the Central and
555 Eastern Alps at the surface. This along-strike change is best seen by comparing the mantle structure
556 in an orogen-parallel profile with the location of the suture in the tectonic map (profile 15 in Fig. 5A)
557 and its projected trace in the horizontal depth slice at a depth of 90 km (Fig. 9). Rather, it coincides
558 with the northward projection of the Giudicarie Belt (Scharf et al., 2013; Verwater et al., 2021;
559 marked GB in Fig. 1), a post-collisional fault of latest Oligocene to Miocene age, which sinistrally
560 offsets the southern part of the Alpine orogenic edifice including the Periadriatic Fault System. This
561 northward projection of the Giudicarie Belt, which lies in the Tauern Window in map view, coincides
562 with the westernmost point of eastward, orogen-parallel extrusion of the Alpine and Western
563 Carpathian lithosphere unit in latest Oligocene to Miocene time (e.g., Pomella et al., 2011; Scharf et
564 al., 2013; Schmid et al., 2013; Favaro et al., 2017). This allochthonous block is referred to in the
565 literature as the ALCAPA mega-unit. The orogenic Moho beneath this block shallows dramatically to
566 the east (e.g., Grad et al., 2009; Kind et al., 2021), reaching a depth of some 20 km beneath the
567 Pannonian Basin (profiles 15 and 5 in Figs. 5A, B). The occurrence of negative V_p anomalies
568 immediately below this shallow orogenic Moho in the Eastern Alps (e.g., profile 12, Fig. 6A,
569 highlighted low V_p area in Fig. 9) strongly suggests that the entire lithospheric mantle reaching from
570 the Tauern Window of the Eastern Alps to their transition with the western Carpathians (profile 5 in
571 Fig. 5B) has been delaminated.

572
573

574 5.2 Pannonian Basin

575 The negative V_p anomaly of the Eastern Alps continues further to the NE into the area of the Vienna
576 Basin and the Central Western Carpathians, as seen in the 90 km and 120 km depth slices (Figs. 2,
577 8). This is the area overlying the slab remnants that have descended into the Mantle Transition Zone
578 (e.g., profile 5 in Fig. 5B). The Central Carpathians host a province of 17-14 Ma post-collisional sub-
579 alkaline magmatism (Seghedi and Downes, 2011; Seghedi et al., 2013) related to Miocene extension
580 of the Pannonian domain, including the Western Carpathians. Given the fact that this magmatism
581 ended some 14 Ma ago, it is uncertain if the low V_p anomaly in the Western Carpathians is solely
582 related to a persistent positive thermal anomaly. In this context, it is relevant to note that the area
583 of the Tisza mega-unit south of the Mid-Hungarian Shear Zone (MHZ in Fig. 1) and characterized by
584 high heat flux (Horvath et al., 2015, their Fig. 12) does not exhibit such a negative V_p anomaly. This
585 indicates that present-day heat production does not everywhere correlate with negative
586 seismological anomalies.

587 Relicts of delaminated and detached European tectosphere can be detected at and below
588 the 410 discontinuity beneath the Pannonian Basin (profiles 5 and 11 in Figs. 5B, 6B) as previously
589 discovered in the passive array swath experiment of Dando et al. (2011). As mentioned in discussing
590 our interpretation thereof (Fig. 7), the 400 km down-dip length of the slab segments is broadly
591 consistent with estimates of shortening since the European slab entered the subduction zone after
592 the closure of Alpine Tethys at around 40 Ma (e.g., Schmid et al., 1996; Handy et al., 2010; Kurz et
593 al., 2008). This suggests that the detached slab remnants comprise mostly European tectosphere
594 (Mitterbauer et al., 2011; Rosenberg et al., 2018; Kästle et al., 2020).

595
596
597

598 5.3 Adriatic Plate



599 The Adriatic Plate is 100-120 km thick as defined by the lower limit of the horizontal $+V_p$ anomalies
600 beneath the Adriatic Sea. We label this as Adriatic lithosphere and regard it as Adriatic tectosphere
601 in a kinematic sense (e.g., profiles 1, 2, 3 and 12 in Figs. 4, 6A). This is less than half the thickness of
602 the European tectosphere. It is generally accepted that in the Alps the former Adriatic Plate formed
603 the upper plate during convergence, whereas in the Dinarides and Apennines, Adria is the
604 subducting plate. The Adriatic slab in the Apennines possibly has a simpler velocity structure than
605 the European slab in the Alps, comprising thinner and compositionally more homogeneous
606 lithosphere with only $+V_p$ anomalies (Fig. 6). In contrast to the European foreland (Franke, 2020),
607 most of the former Adriatic Plate was not affected by high-grade metamorphism and never
608 experienced the closure of various Paleozoic oceans. Instead, it has been interpreted as the
609 southern, Gondwana-derived foreland of the Variscan belt (Molli et al., 2020).

610 The Adriatic tectosphere is underlain by a pronounced low-velocity mantle in depth interval
611 of 150-350 km (profiles B and 3 in Figs. 3C, 4C right hand side; profile 12 in Fig. 6; profiles B, 3, 12,
612 11 in Appendix A). This thick low-velocity zone coincides at the surface in the eastern Po Basin and
613 northern Adriatic Sea with the Veneto volcanic province (Figs. 1, 8), which comprises mostly
614 primitive basalts diluted by a depleted asthenospheric mantle component (Macera et al., 2003). Its
615 age range between Late Paleocene to Late Oligocene (Becculava et al., 2007) spans the transitional
616 time from subduction to collision in the Alps (Handy et al., 2010 and refs therein). It is thus tempting
617 to attribute this magmatism to the combined effects of heat and fluid advection behind the
618 originally S-dipping European slab in the Alps (Macera et al., 2008). The release of water and
619 incompatible elements from deeply buried sediments along the slab interface may have caused
620 hydration of the overlying mantle, giving rise to an overall decrease in seismic velocity, as proposed
621 by Giacomuzzi et al. (2011) to explain the negative anomaly layer beneath the Adriatic Plate.

622
623

624 5.4 Apennines

625 Switches in the polarity of subduction are manifested at the surface by changes in thrust vergence
626 and location of the orogenic fronts at the Alps-Apennines and Alps-Dinarides transitions (Fig. 1). The
627 mantle structure at the Alps-Apennines transition is simpler than the complex surface fault
628 structure due to switching subduction polarity (Molli et al., 2010; Schmid et al., 2017) would
629 suggest. There, the European and Adriatic slabs are easily distinguished in profiles 8 and 7 (Fig. 3A,
630 B). In the horizontal slice at 240 km depth in Fig. 8, the two slabs cannot be distinguished at the
631 resolution of the horizontal depth slice because they are very close to each other (see Figs. 3A, B).
632 However, the horizontal slice at 90 km (Fig. 9) shows them separated by the downward projection
633 of the Alpine Tethys suture. Note that the European slab beneath the Western and Central Alps was
634 subducted to the SE below the Adriatic Plate prior to 35 Ma, ultimately leading to the Alpine Tethys
635 suture depicted in Fig. 9. Adria-Europe suturing occurred before the Apennines formed in latest
636 Oligocene to Miocene and Pliocene time. When considering profiles 8 and 7 in Fig. 3A, as well as
637 profiles 12 and 11 in Figs. 6A and 6B in the following discussion, it is important to note that the
638 Adriatic slab beneath the northern Apennines originally dipped to the SW when it was still attached
639 to the then-still undeformed western part of the Adriatic Plate (Facenna et al. 2004, Schmid et al.
640 2017). Apenninic orogenesis involved E-directed rollback of this former Adriatic Plate that currently
641 makes up the slab below the Northern Apennines.

642 In profile 12 (Fig. 6A) across the northern Apennines, the upper 200 km of the Adriatic slab
643 anomaly dip to the NE and are hence overturned, as pointed out in section 3. This slab is detached
644 from the Adriatic lithosphere and located in the NE foreland of the Apennines. Somewhat more to
645 the south in profile 11 (Fig. 6B) across the central (Tuscan) Apennines, the Adriatic slab is normally



646 inclined, i.e., dips to the SW, and completely detached from the orogenic wedge of the Apennines.
647 In profile 7 (Fig. 3B) running parallel to the strike of the Apennines slab, a subhorizontal tear is
648 clearly visible beneath the Tuscan Apennines at a depth of 80-100 km. We speculate that once the
649 Apennines stopped advancing in Plio-Pleistocene time (e.g., Molli et al., 2010), the heavy Northern
650 Apennines slab steepened. The subhorizontal tear visible in Fig. 3B appears to have propagated
651 from SE to NW, i.e., in a direction of decreasing orogen-normal shortening in the Apennines and
652 towards the pole for Neogene counterclockwise rotation of the Corsica-Sardinia block with respect
653 to Europe (Speranza et al., 2002), also affecting the Apenninic orogen (Maffione et al., 2008). Partial
654 tearing allowed the detached part of the slab in the SE to retreat and sink under its own weight,
655 while the smaller, still-partly attached segment in the NW became vertical and locally overturned
656 (profile 12 in Fig. 6A). The maximum depth (8-9 km) of Plio-Pleistocene fill in the northern Apenninic
657 foreland or “Po” Basin (Bigi et al., 1989) and the deepest Moho beneath the northern Apennines
658 (50-60 km, Spada et al., 2013) are both attributed to the downward pull of this still partially
659 attached slab segment depicted in profile 12 of Fig. 6A (Picotti and Pazzaglia, 2008).

660 The horizontal depth slice at 90 km in Fig. 9 shows the area traversed by profiles 12 and 11
661 discussed above that is characterized by low V_p and interpreted to outline lithospheric delamination
662 during slab detachment. These areas extend from NW to SE along the front of the NE-facing
663 Apennines nappe stack. This indicates that the Adriatic slab below the Apennines has detached
664 from the little-deformed Adriatic Plate in the Adriatic Sea almost all along the strike of the Northern
665 and Central Apennines. Note that this area of delamination is slightly NE of the outline of the
666 detached and subvertical Adriatic slab shown in the horizontal depth slice at 240 km depth (Fig. 8).

667
668

669 5.5 Dinarides

670 Our data only cover the area of the northern Dinarides and the Dinarides-Alps transition area in
671 Slovenia (Stipčević et al., 2011, 2020). Collisional shortening after the closure of the Neotethyan
672 oceanic tract in the northern Dinarides started earlier than in the Alps; major collisional shortening
673 lasted from Late Cretaceous to Oligocene time, with only very minor shortening in the Miocene
674 (e.g., Schmid et al., 2008). In the Alps, collisional shortening after the closure of Alpine Tethys
675 started later, namely in the late Eocene and lasted until Pliocene times. The transition between the
676 Alps and the Dinarides is marked at the surface by the Southern Alpine Front that thrusts the
677 Southern Alps southward over older NW-SE striking Dinaric thrusts (Fig. 1) in the late Miocene.
678 South-directed thrusting in this transition area, combined with dextral strike slip reactivating Dinaric
679 structures, is still seismically active (e.g., Kastelic et al., 2008; see yellow line marking the presently
680 active plate boundary in the Alps in Fig. 1).

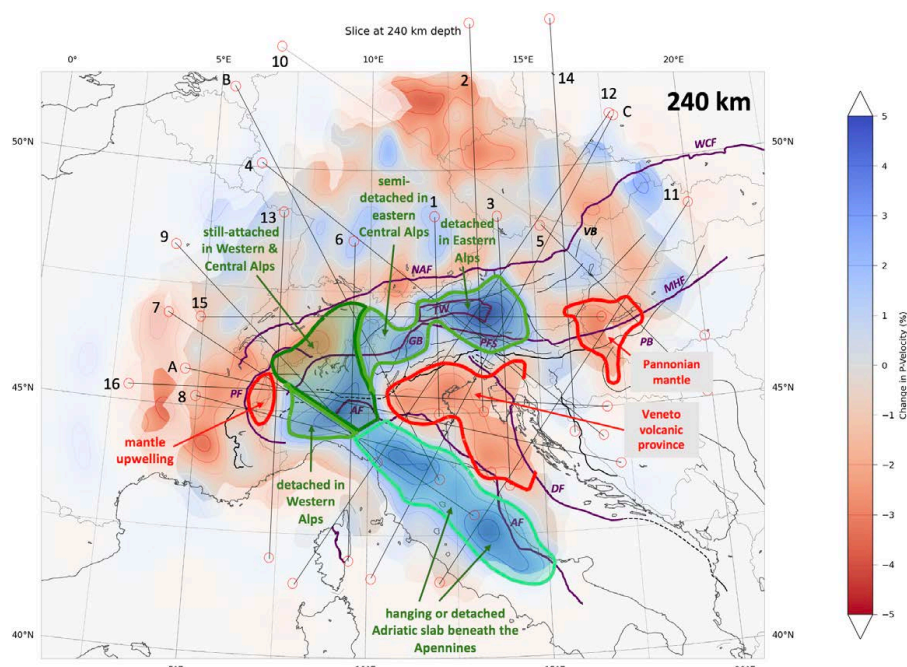
681 An east- to northeast-dipping positive V_p anomaly is partly imaged beneath the Dinarides in
682 profile 16 (Fig. 5C), but is lacking in profile 11 (Fig. 6B) which crosses the frontal Dinarides to the
683 south. Unfortunately, the resolution in this latter profile is very poor. A slab gap in the
684 northernmost Dinarides has been recorded by global tomography (Bijwaard and Spakman, 2000;
685 Piromallo and Morelli, 2003), possibly due to the previous inability of imaging a slab of only ≤ 140
686 km length in this area. Ustaszewski et al. (2008), Schefer et al. (2011) and Horvath et al. (2015)
687 invoked asthenospheric upwelling at the SE limit of the Pannonian basin associated with the
688 breakoff of part of the NE-dipping Adriatic slab. This is thought to have permitted asthenosphere to
689 flow from beneath the Adriatic Plate to below the extending Pannonian Basin in the upper plate of
690 the retreating Carpathian subduction (Jolivet et al., 2009; Handy et al., 2015; Horvath et al., 2015;
691 Kiraly et al., 2018).

692

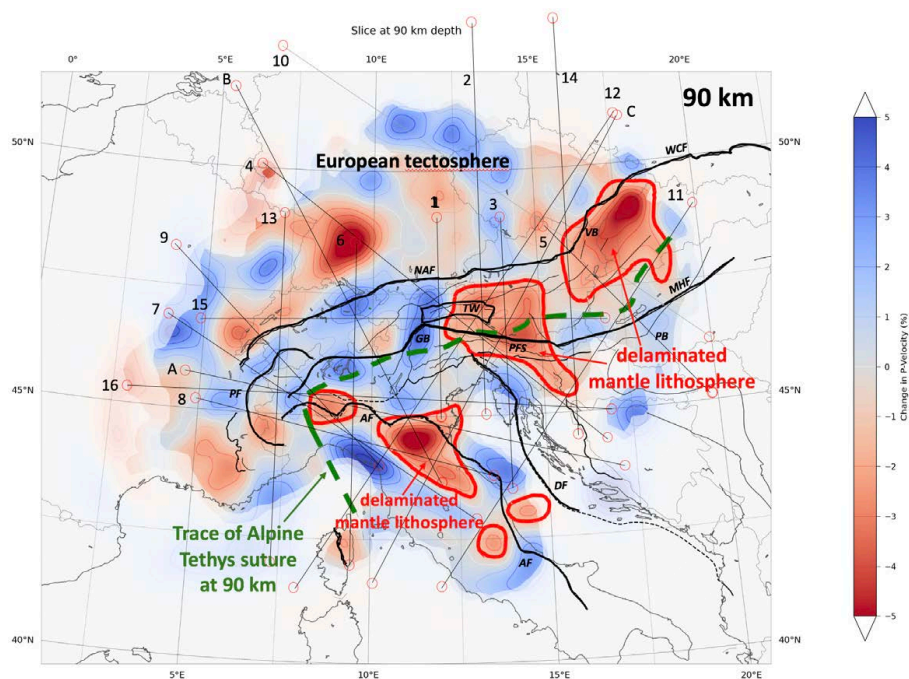


693 **5.6 Summary of the tectonic interpretation**

694 We summarize our interpretations mostly based on inspecting the profiles (see text above and
695 additional profiles in Appendix A) by mainly looking at the map view interpretation of horizontal
696 depth slices (Figs. 8, 9). We chose the 240 km depth slice in Fig. 8 because at this depth a maximum
697 number of slabs can be collected, exhibiting various degrees of attachment of the slabs to their
698 orogenic edifice and their forelands. The horizontal depth slice of Fig. 9 at 90 km was chosen in
699 order to visualize areas characterized by low V_p in the uppermost mantle.
700



701 **Figure 8:** Horizontal V_p tomographic slice at 240 km. Blue and red areas represent fast and slow teleseismic
702 p-wave anomalies, respectively. Isolines indicate deviation in % of P-wave velocities from the mantle model in
703 Paffrath et al. (2021b). Green lines are boundaries of slabs at their intersection with the horizontal plane of the
704 depth slice. The slab boundaries were obtained by projecting the interpreted slab outlines marked with black lines
705 in the 19 profiles found in the text and in Appendix A (traces shown as thin black lines) into the plane of the depth
706 slice. Shades of green denote various degrees of attachment of the European slab to the European tectosphere in
707 the Alpine foreland (see interpreted profiles and text). Red lines outline domains of mantle upwelling. Thick black
708 lines are major Alpine faults: NAF - North Alpine Front, PFS - Periadriatic Fault System, GB - Giudicarie Belt, PF -
709 Penninic Front, TW - Tauern Window, VB - Vienna Basin, PB - Pannonian Basin, MHF - Mid-Hungarian Fault Zone,
710 AF - Apennines Front, DF - Dinarides Front.
711
712
713



714
715 **Figure 9:** Horizontal V_p tomographic slice at 90 km depth. Blue and red areas represent fast and slow teleseismic
716 p-wave anomalies, respectively. Isolines indicate deviation in % of P-wave velocities from the mantle model in
717 Paffrath et al. (2021b). Thick dashed green line is the projection of the suture zone of Alpine Tethys down to 90
718 km based on interpretation of the profiles. This green line marks the southern boundary of the European Plate
719 with the Adriatic Plate and the lithosphere of the Tisza megaunit beneath the Pannonian Basin. Note the variable
720 P-wave velocities within the European tectosphere at this depth due to pre-Alpine tectogenesis. Areas outlined in
721 red indicate areas with low V_p located within the Alpine-age orogens where shallow asthenosphere replaced
722 delaminated mantle lithosphere after slab detachment in the Alps, Western Carpathians and the Apennines
723 occurred.

724
725 Figure 8 shows that in the Alps, slab attachment is only complete in the Central and northern
726 Western Alps between 7° and 10°E. Detachment is complete in the southernmost Western Alps and
727 modest in the eastern Central Alps between 10° and 12°. It is complete in the Eastern Alps east of
728 about 12°E where we observe the detached Eastern Alps slab (Fig. 8) dipping to the NE (e.g.,
729 Lippitsch et al., 2003; see Figs. 4B, 4C and 6A). No significant positive V_p anomaly is seen at 240 km
730 depth in the easternmost Eastern Alps and the Western Carpathians east of 15°E, where the relicts
731 of former slabs reside below the 410 km discontinuity (see Fig. 5). Where detachment is complete,
732 the slabs have been supplanted by upwelling asthenosphere, as is seen by three areas of negative
733 V_p anomalies outlined in the depth slice for 90 km (Fig. 9) in the southern Western Alps, the Veneto
734 volcanic province and the Pannonian basin. In the Apennines, the Adriatic slab is locally hanging, but
735 mostly completely detached from its overlying orogenic root and foreland. There too, upwelling
736 asthenosphere has locally replaced the descending slab in the frontal, i.e., NE parts of the orogen,
737 eliminating the former connection of the slab with the remaining undeformed part of the Adriatic
738 Plate in the Adriatic Sea.

739 Figure 9 also features a dashed green line marking the location of the Alpine Tethys suture zone
740 projected from the crustal down to 90 km, separating the European tectosphere from the Adriatic
741 lithosphere. We emphasize that the downward projection of this suture in the profiles (dashed



742 green lines) is hypothetical in the sense that its mapping involved tracing the suture through
743 domains that were extensively modified during delamination and mantle upwelling. The severe
744 bending of the putative trace of this suture zone at the Alps-Appennines transition reflects
745 counterclockwise rotation of the Corsica-Sardinia block and the Ligurian Alps in Miocene time
746 (Schmid et al., 2017 and references therein). Likewise, bending of the projected suture north of the
747 Mid-Hungarian fault zone is due to the counterclockwise rotation of the Western Carpathians, also
748 in Neogene time (Márton et al., 2015).

749
750

751 6. Discussion

752

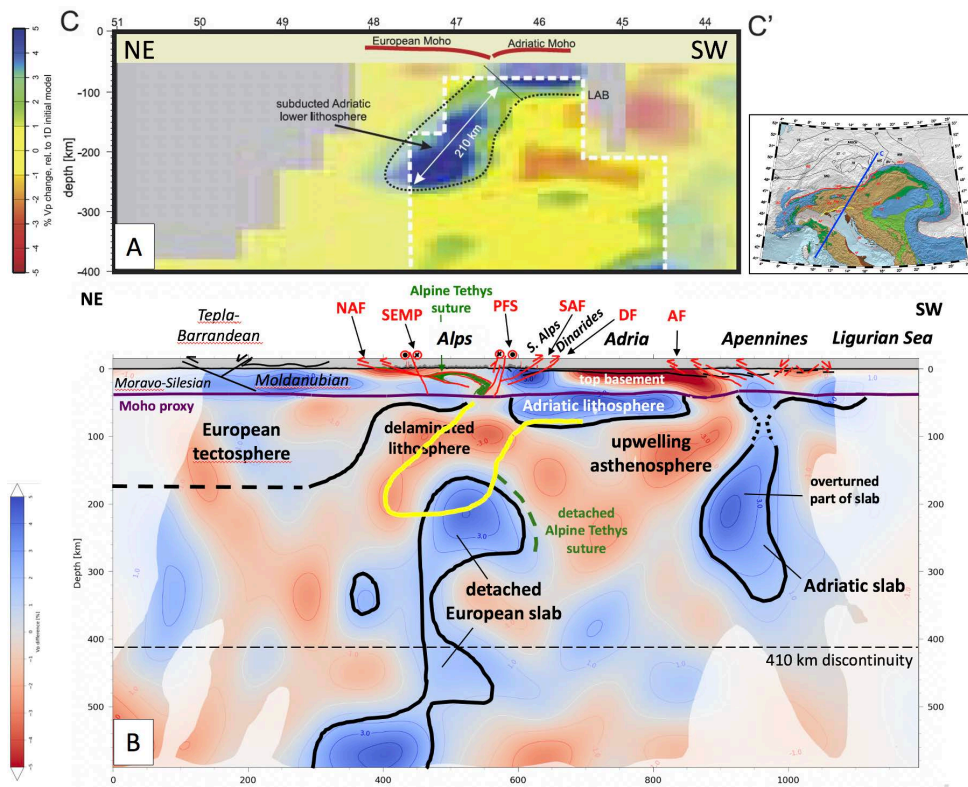
753 6.1 Subduction polarity – was there a switch in the Alps?

754 The polarity of subduction in the Alps, particularly at its junction with the northern Dinarides, has
755 been a bone of contention ever since the publication of P-wave tomographic images showing high
756 velocity anomaly some 200 km long dipping some 50° to the NE beneath the Eastern Alps and
757 connected with the upper mantle of the undeformed Adriatic Plate according to Lippitsch et al.
758 (2003). This Eastern Alps slab, first detected by the pioneering work of Babuska et al. (1990) as
759 distinct from the Western and Central Alps slab. The Eastern Alps slab was thought to be separated
760 from the SE-dipping European slab anomaly in the Central and Western Alps by a decrease in
761 strength of the positive anomaly, interpreted by Babuska et al. (1990) and Lippitsch et al. (2003) as
762 a slab gap in map view. The attribution of the Eastern Alps slab to the Adriatic Plate by Lippitsch et
763 al. (2003) was challenged by the teleseismic model of Mitterbauer et al. (2011), showing a steeper
764 (75° or more) and longer Eastern Alps slab reaching the 410 km discontinuity. The Eastern Alps slab
765 was thought to have been Adriatic lithosphere that had been laterally wedged from the Dinarides
766 (Lippitsch et al., 2003) or subducted beneath the Eastern Alps in Neogene time (Schmid et al., 2004;
767 Kissling et al., 2006; Handy et al., 2015). Although N-directed subduction was inconsistent with
768 north-vergent nappe stacking along strike of the entire Alpine chain, which supported uniformly
769 south-directed subduction of the European lithosphere beneath the Adriatic Plate during the closing
770 of Alpine Tethys, these authors postulated a late-stage switch in subduction polarity that was
771 thought to have occurred in Miocene times, i.e., after nappe stacking. Another possible problem
772 with a Miocene switch in subduction polarity is that the easternmost part of the slab anomaly
773 discovered by Lippitsch et al. (2003) is significantly longer (200 km) than the estimated amount of
774 south-directed shortening in the eastern Southern Alps, which amounts to ≥ 50 km (Schönborn,
775 1999; Nussbaum, 2000). One way to explain the excess slab length was also to take into account
776 some 85 km Miocene N-S shortening accommodated in the Eastern Alps and some 55 km Miocene
777 shortening taken up at the front of the northernmost Dinarides (Ustaszewski et al., 2008, their fig.
778 6). Another way to explain the excess slab length was to assume that the eastern part of the slab is
779 partly of European origin (Handy et al., 2015). Indeed, recent models based on pre-AlpArray
780 seismological data have combined ambient noise and P-wave tomography to propose that Eastern
781 Alps slab is actually a composite of predominantly European and a subordinate amount of Adriatic
782 lithospheres (Kästle et al., 2020).

783 Our new results clearly show that there is only one slab below the Alps, rather than the two
784 proposed by adherents of a switch in subduction polarity. A switch in the polarity of subduction
785 beneath the Alps can thus be ruled out based on our new data. The notion of only one continuous
786 European slab beneath the Alps was previously advanced by Mitterbauer et al. (2011), with the
787 added observation that this slab is overturned and acquires a northward dip in the Eastern Alps, as
788 also noted in our profiles (Fig. 4). A comparison of profiles across the Eastern Alps between the



789 model of Lippitsch et al. (2003) in Fig. 10A and this work (Fig. 10B) demonstrates the poor fit of the
 790 models and highlights why mantle delamination and slab detachment rather than a change in
 791 subduction polarity are the most recent processes to leave their imprint in the Eastern Alps. The
 792 most striking difference, apart from the length of the slab, is that the detached European slab
 793 according to our model has no connection to the Adriatic lithosphere from which it is separated by
 794 low-velocity upper mantle (Fig. 10B).
 795



796
 797 **Figure 10:** Two tomographic profiles along the trace of profile C (given in inset map) on the same scale: (A)
 798 Lippitsch et al. 2003; (B) this work. Yellow line in (B) is the outline of the slab anomaly in (A). The profiles show
 799 moderate agreement regarding slab detachment beneath the Eastern Alps, but disagreement regarding the dip
 800 and length of the slab anomaly. Our preferred model in (B) provides evidence for delamination of most of the
 801 underpinnings of Adria and Europe beneath the Alps, Adria and Apennines. A direct connection of the NE-dipping
 802 slab beneath the Eastern Alps to the Adriatic lithosphere shown in (A) becomes untenable in light of the new data
 803 presented in (B).
 804

805 The length of the slab measured in profiles varies along strike between 220 and ≥ 500 km,
 806 with even the latter estimates regarded as minima given that in some profiles the positive
 807 anomalies continue below the 410 km discontinuity into the Mantle Transition Zone (e.g., profile 8
 808 in Fig. 3A and profiles 6, 8, A and C in Appendix A). These lengths are not a reliable measure of the
 809 amount of subducted lithosphere, because the slabs appear to be highly deformed and, anyway,
 810 resolution decreases at such depths (Foulger, 2013). Nevertheless, the range of lengths overlaps
 811 with palinspastic estimates of the total width of the Alpine Tethyan domain and its continental
 812 margins subducted between 84 and 35 Ma as measured in a NNW-SSE direction parallel to Adria-



813 Europe convergence (350-400 km, Le Breton et al., 2021; van Hinsbergen et al., 2020; 600 km,
814 Handy et al., 2010). An interesting implication of this overall consistency between subducted and
815 seismically imaged lithosphere is that potentially more of the Alpine subduction is preserved than
816 hitherto thought. Based on earlier teleseismic tomography, Handy et al. (2010) estimated a deficit
817 between subducted and imaged lithosphere of between 10 and 30%, depending on the contour
818 intervals of positive P-wave anomalies used in their areal assessments of positive anomalies.

819 The steep northward dip of the part of the European slab beneath the Eastern Alps must
820 have been acquired after southward subduction of the European tectosphere stopped in this part of
821 the Alps. The youngest exhumed high-pressure rocks that are testimony to an exhumed subduction
822 zone in this part of the Alps are found in the central Tauern Window (Gross et al., 2000) and the age
823 of subduction-related metamorphism is estimated to be around 35-45 Ma (Kurz et al., 2008;
824 Ratschbacher et al., 2004 and refs. therein). A younger age range for this metamorphism was
825 proposed (32-35 Ma, allanite U-Pb, Smye et al. 2011; Lu-Hf, Nagel et al., 2013), but these are
826 inconsistent with evidence for substantial exhumation of high-pressure units before the intrusion of
827 the Periadriatic plutons and the onset of movements along the Periadriatic Fault System
828 (Rosenberg, 2004). The 35-45 Ma age range for HP metamorphism certainly pre-dates indentation
829 of the eastern Southern Alps along the Giudicarie Belt starting at around 23 Ma (Scharf et al., 2013).
830 Hence, roll back and steepening of the European slab, followed by slab detachment and rotation of
831 the detached Eastern Alps slab into a steeply N-dipping orientation most likely occurred sometimes
832 within the 39-23 Ma time interval, most likely at around 23 Ma according to geological evidence
833 (e.g. Scharf et al., 2013). The mechanisms of such rotation and verticalization during opening of the
834 Pannonian backarc behind the subducting European slab beneath the Eastern Carpathians are
835 unclear. The slab might have been twisted while still attached to a descending slab relict beneath
836 the Pannonian basin (profile 5 in Fig. 5B; Dando et al., 2011). However, we favor reorientation of
837 the slab by asthenospheric flow, either during northward Adriatic indentation in Neogene time (e.g.,
838 Ratschbacher et al., 1991; Favaro et al., 2017), or alternatively, during equilibration of the slab after
839 it had detached. The arcuate convex-northward pattern of fast SKS directions beneath the Eastern
840 Alps are suggestive of east-directed asthenospheric flow (e.g., Qorbani et al., 2015) and would be
841 consistent with both of these interpretations.

842
843

844 6.2 Slab attachment and detachment

845 An intact slab dipping down to a depth of 300 km and beyond is only observed beneath the Western
846 to Central (Swiss-Italian) Alps between latitudes 7°E and 10°E (see area marked as un-detached in
847 Fig. 8; profiles 6 and 9 in Appendix A. Interestingly, Singer et al. (2014) noticed that lower crustal
848 seismicity in the European tectosphere is restricted to this same range of latitudes. They proposed
849 that this deep crustal seismicity is driven by stresses transferred to the foreland from the still-
850 attached segment of the European slab, which they argue is steepening as it retreats toward the
851 foreland. Kissling and Schlunegger (2018; their fig. 5c) present a schematic 3-D diagram of this
852 remaining undetached European slab, arguing that such slab retreat during attachment is
853 responsible for the striking isostatic disequilibrium between the low surface topography and the
854 thick crustal root (some 50 km, e.g., Spada et al. 2013) found beneath this segment of the Alps.

855 Complete delamination during the advanced stages of detachment of the European
856 tectosphere occurred in the Eastern Alps and resulted in a broad zone of low-velocity mantle
857 interpreted to be caused by upwelling mantle (Fig. 9), typically at a depth between 70km and 130
858 km (e.g., profile 15 in Fig. 5A) east of 12°E (i.e., east of the western Tauern Window, Fig. 1). East of
859 15° E no substantial remnants of the European slab are found above the 410 km discontinuity (Fig. 8



860 and profiles 5, 11, 10 in Appendix A). This conforms with the findings of Dando et al. (2011) and
861 indicates that roll back in the Carpathians followed by detachment of the European slab played a
862 fundamental role during the formation of the greater Pannonian area (Horvath et al., 2006;
863 Matenco and Radivojević, 2012). West of the Tauern window, between 12° and about 9.5°E
864 traversed by profile B (Fig. 3C), detachment is only moderate. A third area in the Alps where
865 substantial detachment occurs is the southern part of the Western Alps (profiles 8 in Fig. 3A, and A
866 in Appendix A) that is transitional to the northern Apennines. Such detachment was first noticed by
867 Lippitsch et al (2003; their profile A-A'), but recently refuted by Zhao et al. (2016). There, the
868 detached European slab of the Alps slab resides beneath the westernmost Apennines at a depth of
869 240 km, while upwelling mantle occupies the area beneath the Western Alps at this same depth
870 (Fig. 8).

871 The completely detached slab beneath most of the Northern Apennines (except for the
872 westernmost parts) hangs subvertically (profiles 11 and 12 in Fig. 6; profile C in Appendix A),
873 confirming the findings of Giacomuzzi et al. (2011, 2012) from teleseismic tomography. A clear
874 boundary between the European slab under the westernmost Apennines and the delaminated
875 Adriatic mantle lithosphere of the Northern Apennines slab cannot be resolved in the horizontal
876 depth slices, but is evident in profiles (e.g., Fig. 3A), where we interpret the boundary between the
877 two slabs to coincide with the Alpine Tethys suture.

878
879

880 6.3 Nature of low velocity domains in the greater Alpine area

881 In text and profiles above, we interpreted low V_p areas within the greater Alpine area as resulting
882 from upwelling mantle material, while low V_p areas at the base of European tectosphere reflect
883 compositional differences inherited Variscan or pre-Variscan features rather than present enhanced
884 temperature. This raises the question if the younger low V_p volumes attributed to asthenospheric
885 upwelling during Alpine orogeny still represent volumes of substantially elevated temperatures
886 today. In view of the fact that water content and other features besides temperature generally are
887 the most important factors influencing seismic wave velocities in the mantle (Karato and Jung,
888 1998; Shito et al., 2006) we propose that at least in the case of the Veneto volcanic province (Fig. 8)
889 temperature is unlikely to be the dominant factor, especially given that present-day heat flow in the
890 Adriatic region is low (Giacomuzzi et al., 2011).

891
892

893 6.4 Timing of slab detachment and its consequences

894 A rough estimate of the time since slab detachment in the Eastern Alps can be obtained from the
895 average sink rate of slabs around the world (12 mm/a, van der Meer et al., 2010, 2018). The rate is
896 derived from a compilation of teleseismically imaged slabs of known lengths and ages that are still
897 attached to their lower plate lithospheres, mostly in Circum-Pacific convergent zones. When applied
898 to the Eastern Alps where the slabs are detached (Figs. 4 and 6), this approach yields minimum
899 values of the time since detachment. They range from 10 to 25 Mas, respectively, beneath the
900 Eastern Alps and the Pannonian Basin. The 10-25 Ma time range since slab detachment
901 encompasses the period of orogen-parallel extension and rapid exhumation and lateral escape in
902 the Tauern Window (23-11 Ma, e.g., Scharf et al., 2013) and overlaps with the duration of extension
903 in the Pannonian Basin (21-15 Ma, Horvath et al., 2015 and references therein). This supports our
904 suggestion that slab detachment and asthenospheric upwelling were instrumental in triggering
905 decoupling that enabled Neogene orogen-parallel lateral extrusion of the ALCAPA tectonic
906 megaunit (upper plate crustal edifice of Alps and Carpathians) towards the Pannonian Basin. This



907 raises questions about the depth of detachment at the base of the ALCAPA megaunit during its
908 lateral extrusion and the nature of the Moho beneath the Pannonian Basin. Horvath et al. (2015)
909 proposed that during lateral extrusion the extending crust of the ALCAPA megaunit could directly
910 overlay the hot asthenosphere of the Carpathian embayment and that since then, most of the
911 Pannonian Basin cooled, allowing a new mantle lithosphere to grow. If correct, this would imply
912 that the Moho imaged beneath the Pannonian basin is of Miocene or younger age.

913 An intriguing aspect of Adriatic indentation and Alpine slab detachment is their potential
914 effects on the fore- and hinterland basins of the Alps. The 25-10 Ma time window for slab
915 detachment brackets the time when thrusting in the eastern Molasse basin stopped advancing (21-
916 22 Ma) and changed from in-sequence to out-of-sequence (wedge-top) mode (Hinsch, 2013). It also
917 includes the time when the basin rapidly filled with terrigenous components at 19-18 Ma (Grunert
918 et al., 2013), leading to a shift in the paleo-drainage direction from eastward to northwestward
919 (Kuhleemann and Kempf, 2002). Subsequent uplift and erosion of the entire Molasse Basin at 10 to 5
920 Ma (Cederbom et al., 2011) was greater in the E (0.3-0.5 km) than the W (0.5-1.5 km, Baran et al.,
921 2014). These first-order orogen-parallel variations in foreland basin fill and erosion may be related
922 to the degree of slab attachment, with full attachment in the Central Alps lengthening the flexural
923 response of the foreland to slab loading, whereas complete slab detachment and delamination in
924 the east after 25-20 Ma (Handy et al., 2015) favored a very rapid decrease in basin depth (Genser et
925 al., 2007). This period at 23 Ma coincided with the aforementioned onset of rapid exhumation in the
926 Tauern Window (Fügenschuh et al., 1997) and eastward escape of the Eastern Alps into the
927 Pannonian Basin in the upper plate of the retreating Carpathians (Ratschbacher et al., 1991; Scharf
928 et al., 2013).

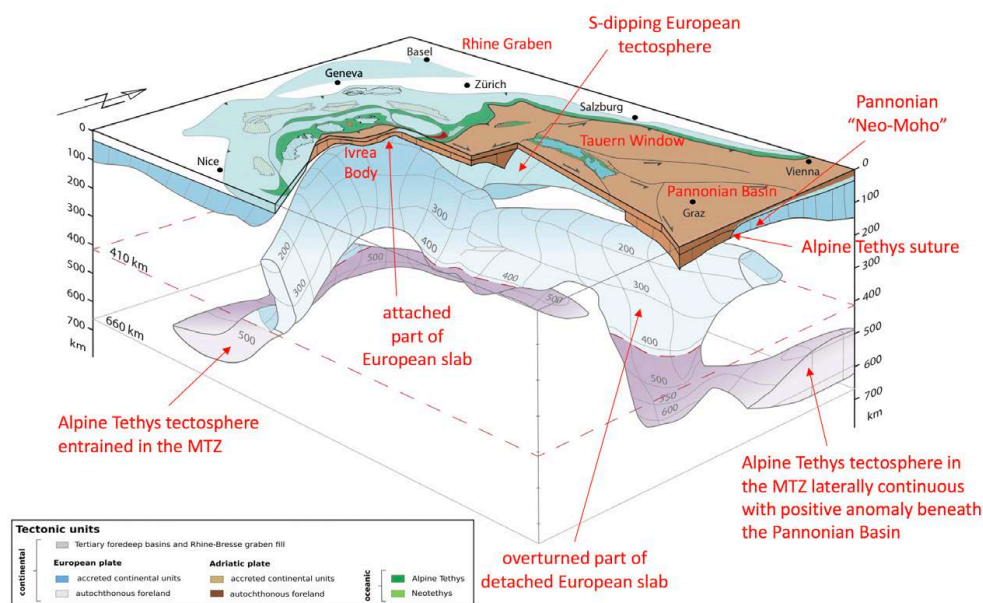
929 Finally, a rather vexing consequence of the calculations above is that the 25-10 Ma time window
930 for slab detachment is far younger than the 34-28 Ma age range of the Periadriatic calc-alkaline
931 intrusive suite along the Periadriatic Fault (e.g., Rosenberg, 2004), which has been attributed to slab
932 breakoff (von Blanckenburg and Davies, 1995). Either our estimates of detachment times above are
933 based on questionable assumptions and the time since detachment was far longer than 25 Ma, or
934 calc-alkaline magmatism with a lithospheric mantle component reflects deep-seated processes
935 other than slab breakoff. We note that the calc-alkaline intrusives occur all along the Periadriatic
936 Fault, extending from the Western Alps to the Mid-Hungarian Fault Zone in the Pannonian Basin
937 (Fig. 1). Its lateral extent (7.5-19°E, Fig. 1) is thus far beyond the narrow corridor of slab attachment
938 between 7-10°E (Fig. 8), suggesting that the detachment observed in this study had little, if
939 anything, to do with Periadriatic magmatism.

940
941

942 **7. Conclusions**

943 The exciting images presented here resolve some long-standing debates while compelling us to
944 reassess the role of plate structure in mountain-building. Figure 11 is a graphic attempt to visualize
945 the complex 3-D geometry of mantle structure in the area covered by AlpArray. This figure is a
946 composite view of the Alps seen from the SE, i.e., from a vantage point above the Dinarides, with
947 the Adriatic Plate removed to reveal the slabs. The slabs and foreland structures were constructed
948 from the interpreted outlines in the 18 profiles in Appendix A.

949



950
951

Figure 11: 3D-sketch of the slab beneath the Alps as viewed from the southeast. Slab geometry based on projections of all vertical tomographic profiles in Appendix B. Tectonic map of the surface is simplified from maps of Schmid et al. (2004) and Schmid et al. (2008).

952
953
954
955

A prime outcome of this study is that the European and Adriatic Plates involved in Alpine collision have first-order differences in structure and composition: the downgoing European tectosphere is thick (150-180 km) and comprises compositional heterogeneities that are marked by strong positive and negative P-wave anomalies. These are believed to be of inherited Variscan or pre-Variscan features. In the Central (Swiss-Italian Alps), they descend as part of a coherent slab from the Alpine foreland to beneath the Northern Alpine Front. In contrast, the Adriatic Plate is thinner (100-120 km) and has a poorly defined base at the lower boundary of $+V_p$ anomalies. The underlying negative anomaly in the depth interval of 120-270 km is attributable partly to compositional effects (e.g., mantle hydration due to upwelling fluids from the Alpine slab) and partly to upwelling asthenosphere in the aftermath of slab detachment in the Alps and Apennines.

956
957
958
959
960
961
962
963
964
965

This fundamental difference in the structure of the lower and upper plates may be responsible for two of the most striking features of the Alps compared to other Alpine-Mediterranean orogens, namely the rugged, high altitude Alpine topography and the disproportionately large amount of accreted, deeply subducted and exhumed lower-plate units exposed in the deeply eroded core of the Alps (Fig. 11). Thick tectosphere is expected to be relatively stiff and buoyant upon entering collision, favoring tectonic underplating of accreted and subducted tectonic units as subduction proceeds. By comparison, "normal" lithosphere, as found in the Adriatic Plate and its slab beneath the Apennines, is expected to sink more easily under its own weight, favoring roll-back subduction, the development of low topography and upper plate extension with only limited exhumation of subducted units.

966
967
968
969
970
971
972
973
974
975

Another new outcome of this study is the widespread delamination and detachment of slabs observed in both the Alps and the Apennines. Detachment is complete in the southwesternmost Alps, and on a much larger scale, in the Eastern Alps (Fig. 11) and Western Carpathians. There, relicts of European tectosphere hang at various depth intervals, with generally greater depths

976
977
978
979



980 towards the east extending down to the MTZ beneath the Pannonian Basin. The response of the
981 mantle to delamination of the European tectosphere and downward motion of detached slabs since
982 at least 25 Ma has been large-scale upwelling of asthenosphere. The asthenosphere above
983 delaminated areas occupies very shallow depths, in some cases immediately below the Moho
984 marking the base of thinned Alpine orogenic crust, which was stretched in Neogene time during
985 lateral orogenic escape and upper-plate extension of the Pannonian Basin.

986 In this study, we claim to have resolved the debate over the polarity of Alpine subduction
987 beneath the Eastern Alps in favor of the model of a single European slab that originally subducted to
988 the south. The presently steep, northward dip of the Eastern Alps slab segment (Fig. 11), which gave
989 rise to the alternative view of Adriatic subduction in the first place, is clearly a secondary feature
990 acquired during or after slab detachment.

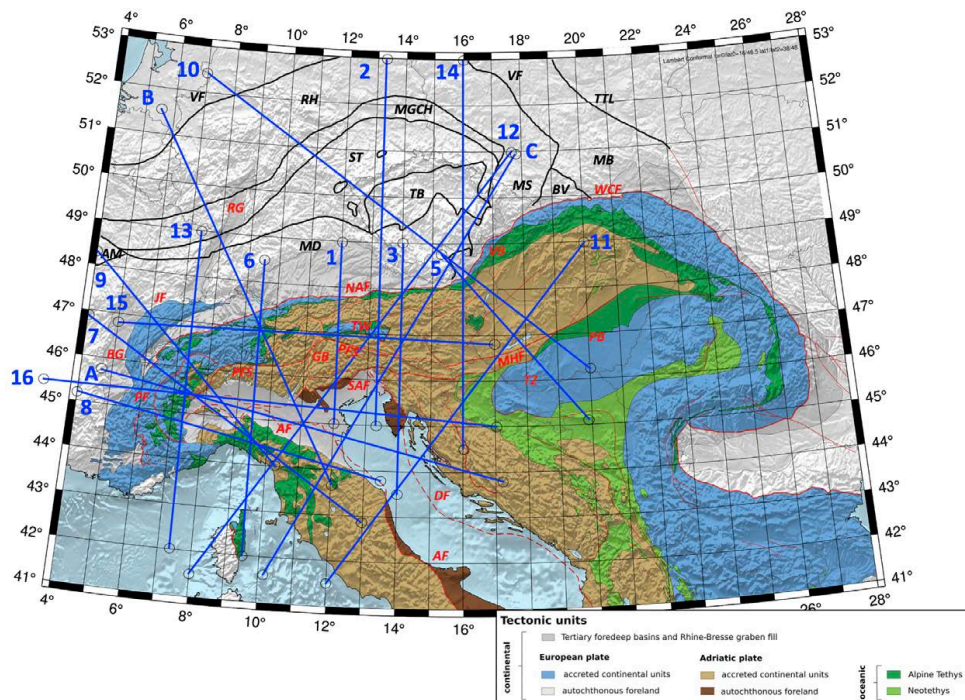
991 A lesson learned in collating and interpreting this extraordinary data set has been that, after
992 initially acquiring and processing seismological data, methodological development and tectonic
993 interpretation must go hand-in-hand if they are to yield a meaningful, testable model. Figure 11 is
994 an initial model of tectonic boundaries based on a qualitative assessment of both positive and
995 negative anomalies in a plate kinematic context. The next step is obviously to parameterize this
996 model in order to compare it with independent sources of data and determine its thermo-
997 mechanical characteristics.

998
999

1000 Appendices

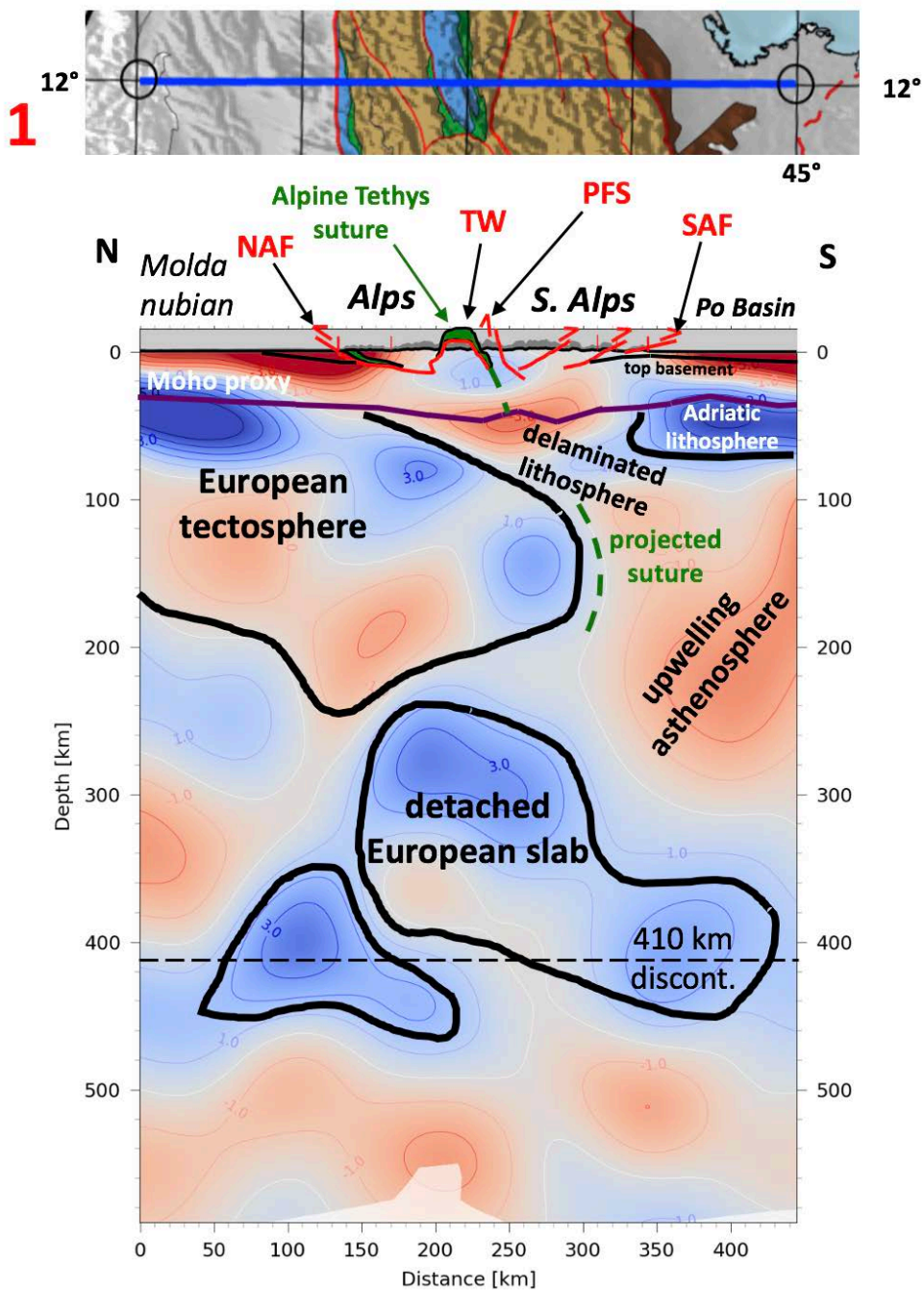
1001 A. Profiles used in interpretations

1002

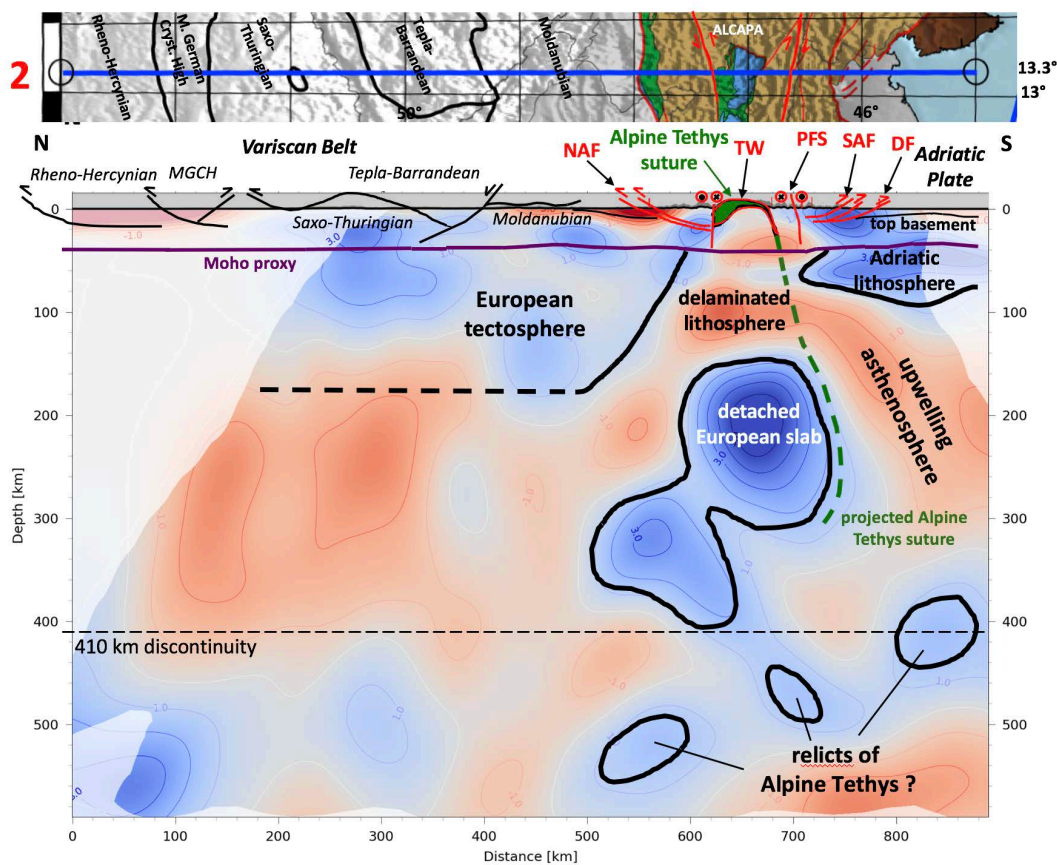


1003
1004
1005

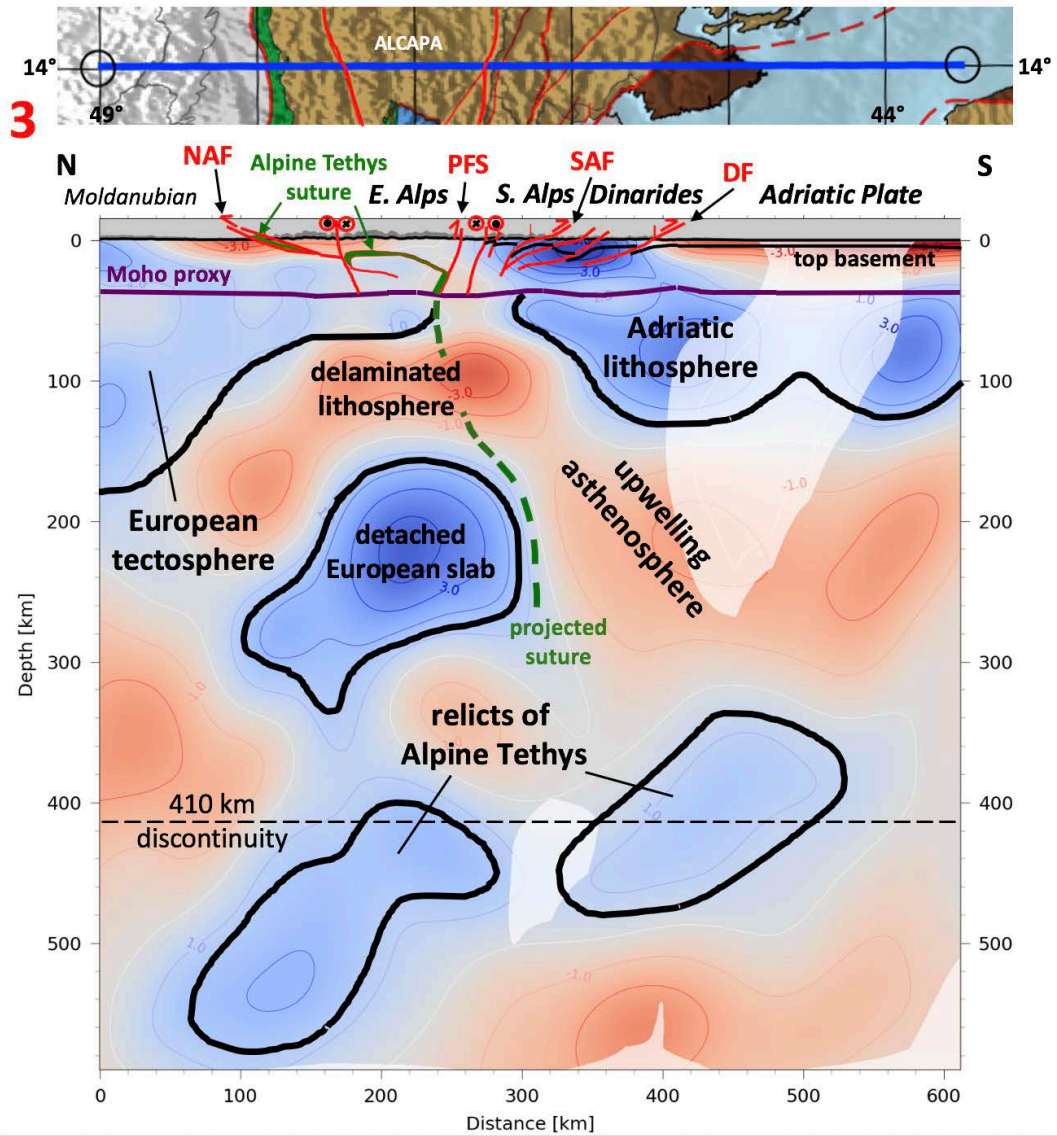
Fig. A0 Tectonic map with traces of all tomographic profiles used in this study



1006
1007 Fig. A1 Profile 1

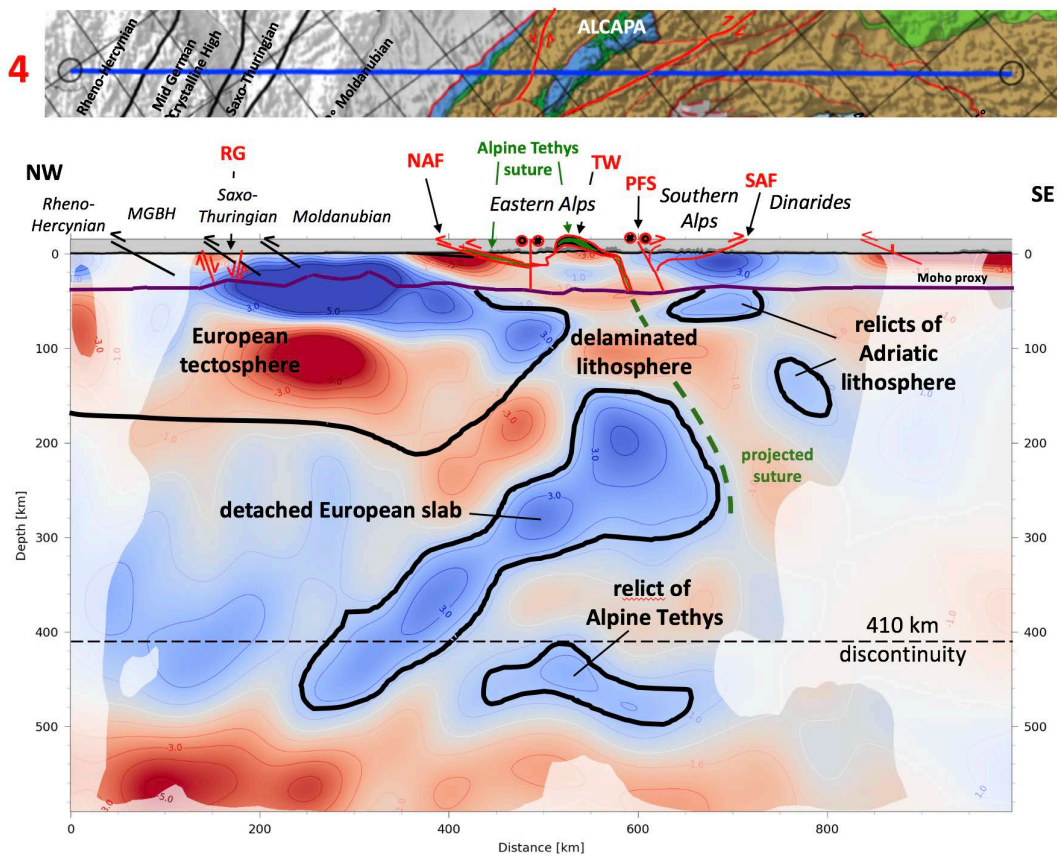


1008
 1009 Fig. A2 Profile 2

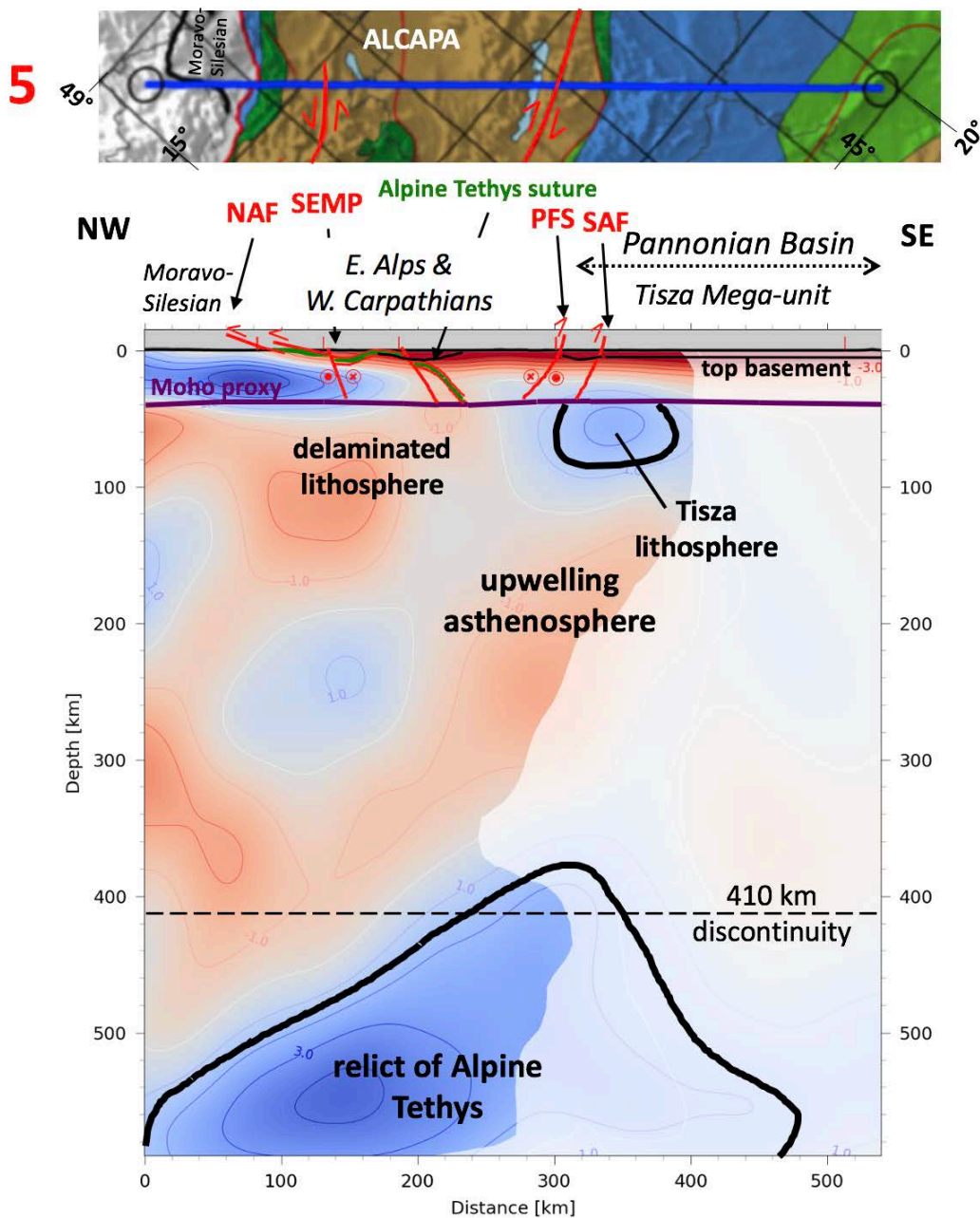


1010
 1011

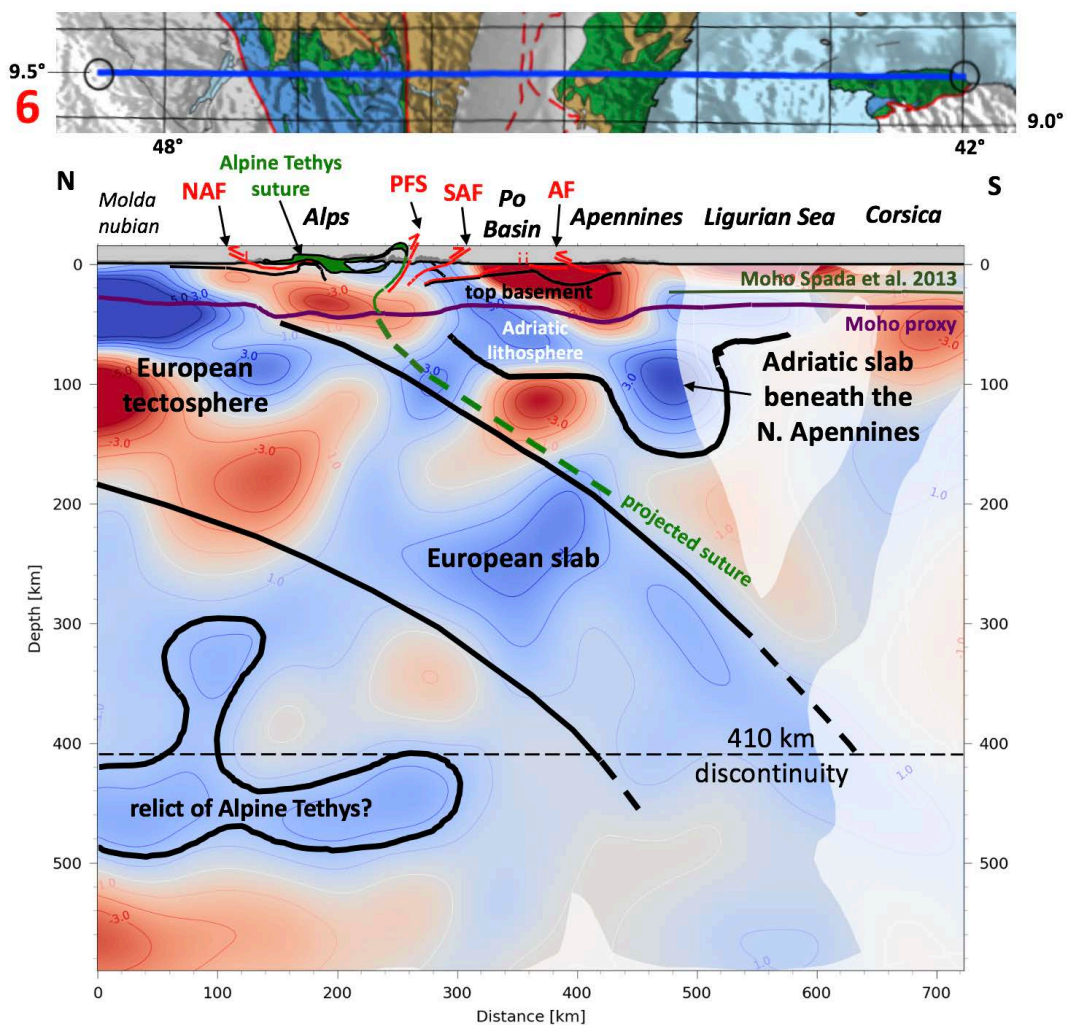
Fig. A3 Profile 3



1012
 1013 Fig. A4 Profile 4

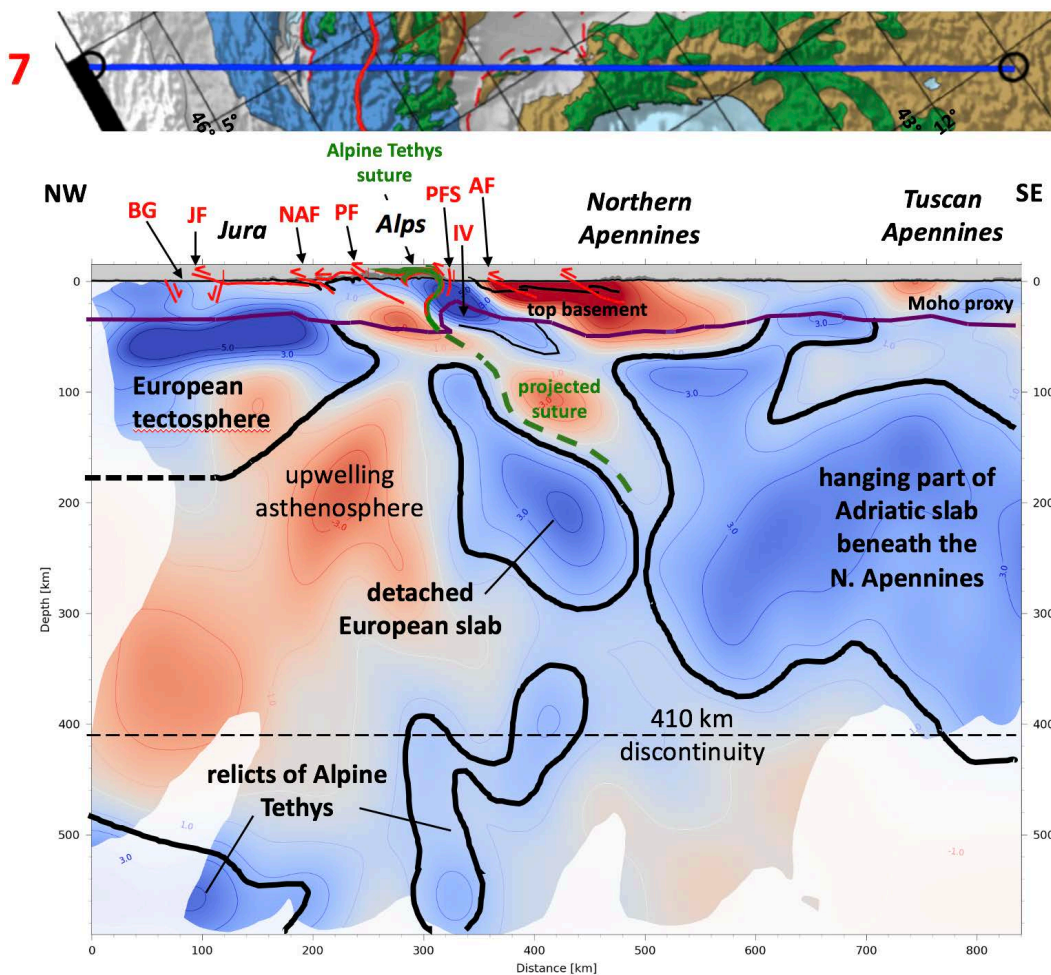


1014
 1015 Fig. A5 Profile 5

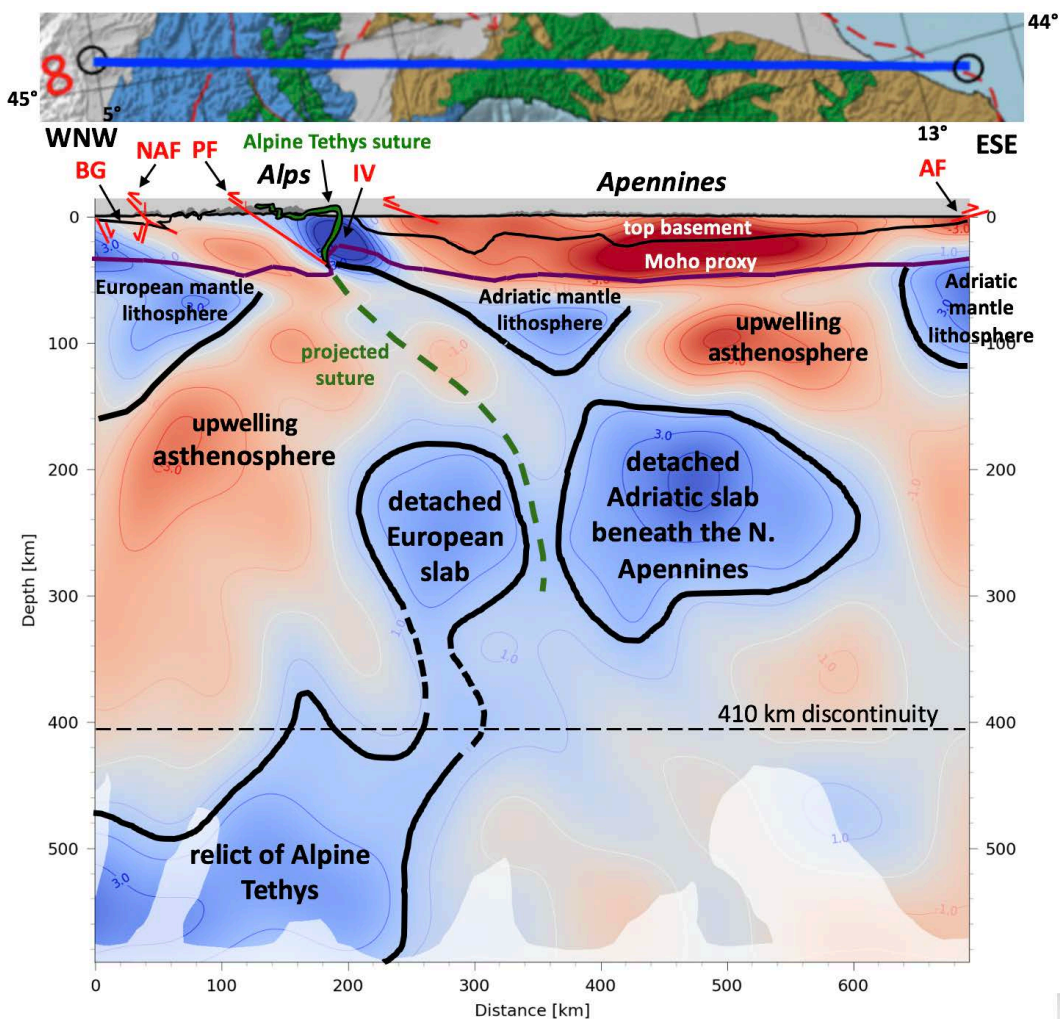


1016
1017

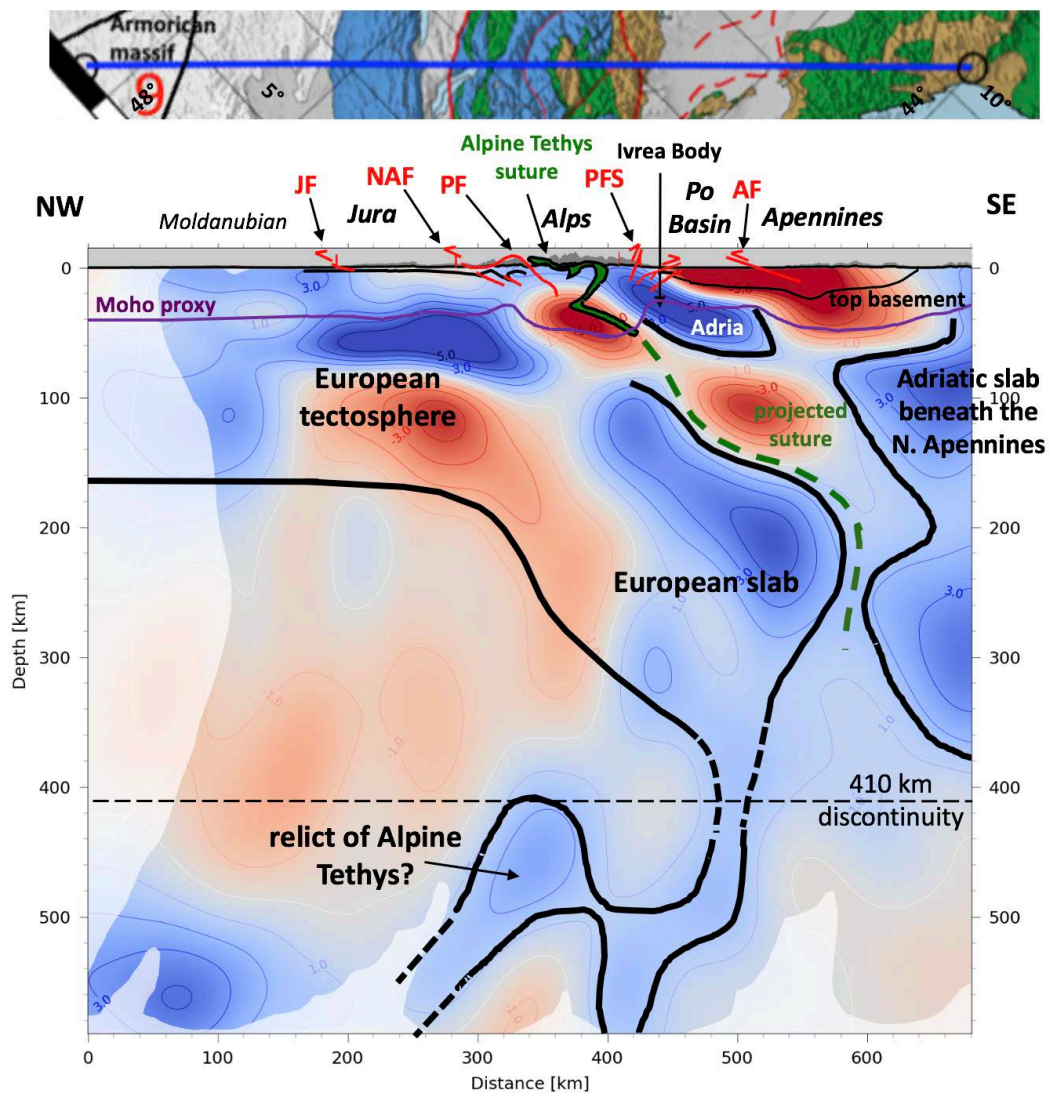
Fig. A6 Profile 6



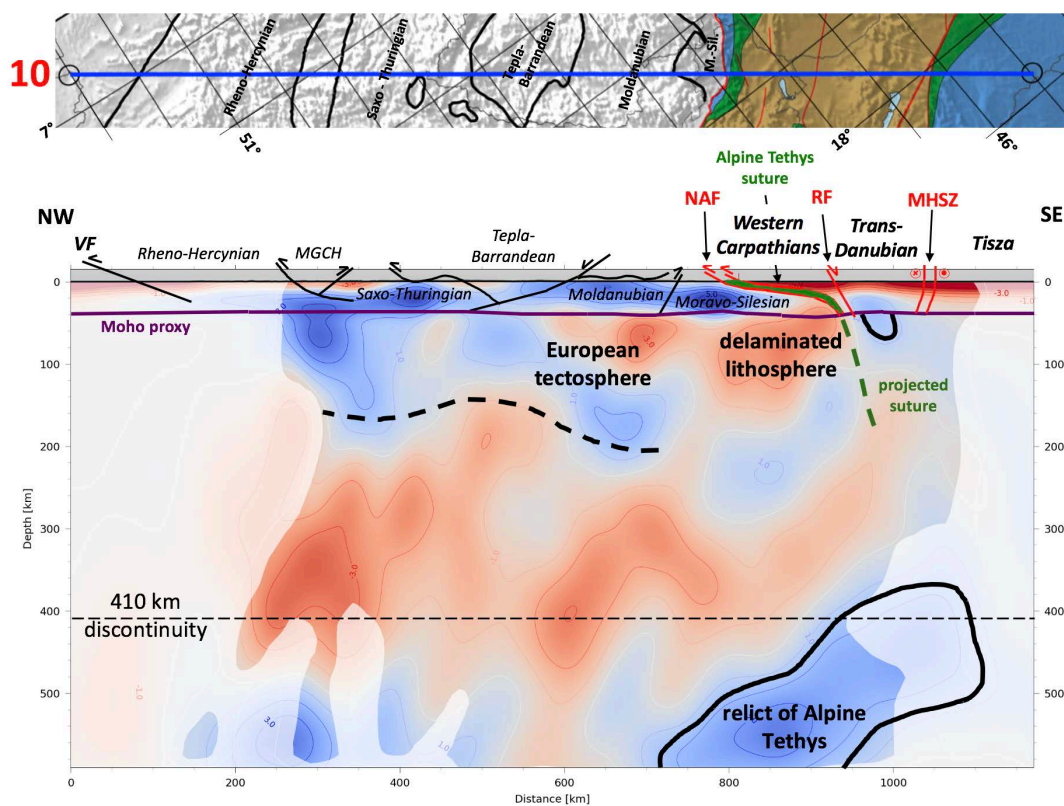
1018
 1019 Fig. A7 Profile 7



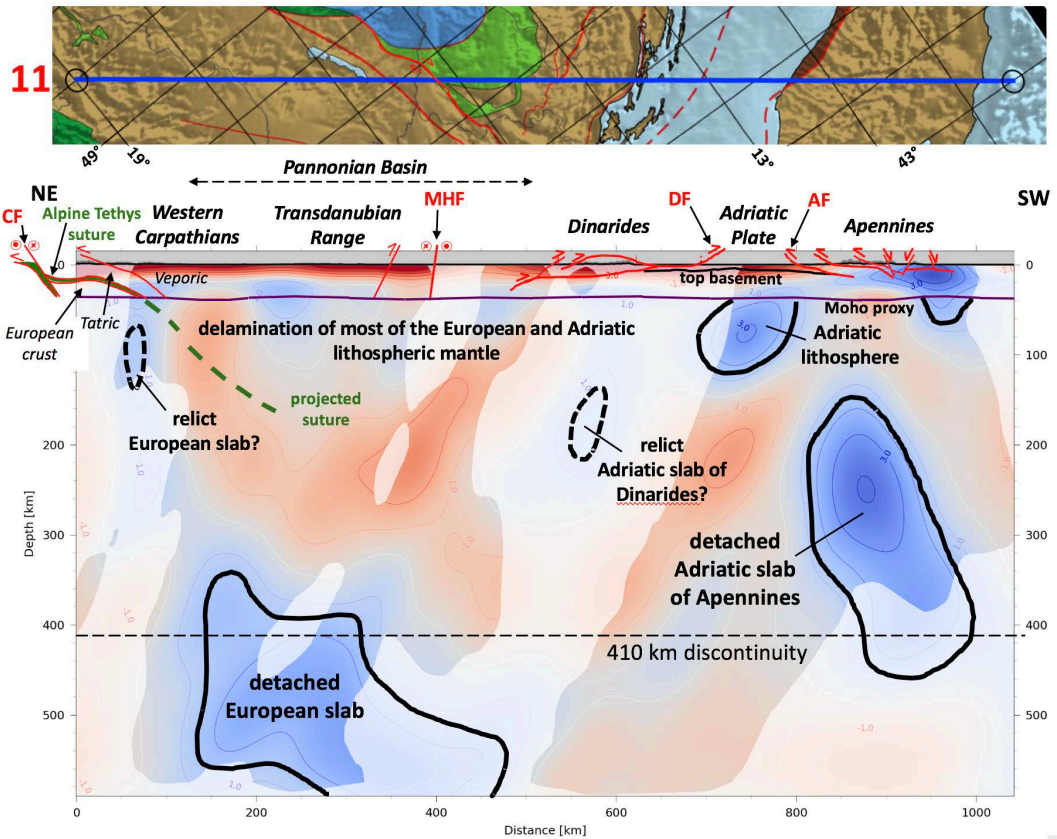
1020
 1021 Fig. A8 Profile 8



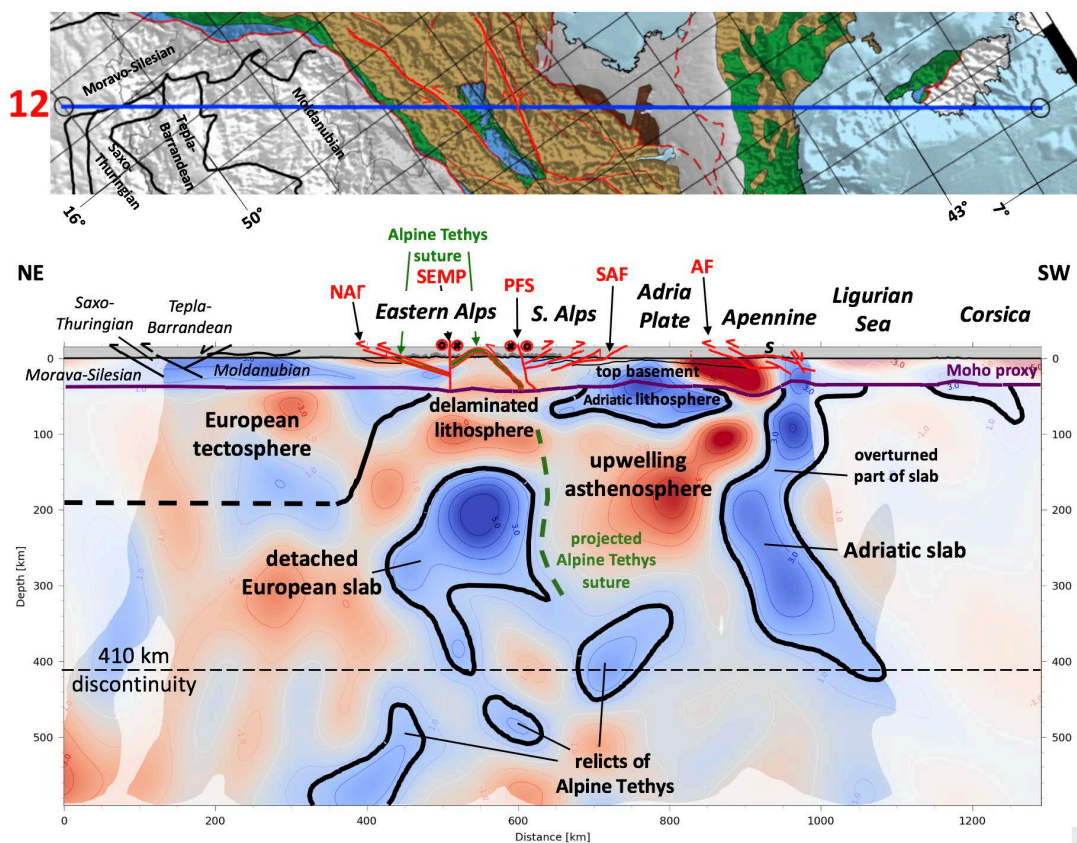
1022
 1023 Fig. A9 Profile 9



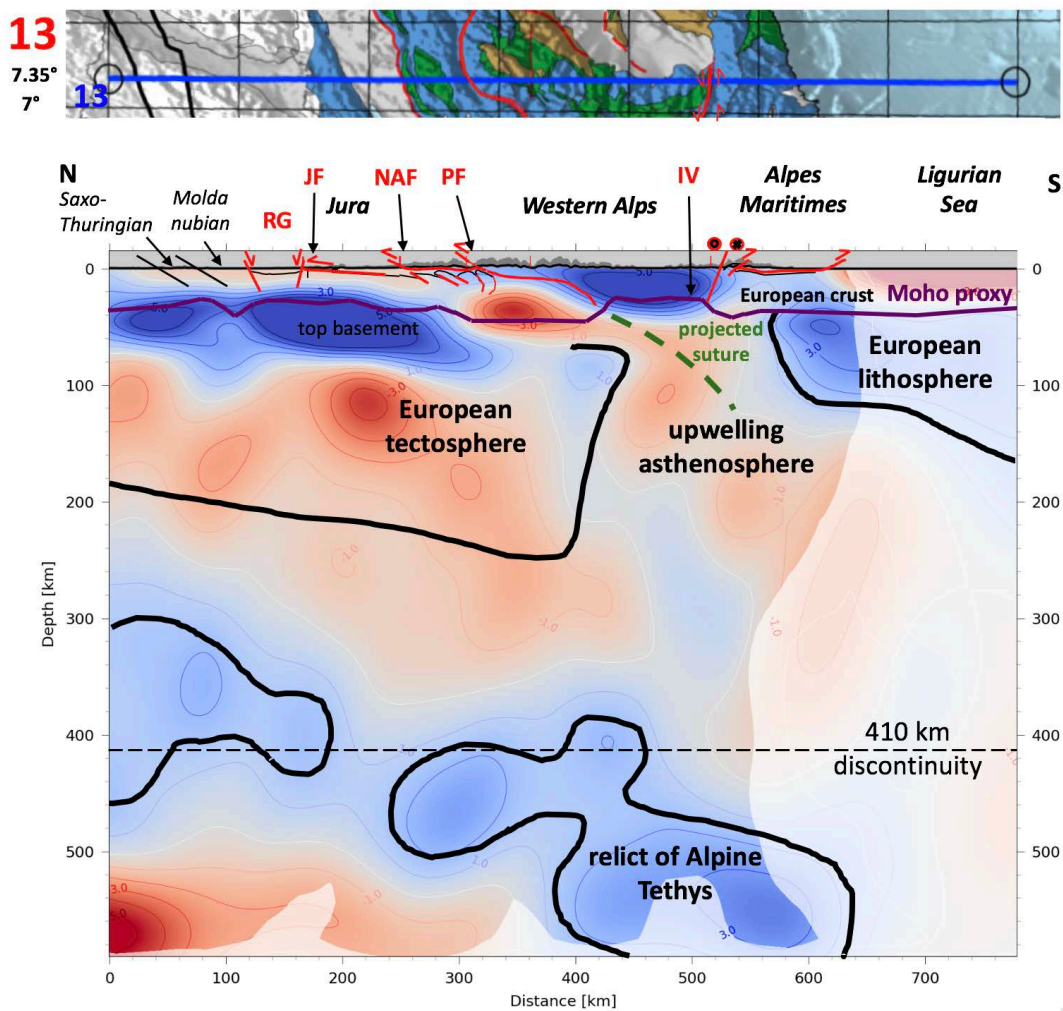
1024 Fig. A10 Profile 10
 1025



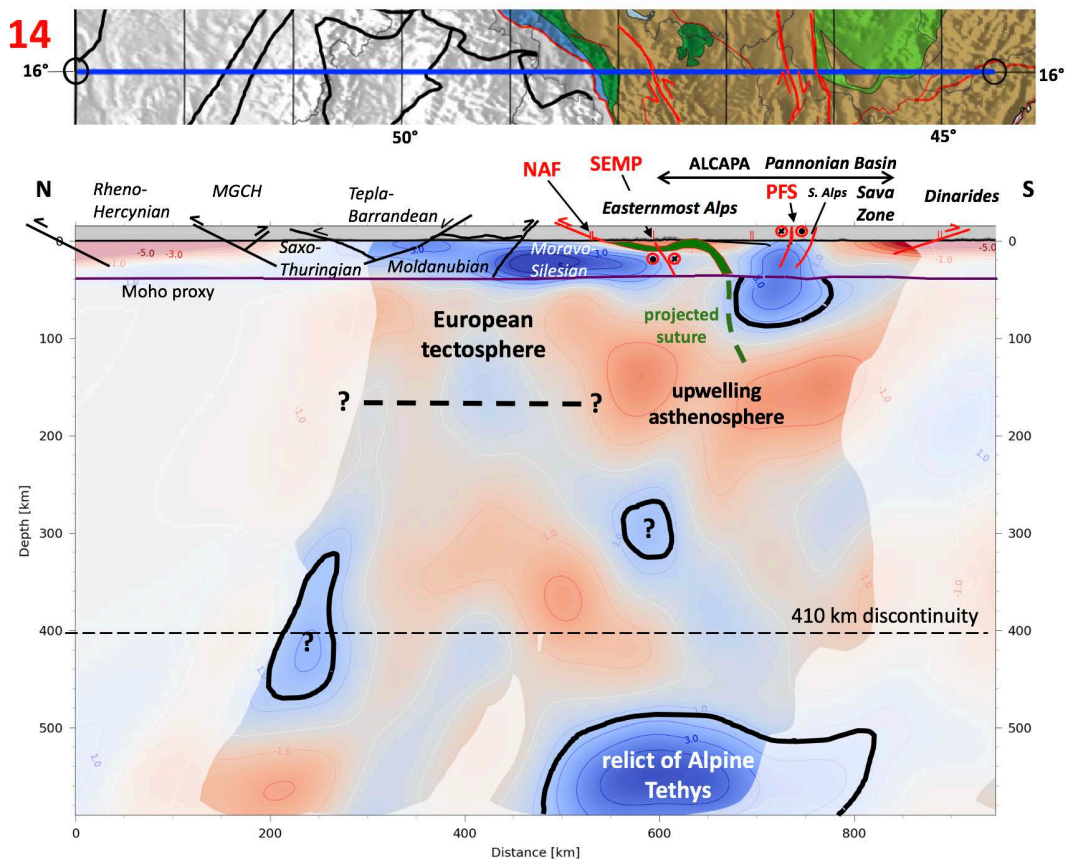
1026
 1027 Fig. A11 Profile 11



1028
 1029 Fig. A12 Profile 12

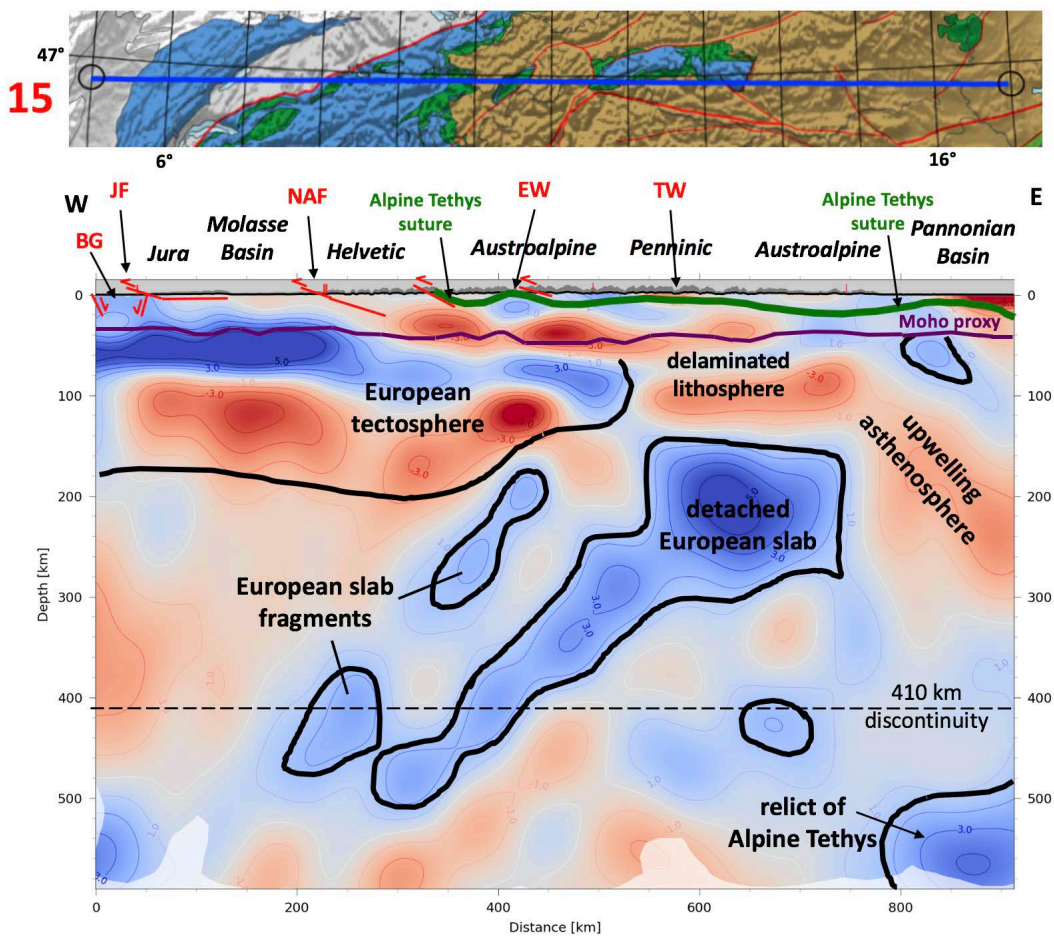


1030
1031 Fig. A13 Profile 13

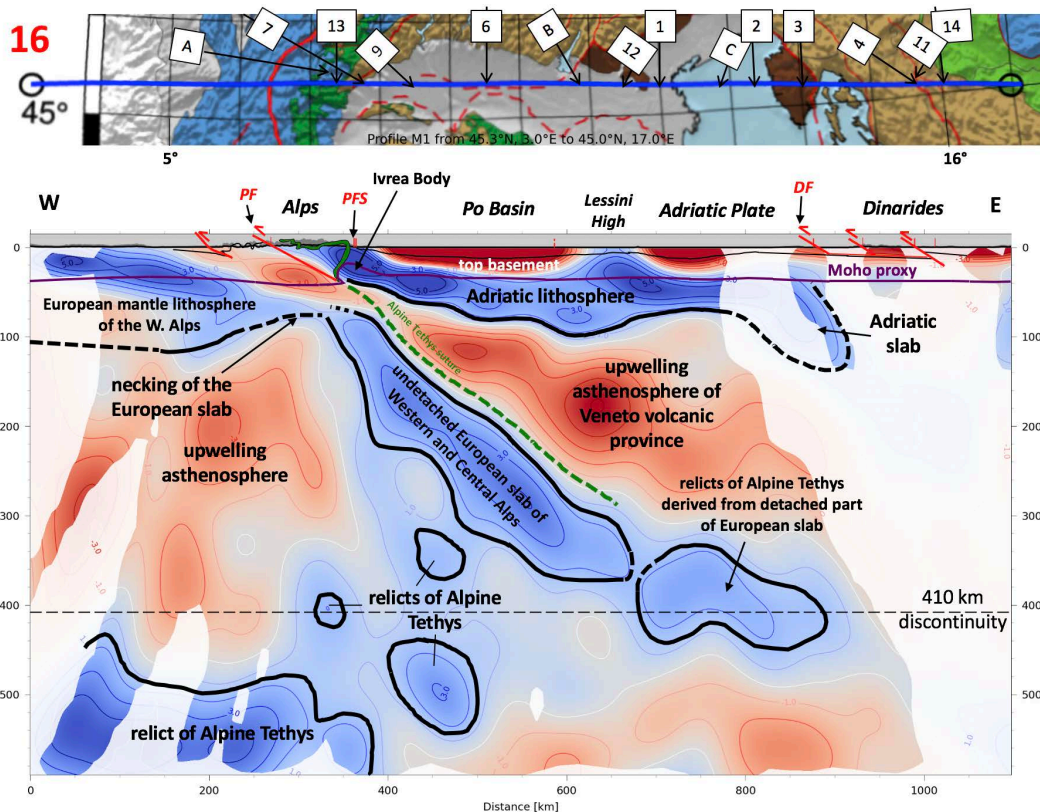


1032
 1033

Fig. A14 Profile 14

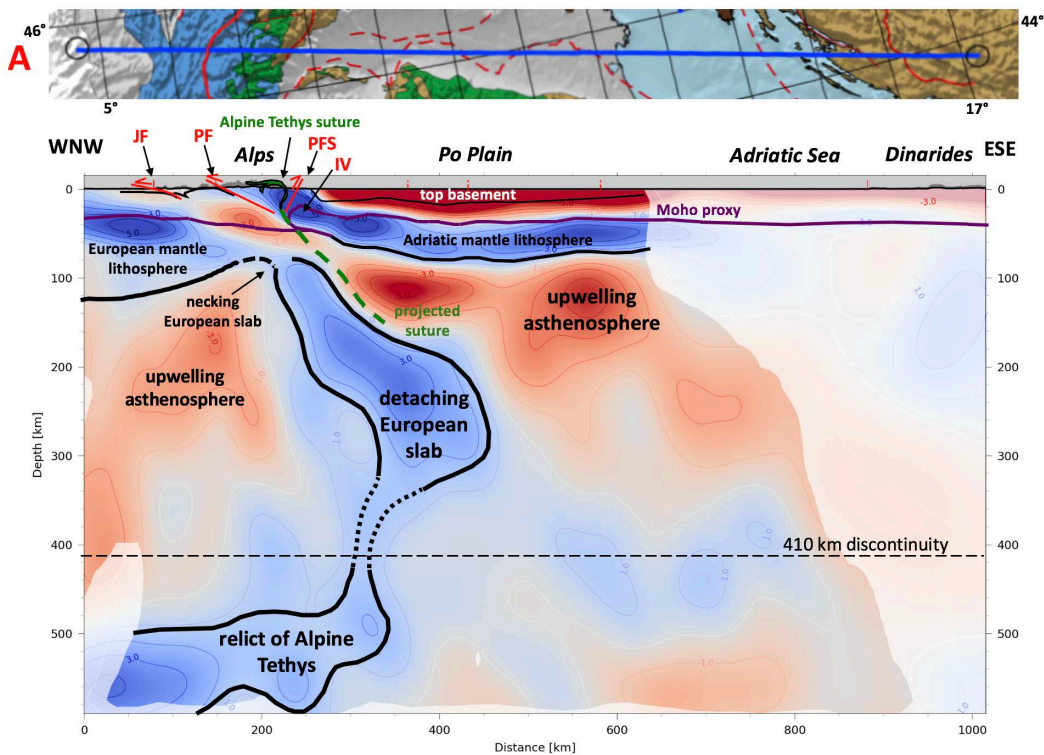


1034
 1035 Fig. A15 Profile 15

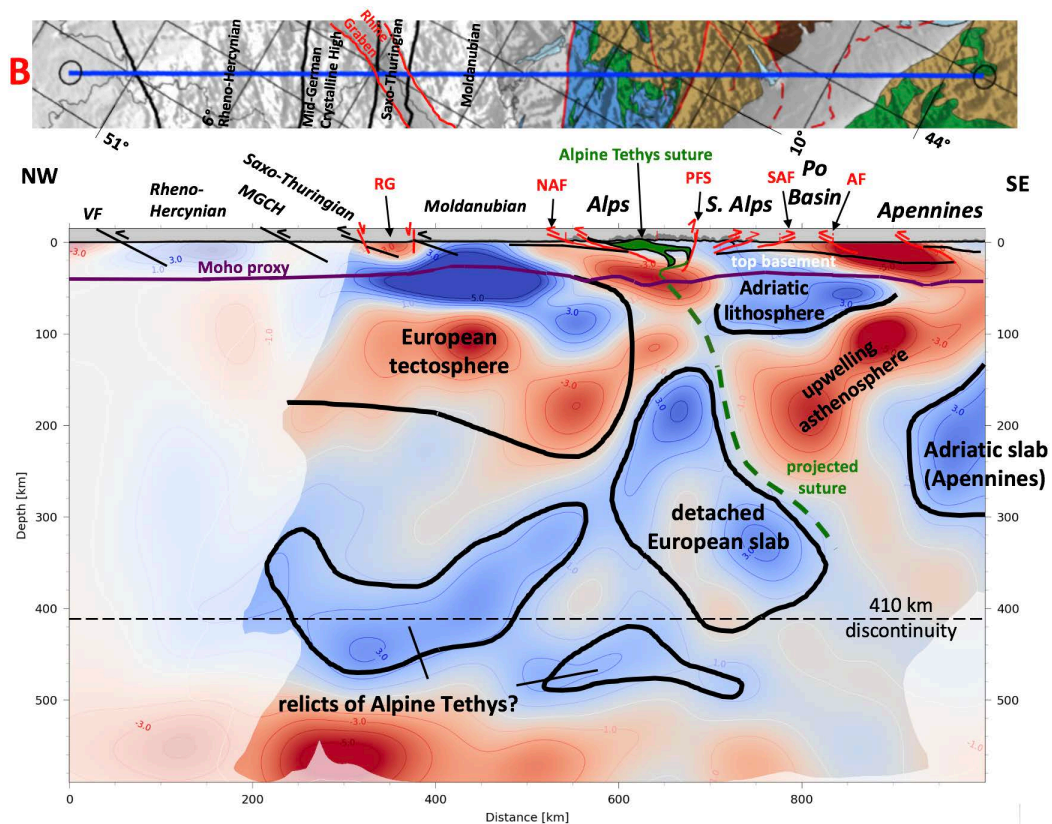


1036
 1037

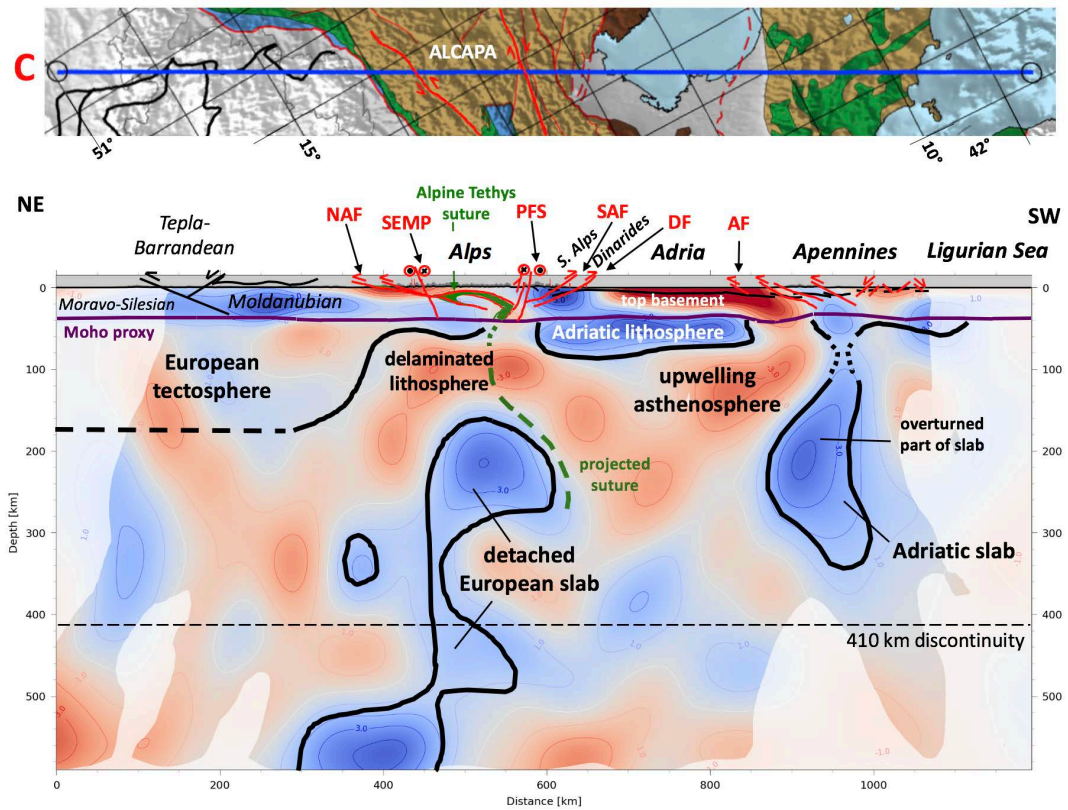
Fig. A16 Profile 16. Numbered labels at top indicate intersecting profiles



1038
1039 Fig. A17 Profile A



1040
 1041 Fig. A18 Profile B

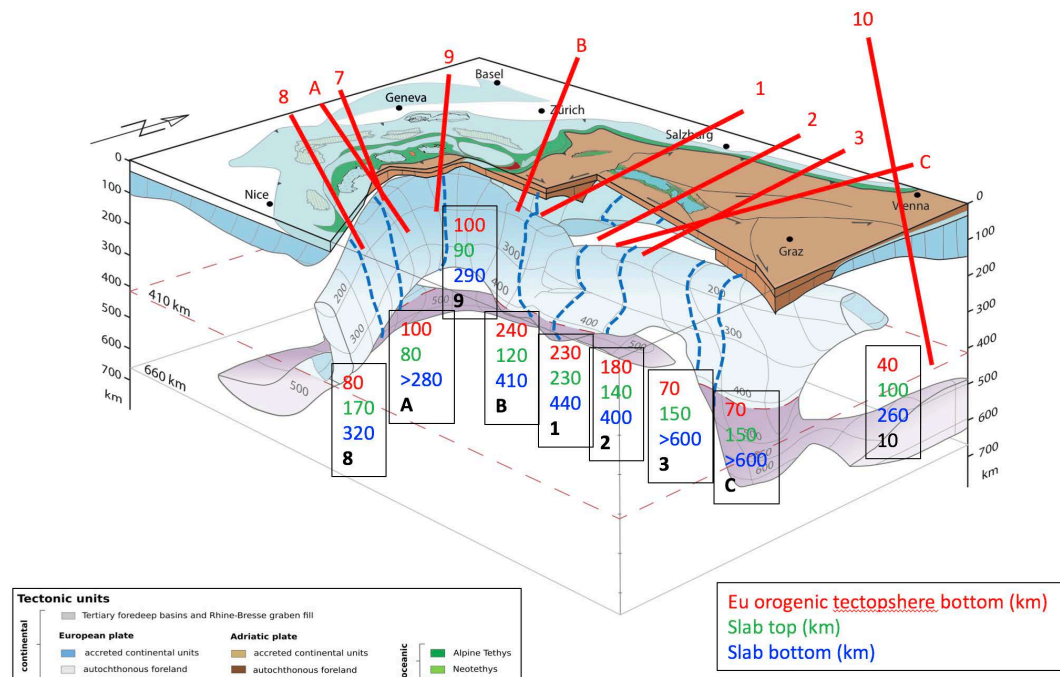


1042
 1043
 1044
 1045

Fig. A19 Profile C



1046 3D-slab image
 1047

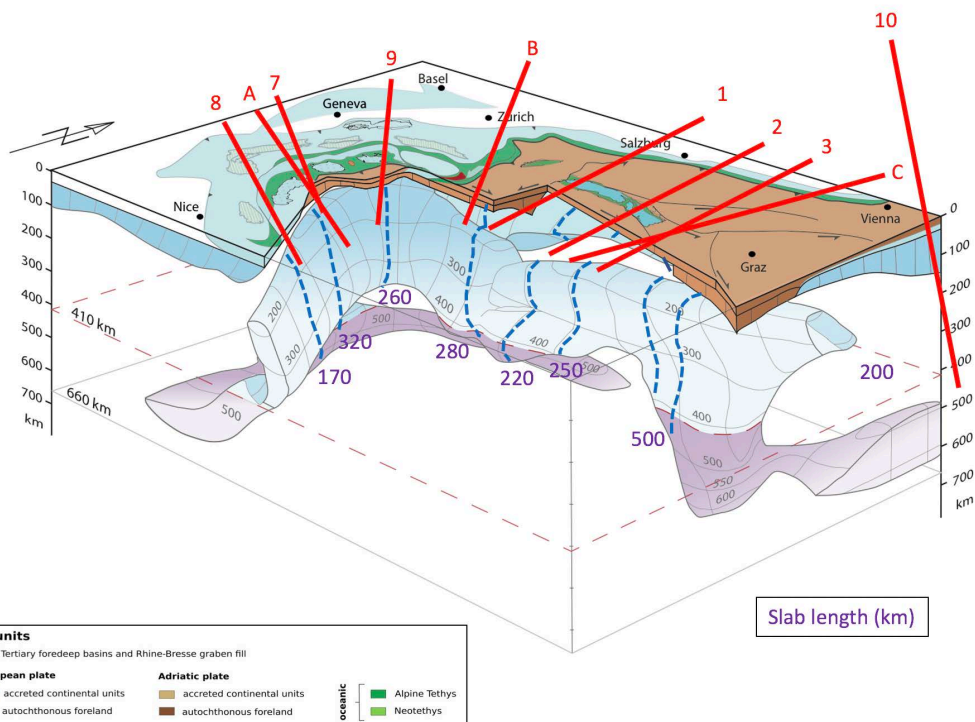


1048
 1049
 1050

Fig. B1 3D block diagram with depths to slab tops and bottoms



1051



1052
1053
1054
1055
1056
1057
1058
1059
1060
1061

Fig. B2 3D block diagram with slab lengths



1062 **Team List**

- 1063 1. Mark R. Handy - Institut für Geologische Wissenschaften, Freie Universität Berlin, Malteserstr.
1064 74-100, 12249 Berlin, Germany; Institut für Geologie, ETH-Zürich, Sonneggstr. 5, 8092 Zürich
1065 2. Stefan M. Schmid - Institut für Geophysik, ETH-Zürich, Sonneggstr. 5, 8092 Zürich
1066 3. Marcel Paffrath - Institut für Geologie, Mineralogie, Geophysik, Ruhr-Universität Bochum, 44780
1067 Bochum, Germany
1068 4. Wolfgang Friederich - Institut für Geologie, Mineralogie, Geophysik, Ruhr-Universität Bochum,
1069 44780 Bochum, Germany
1070 5. AlpArray Working Group: [http://www.alparray.ethz.ch/en/seismic_network/backbone/data-](http://www.alparray.ethz.ch/en/seismic_network/backbone/data-policy-and-citation/)
1071 [policy-and-citation/](http://www.alparray.ethz.ch/en/seismic_network/backbone/data-policy-and-citation/).

1072

1073 **Author contributions**

1074 Mark Handy and Stefan Schmid interpreted the tomographic profiles and slices that were provided in
1075 raw form by Marcel Paffrath. The latter co-author and Wolfgang Friederich provided methodological
1076 insights that are relevant to the interpretations. Mark Handy conceived of and prepared the
1077 manuscript with contributions from all co-authors.

1078 **Competing interests** – Mark Handy is a member of the editorial board of this special issue

1079 **Disclaimer** - none

1080 **Special Issue Statement** – this manuscript has been submitted for inclusion in the special issue „New
1081 insights on the tectonic evolution of the Alps and the adjacent orogens“

1082

1083 **Acknowledgements**

1084

1085 We acknowledge the generous funding of the German Science Foundation. (DFG) in the form of
1086 Special Priority Program 2017 “Mountain-Building in Four-Dimensions (4D-MB). This is an arm of the
1087 European “AlpArray” project, which involved the following subprojects: Ha-2403/22-1, Ha-2403/23-1,
1088 Ha-2403/24-1 and FR 1146/12-1. We thank our colleagues in AlpArray for discussions on various
1089 topics, some who were only marginally related to this paper, but all of whom provided a stimulating
1090 research background for the ideas presented here: Tobias Diehl, György Hetényi, the late Frank
1091 Horvath, Rainer Kind, Edi Kissling, Eline Le Breton, Frederick Link, Thomas Meier, Jan Pleuger, Georg
1092 Rumpker, Wim Spakman, Frederik Tilmann, Claudia Piromallo, Jean-Mathieu Nocquet, Nicola
1093 d’Agostino, , Anne Bernhardt, Vincent Verwater, Philip Groß, Julian Hülscher. A complete list of
1094 members of the AlpArray Working Group can be found here:
1095 http://www.alparray.ethz.ch/en/seismic_network/backbone/data-policy-and-citation/.

1096

1097

1098

1099



1100 **References**

- 1101
- 1102 Agard, P., and Handy, M.R.: Ocean subduction dynamics in the Alps, in: Shedding Light on the
1103 European Alps, McCarthy, A. and Müntener, O., Guest Editors, *Elements* 17, 1, 2021.
1104
- 1105 Argand, E.: Des Alpes et de l'Afrique: Bulletin de la Société Vaudoise des Sciences Naturelles, 55,
1106 233–236, 1924.
1107
- 1108 Artemieva, I.: *The Lithosphere: An Interdisciplinary Approach*, Cambridge University Press
1109 Monograph, 794 pp., ISBN 9780521843966, 2011.
1110
- 1111 Babuska, V., Plomerova, J., and Granet, M.: The deep lithosphere in the Alps: a model inferred from P
1112 residuals, *Tectonophysics*, 176, 137–165, [https://doi.org/10.1016/0040-1951\(90\)90263-8](https://doi.org/10.1016/0040-1951(90)90263-8), 1990.
1113
- 1114 Baran, R., Friedrich, A. M., and Schlunegger, F.: The late Miocene to Holocene erosion pattern of the
1115 Alpine foreland basin reflects Eurasian slab unloading beneath the western Alps rather than
1116 global climate change, *Lithosphere*, 6/2, 124–131, doi: 10.1130/L307.1, 2014.
1117
- 1118 Beccaluva, L., Bianchini, G., Bonadiman, C., Coltorti, M., Milani, L., Salvini, L., Siena, F., and Tassinari,
1119 R.: Intraplate lithospheric and sublithospheric components in the Adriatic domain: Nephelinite
1120 to tholeiite magma generation in the Paleogene Veneto volcanic province, southern Alps,
1121 *Geological Society of America Special Paper*, 418, 131–152, doi:10.1130/2007.2418(07), 2007.
1122
- 1123 Behm, M., Brückl, E., Chwatal, W., and Thybo, H.: Application of stacking and inversion techniques
1124 to three-dimensional wide-angle reflection and refraction data of the Eastern Alps, *Geophys. J.*
1125 *Int.* 170, 275–298, doi.org/10.1111/j.1365-246X.2007.03393.x, 2007
1126
- 1127 Bigi, G., Castellarin, A., Catalano, R., Coli, M., Cosentino, D., Dal Piaz, G.V., Lentini, F., Parotto, M.,
1128 Patacca, E., Praturlon, A., Salvini, F., Sartori, R., Scandone, P., and Vai, G.: Synthetic structural
1129 kinematic map of Italy, Sheets 1 and 2, C.N.R., Progetto Finalizzato Geodinamica, SELCA Firenze,
1130 1989.
1131
- 1132 Bijwaard, H., and Spakman, W.: Non-linear global P-wave tomography by iterated linearized
1133 inversion, *Geophys. J. Int.*, 141,71–82, doi.org/10.1046/j.1365-246X.2000.00053.x, 2000.
1134
- 1135 Brenker, F.E., and Brey, G.P.: Reconstruction of the exhumation path of the Alpe Arami garnet-
1136 peridotite from depths exceeding 160 km. *J. metamorphic Geol.*, 15, 581–592,
1137 doi/abs/10.1111/j.1525-1314.1997.tb00637.x, 1997.
1138
- 1139 Brückl, E., Bleibinhaus, F., Gosar, A., et al.: Crustal structure due to collisional and escape tectonics
1140 in the Eastern Alps region based on profiles Alp01 and Alp02 from the ALP 2002 seismic
1141 experiment. *J. Geophys. Res.* 112, B06308, doi:10.1029/2006JB004687, 2007.
1142
- 1143 Cammarano, F., Goes, S., Vacher, P., and Giardini, D.: Inferring upper-mantle temperatures from
1144 seismic velocities, *Physics of the Earth and Planetary Interiors*, 138, 197–222,
1145 doi:10.1016/S0031-9201(03)00156-0, 2003.
1146



- 1147 Cassano, E., Anelli, L., Fichera, R., and Cappelli, V.: Pianura Padana: Interpretazione integrate di dati
1148 Geofisici e geologici, 73° Congresso Società Geologica Italiana, Roma, AGIP, 27 pp, 1986.
1149
- 1150 Champagnac, J.D., Molnar, P., Anderson, R.S., Sue, C., and Delacou, B.: Quaternary erosion-induced
1151 isostatic rebound in the western Alps, *Geology*, 35; 195-198, doi: 10.1130/G23053A.1, 2007.
- 1152 Chopin, C.: Coesite and pure pyrope in high-grade blueschists of the Western Alps: a first record and
1153 some consequences, *Contr. Mineral. and Petrol.* 86, 107–118,
1154 <https://doi.org/10.1007/BF00381838>, 1984.
- 1155 Cederbom C.E., van der Beek, P., Schlunegger, F., Sinclair, H.D., and Oncken, O.: Rapid extensive
1156 erosion of the North Alpine foreland basin at 5-4 Ma, *Basin Research*, 23, 528–550, doi:
1157 10.1111/j.1365-2117.2011.00501.x, 2011.
- 1158 Dando B.D.E., Stuart, G.W., Houseman, G.A., Hegedüs, E., Brückl. E., and Radovanovic, S.:
1159 Teleseismic tomography of the mantle in the Carpathian–Pannonian region of central Europe.
1160 *Geophys. J. Int.*, 186, 11–31, doi: 10.1111/j.1365246X.2011.04998.x, 2011.
1161
- 1162 Diehl, T., Husen, S., Kissling, E., and Deichmann, N.: High-resolution 3-D P-wave model of the Alpine
1163 crust, *Geophys. J. Int.*, 179, 1133–1147, doi: 10.1111/j.1365246X.2009.04331.x, 2009.
1164
- 1165 Faccenna, C., Piromallo, C., Crespo-Blanc, A., Jolivet, L., and Rossetti, F.: Lateral slab deformation and
1166 the origin of the western Mediterranean arcs, *Tectonics*, 23, TC1012,
1167 doi:10.1029/2002TC001488, 2004.
1168
- 1169 Favaro S., Handy, M.R., Scharf, A., and Schuster, R.: Changing patterns of exhumation and
1170 denudation in front of an advancing crustal indenter, Tauern Window (Eastern Alps), *Tectonics*,
1171 36, 1053-1071, doi: 10.1002/2016TC004448, 2017.
1172
- 1173 Foulger, G. R., Panza, G. F., Artemieva, I. M., Bastow, I. D., Cammarano, F., Evans, J. R., Hamilton, W.
1174 B., Julian, B. R., Lustrino, M., Thybo, H., and Yanovskaya, T. B.: Caveats on tomographic images,
1175 *Terra Nova*, 25, 259-281, doi: 10.1111/ter.12041, 2013.
1176
- 1177 Fox, M., Herman, F., Kissling E., and Willet, S.D.: Rapid exhumation in the Western Alps driven by
1178 slab detachment and glacial erosion, *Geology*, doi:10.1130/G36411.1, 2015.
1179
- 1180 Fox, M., Herman F., Willett, S.D., and Schmid, S.M.: The exhumation history of the European Alps
1181 inferred from linear inversion of thermochronometric data: *American Journal of Science*, 316,
1182 505-541, doi: 10.2475/06.2016.01, 2016.
1183
- 1184 Franke, W.: The Mid-European segment of the Variscides: tectonostratigraphic units, terrane
1185 boundaries and plate tectonics evolution, *Geological Society, London, Special Publications*, 179,
1186 35-61, <https://doi.org/10.1144/GSL>, 2000.
1187
- 1188 Franke, W., Cock, L.R.M., and Torsvik, T.H.: The Palaeozoic Variscan oceans revisited. *Gondwana*
1189 *Research*, 48, 257-284, <http://dx.doi.org/10.1016/j.gr.2017.03.005>, 2017.
1190



- 1191 Fügenschuh, B., Seward, D., and Mancktelow, N.S.: Exhumation in a convergent orogen: the western
1192 Tauern Window. *Terra Nova*, 9, 213–217, doi: 10.1111/j.1365-3121.1997.tb00015.x, 1997
1193
- 1194 Geissler, W.H., Sodoudi, F., and Kind, R.: Thickness of the central and eastern European lithosphere
1195 as seen by S receiver functions: *Geophysical Journal International*, 181, 604–634, doi:
1196 10.1111/j.1365-246X.2010.04548.x, 2010.
1197
- 1198 Genser, J., Cloetingh, S. A. L., and Neubauer, F.: Late orogenic rebound and oblique Alpine
1199 convergence: New constraints from subsidence analysis of the Austrian Molasse basin, *Global
1200 and Planetary Change*, 58, 1–4, 214–223, doi: 10.1016/j.gloplacha.2007.03.010, 2007.
1201
- 1202 Giacomuzzi, G., Chiarabba, C., and De Gori, P.: Linking the Alps and Apennines subduction systems:
1203 New constraints revealed by high-resolution teleseismic tomography. *Earth and Planetary
1204 Science Letters*, 301, 531–543, doi:10.1016/j.epsl.2010.11.033, 2011.
1205
- 1206 Giacomuzzi, G., Civalleri, M., DeGori, P., and Chiarabba, C.: A 3D Vs model of the upper mantle
1207 beneath Italy: Insight on the geodynamics of central Mediterranean, *Earth and Planetary
1208 Science Letters*, 335–336, 105–120, doi.org/10.1016/j.epsl.2012.05.004, 2012.
1209
- 1210 Goes, S., Govers, R., and Vacher, P.: Shallow mantle temperatures under Europe from P and S wave
1211 tomography: *Journal of Geophysical Research* 105/B5, 11153–11169,
1212 doi.org/10.1029/1999JB900300, 2000.
1213
- 1214 Grad, M., Tiira, T., and ESC Working Group: The Moho depth map of the European Plate. *Geophys. J.
1215 Int.* 176, 279–292, doi: 10.1111/j.1365-246X.2008.03919.x, 2009.
1216
- 1217 Grenerczy, G., Sella, G., Stein, S., Kenyeres, A.: Tectonic implications of the GPS velocity field in the
1218 northern Adriatic region, *Geophysical Research Letters*, 32, doi:10.1029/2005GL022947, 2005.
1219
- 1220 Gross, P., Handy, M. R., John, T., Pestal, G., and Pleuger, J.: Crustal-scale sheath folding at HP
1221 conditions in an exhumed Alpine subduction zone (Tauern Window, Eastern Alps), *Tectonics*,
1222 39, doi.org/10.1029/2019TC005942, 2020.
1223
- 1224 Grunert, P., Hinsch, R., Sachsenhofer, R. F., Bechtel, A., Ćorić, S., Harzhauser, M., Piller, W.E., and
1225 Sperl, H.: Early Burdigalian infill of the Puchkirchen Trough (North Alpine Foreland Basin,
1226 Central Paratethys): Facies development and sequence stratigraphy. *Marine and Petroleum
1227 Geology*, 39/1, 164–186, doi: 10.1016/j.marpetgeo.2012.08.009, 2013.
1228
- 1229 Handy, M. R., Schmid, S. M., Bousquet, R., Kissling, E., and Bernoulli, D.: Reconciling plate-tectonic
1230 reconstructions with the geological-geophysical record of spreading and subduction in the Alps,
1231 *Earth Science Reviews*, 102, 121–158, doi:10.1016/j.earscirev.2010.06.002, 2010.
1232
- 1233 Handy, M. R., Ustaszewski, K., and Kissling, E.: Reconstructing the Alps–Carpathians–Dinarides as a
1234 key to understanding switches in subduction polarity, slab gaps and surface motion, *Int. J. Earth
1235 Sci. (Geol. Rundsch.)*, 104, 1–26 doi, 10.1007/s00531-014-1060-3, 2015.
1236
- 1237 Hetényi, G., Molinari, I., Clinton, J., Bokelmann, G., Bondár, I., Crawford, W.C., Dessa, J.X., Doubre, C.,



- 1238 Friederich, W., Fuchs, F., Giardini, D., Gráczér, Z., Handy, M.R., Herak, M., Jia, Y., Kissling, E.,
1239 Kopp, H., Korn, M., Margheriti, L., Meier, T., Mucciarelli, M., Paul, A., Pesaresi, D., Piromallo, C.,
1240 Plenefisch, Th., Plomerová, J., Ritter, J., Rümpker, G., Šipka, V., Spallarossa, D., Thomas, Ch.,
1241 Tilmann, F., Wassermann, J., Weber, M., Wéber, Z., Wesztergom, V., Živčić, M., and AlpArray
1242 Seismic Network Team , AlpArray OBS Cruise Crew, AlpArray Working Group: The AlpArray
1243 Seismic Network: A large-scale European experiment to image the Alpine orogen. *Surveys in*
1244 *Geophysics*, 39, 1009-1033, doi.org/10.1007/s10712-018-9472-4, 2018.
1245
1246 Hirsch, R.: Laterally varying structure and kinematics of the Molasse fold and thrust belt of the
1247 Central Eastern Alps: Implications for exploration, *AAPG Bulletin*, 97, 10, 1805–1831.
1248 doi:10.1306/04081312129, 2013.
1249
1250 Horváth, F., Bada, G., Szafian, P., Tari, G., Adam, A. and Cloetingh, S.: Formation and deformation of
1251 the Pannonian Basin: constraints from observational data. In: Gee, D. G. & Stephenson, R. A.
1252 (eds), *European Lithosphere Dynamics*, Geological Society London Memoirs, 32, 191–206,
1253 doi.org/10.1144/GSL.MEM.2006.032.01.11, 2006.
1254
1255 Horváth, F., Musitz, B., Balázs, A., Véghe, A., Uhrin, A., Nádor, A., Koroknai, B., Pap, N., Tóth, T., and
1256 Wórum, G.: Evolution of the Pannonian basin and its geothermal resources. *Geothermics*, 53,
1257 328–352, doi.org/10.1016/j.geothermics.2014.07.009, 2015.
1258
1259 Jolivet, L., Faccenna, C., and Piromallo, C.: From mantle to crust: Stretching the Mediterranean,
1260 *Earth and Planetary Science Letters*, 285, 1–2, 198-209.
1261 https://doi.org/10.1016/j.epsl.2009.06.017, 2009.
1262
1263 Jones, A., G., Plomerova, J., Korja, T., Sodoudi, F., and Spakman, W.: Europe from the bottom up: A
1264 statistical examination of the central and northern European lithosphere–asthenosphere
1265 boundary from comparing seismological and electromagnetic observations, *Lithos*, 120, 14-29,
1266 doi:10.1016/j.lithos.2010.07.013, 2010.
1267
1268 Jordan, T.H.: The Continental Tectosphere, *Reviews of Geophysics and Space Physics*, 13/3,
1269 doi.org/10.1029/RG013i003p00001, 1975.
1270
1271 Jordan, T.H.: Continents as a chemical boundary layer, *Phil. Trans. R. Soc. Lond.*, A 301, 359-373,
1272 1981.
1273
1274 Karato, S., and Jung, H.: Water, partial melting and the origin of the seismic low velocity and high
1275 attenuation zone in the upper mantle, *Earth and Planetary Science Letters*, 157, 193–207, 1998.
1276
1277 Karousová, H., Babuška, V., and Plomerová, J.: Upper-mantle structure beneath the southern
1278 Bohemian Massif and its surroundings imaged by high-resolution tomography, *Geophys. J. Int.*,
1279 194, 1203–1215, https://doi.org/10.1093/gji/ggt159, 2013.
1280
1281 Kastelic, V., Vrabec, M., Cunningham, D., and Gosar, A.: Neo-Alpine structural evolution and
1282 present-day tectonic activity of the eastern Southern Alps: The case of the Ravne Fault, NW
1283 Slovenia, *Journal of Structural Geology*, 30, 963-975, doi:10.1016/j.jsg.2008.03.009, 2008.
1284



- 1285 Kästle, E.D., Rosenberg, C., Boschi, L., Bellahsen, N., Meier, T., El-Sharkawy, A.: Slab break-offs in
1286 the Alpine subduction zone. *Int. J. Earth Sci. (Geol Rundsch)*, 109, 587–603,
1287 <https://doi.org/10.1007/s00531-020-01821-z>, 2020.
1288
- 1289 Kind, R., Schmid, S. M., Yuan, X, Heit, B., Meier, T., and the AlpArray and AlpArray-SWATH-D
1290 Working Groups: Moho and uppermost mantle structure in the greater Alpine area from S-to-P
1291 converted waves, *Solid Earth*, this volume, 2021.
1292
- 1293 Király, Á., Faccenna, C., and Funicello, F: Subduction zones interaction around the Adria microplate
1294 and the origin of the Apenninic arc: *Tectonics*, 37, 3941–3953,
1295 <https://doi.org/10.1029/2018TC00521>, 2018.
1296
- 1297 Kissling, E., and Schlunegger, F.: Rollback orogeny model for the evolution of the Swiss Alps,
1298 *Tectonics*, 37, doi.org/10.1002/2017TC004762, 2018.
1299
- 1300 Kissling, E., Schmid, S. M., Lippitsch, R., Ansorge, J., and Fügenschuh, B.: Lithosphere structure and
1301 tectonic evolution of the Alpine arc: new evidence from high-resolution teleseismic
1302 tomography, *Geological Society of London Memoirs*, 32, 129-145,
1303 doi.org/10.1144/GSL.MEM.2006.032.01.08, 2006.
1304
- 1305 Koulakov, I., Kaban, M., Tesauro, M., and Cloetingh, S.: P-and S-velocity anomalies in the upper
1306 mantle beneath Europe from tomographic inversion of ISC data, *Geophys. J. Int.*, 179, 345–366,
1307 [doi: 10.1111/j.1365-246X.2009.04279.x](https://doi.org/10.1111/j.1365-246X.2009.04279.x), 2009.
1308
- 1309 Kuhlemann, J., and Kempf, O.: Post-Eocene evolution of the North Alpine Foreland Basin and its
1310 response to Alpine tectonics, *Sedimentary Geology*, 152, 45–78, [doi.org/10.1016/S0037-](https://doi.org/10.1016/S0037-0738(01)00285-8)
1311 [0738\(01\)00285-8](https://doi.org/10.1016/S0037-0738(01)00285-8), 2002.
1312
- 1313 Kurz, W., Handler, R., and Bertoldi, C.: Tracing the exhumation of the Eclogite Zone (Tauern
1314 Window, Eastern Alps) by ⁴⁰Ar/³⁹Ar dating of white mica in eclogites, *Swiss J. Geosci.* 101,
1315 Supplement 1, S191–S206, [10.1007/s00015-008-1281-1](https://doi.org/10.1007/s00015-008-1281-1), 2008.
1316
- 1317 Le Breton, E., Brune, S., Ustaszewski, K., Zahirovic, S., Seton, M., and Müller, R. D.: Kinematics and
1318 extent of the Piemonte-Liguria Basin – implications for subduction processes in the Alps, *Solid*
1319 *Earth*, <https://doi.org/10.5194/se-2020-161>, 2021.
1320
- 1321 Lippitsch, R., Kissling, E., and Ansorge, J.: Upper mantle structure beneath the Alpine orogen from
1322 high-resolution teleseismic tomography, *J. Geophys. Res.*, 108(B8), 2376,
1323 [doi:10.1029/2002JB002016](https://doi.org/10.1029/2002JB002016), 2003.
1324
- 1325 Macera, P., Gasperini, D., Piromallo, C., Blichert-Toft, J., Bosch, D., Del Moro, A., and Martin, S.:
1326 Geodynamic implications of deep mantle upwelling in the source of Tertiary volcanics from the
1327 Veneto region (South-Eastern Alps), *Journal of Geodynamics*, 36, 563–590,
1328 [doi:10.1016/j.jog.2003.08.004](https://doi.org/10.1016/j.jog.2003.08.004), 2003.
1329



- 1330 Macera, P., Gasperini, D., Ranalli, G., and Mahatsente, R.: Slab detachment and mantle plume
1331 upwelling in subduction zones: an example from the Italian South-Eastern Alps, *Journal of*
1332 *Geodynamics*, 45, 32–48, doi:10.1016/j.jog.2007.03.004, 2008.
1333
- 1334 Maffione, M., Speranza, F., Faccenna, C., Cascella, A., Vignaroli, G., and Sagnotti, L.: A synchronous
1335 Alpine and Corsica-Sardinia rotation: *Journal of Geophysical Research*, 113, B03104,
1336 doi:10.1029/2007JB005214, 2008.
- 1337 Márton, E., Grabowski, J., Tokarski, A.K., and Túnyi, I.: Palaeomagnetic results from the fold and
1338 thrust belt of the Western Carpathians: an overview, *Geological Society, London, Special*
1339 *Publications*, 425, 7-36, <https://doi.org/10.1144/SP425.1>, 2015.
- 1340 Matenco, L., and Radivojević, D.: On the formation and evolution of the Pannonian Basin:
1341 Constraints derived from the structure of the junction area between the Carpathians and
1342 Dinarides, *Tectonics*, 31, TC6007, doi:10.1029/2012TC003206, 2012.
- 1343 Mazur, S., Aleksandrowski, P., Gągała, Ł., Krzywiec, P., Żaba, J., Gaidzik, K., and Sikora, R.: Late
1344 Palaeozoic strike-slip tectonics versus oroclinal bending at the SW outskirts of Baltica: case of
1345 the Variscan belt's eastern end in Poland, *International Journal of Earth Sciences*, 109, 1133–
1346 1160, doi:10.1007/s00531-019-01814-7, 2020.
1347
- 1348 Mey, J., Scherler, D., Wickert, A. D., Egholm, D. L., Tesauero, M., Schildgen, T. F., and Strecker M. R.:
1349 Glacial isostatic uplift of the European Alps, *Nature Communications*, 7: 13382,
1350 doi:10.1038/ncomms13382, 2016.
1351
- 1352 Mitchell, B.J.: Anelastic structure and evolution of the continental crust and upper mantle from
1353 seismic surface wave attenuation, *Reviews of Geophysics*, 33, 441-462,
1354 <https://doi.org/10.1029/95RG02074>
1355
- 1356 Mitterbauer, U., Behm, M., Brückl, E., Lippitsch, R., Guterch, A., Keller, G. R., Koslovskaya, E.,
1357 Rumpfhuber, E. M., and Šumanovac, F.: Shape and origin of the East-Alpine slab constrained by
1358 the ALPASS teleseismic model, *Tectonophysics* 510, 195–206, doi:10.1016/j.tecto.2011.07.001,
1359 2011.
1360
- 1361 Molli, G., Crispini, L., Mosca, P., Piana, P., and Federico, L.: Geology of the Western Alps-Northern
1362 Apennine junction area: a regional review. *Journal of the Virtual Explorer*, 36/9, 1-49,
1363 doi:10.3809/jvirtex.2010.00215, 2010.
1364
- 1365 Molli, G., Brogi, A., Caggianelli, A., Capezzuoli, E., Liotta, D., Spina, A., and Zibra, I.: Late Palaeozoic
1366 tectonics in Central Mediterranean: a reappraisal, *Swiss Journal of Geosciences*, 113,
1367 doi.org/10.1186/s00015-020-00375-1, 2020.
1368
- 1369 Nagel, T. J., Herwartz, D., Rexroth, S., Münker, C., Froitzheim, N., & Kurz, W.: Lu-Hf dating,
1370 petrography, and tectonic implications of the youngest Alpine eclogites (Tauern Window,
1371 Austria), *Lithos*, 170, 179–190, <https://doi.org/10.1016/j.lithos.2013.02.008>, 2013.
1372
- 1373 Nussbaum, C.: Neogene tectonics and thermal maturity of sediments of the easternmost Southern



- 1374 Alps (Friuli are, Italy), unpublished PhD thesis Université de Neuchâtel, Switzerland, 2000.
1375
- 1376 Paffrath, M. H., Friederich, W., and AlpArray & AlpArray-SWATH D Working Groups: Teleseismic P-
1377 waves at the AlpArray seismic network: Wave fronts, absolute traveltimes and traveltime
1378 residuals, *Solid Earth*, <https://doi.org/10.5194/se-2020-189>, this volume, 2021a.
1379
- 1380 Paffrath, M. H., Friederich, W., and AlpArray & AlpArray-SWATH D Working Groups: Teleseismic
1381 traveltome tomography of the greater Alpine region. *Solid Earth*, this volume, 2021b.
1382
- 1383 Perry, H. K. C., Jaupart, C., Mareschal, J.-C., and Shapiro, N. M.: Upper mantle velocity-temperature
1384 conversion and composition determined from seismic refraction and heat flow, *J. Geophys.
1385 Res.*, 111, B07301, doi:10.1029/2005JB003921, 2006.
1386
- 1387 Pfiffner, O.A., Lehner, P., Heitzmann, P., Mueller, St., and Steck, A. (Eds.) : Deep Structure of the
1388 Swiss Alps: Results of NRP 20: Birkhäuser et al., Basel, 460pp., ISBN 3-7643 5254 X, 1997.
1389
- 1390 Pfiffner, O. A., and Hitz, L.: Geologic interpretation of the seismic profiles in the Eastern Traverse
1391 (lines E1 – E3, E7-E9): eastern Alps, Chapter 9 in Pfiffner et al. (Eds.) Deep Structure of the Alps:
1392 Results of NRP 20, Birkhäuser et al., Basel, 73-100, 1997.
1393
- 1394 Picotti, V., and Pazzaglia, F. J.: A new active tectonic model for the construction of the Northern
1395 Apennines mountain front near Bologna (Italy), *J. Geophys. Res.*, 113, B08412,
1396 doi:10.1029/2007JB005307, 2008.
1397
- 1398 Piromallo, C., and Morelli, A.: P wave tomography of the mantle under the Alpine-Mediterranean
1399 area. *J. Geophys. Res.*, 108(B2), 2065, doi:10.1029/2002JB001757, 2003.
1400
- 1401 Pomella, H., Klötzli, U., Scholger, R., Stipp, M., and Fügenschuh, B.: The Northern Giudicarie and the
1402 Meran-Mauls fault (Alps, Northern Italy) in the light of new paleomagnetic and
1403 geochronological data from boudinaged Eo-Oligocene tonalites, *Int. J. Earth Sci.*, 100, 1827–
1404 1850, doi:10.1007/s00531-010-0612-4, 2011.
1405
- 1406 Qorbani, E., Bianchi, I., and Bokelmann, G.: Slab detachment under the Eastern Alps seen by seismic
1407 anisotropy, *Earth and Planetary Science Letters*, 409, 96-108,
1408 doi.org/10.1016/j.epsl.2014.10.049, 2015.
1409
- 1410 Ratschbacher, L., Frisch, W., Linzer, H.-G., and Merle, O.: Lateral extrusion in the Eastern Alps, part
1411 2: Structural analysis. *Tectonics*, 10(2), 257–271 <https://doi.org/10.1029/90TC02623>, 1991.
1412
- 1413 Ratschbacher, L., Dingeldey, C., Miller, C., Hacker, B. R., and McWilliams, M. O.: Formation,
1414 subduction, and exhumation of Penninic oceanic crust in the Eastern Alps: Time constraints
1415 from 40 Ar/39 Ar geochronology, *Tectonophysics*, 394(3), 155–170,
1416 <https://doi.org/10.1016/j.tecto.2004.08.003>, 2004.
1417
- 1418 Rawlinson, N., and Sambridge, M.: The Fast Marching Method: An Effective Tool for Tomographic
1419 Imaging and Tracking Multiple Phases in Complex Layered Media, *Exploration Geophysics*, 36:4,
1420 341-350, doi:10.1071/EG05341, 2005.



- 1421
1422 Rawlinson, N., Reading, A. M., and Kennett, B. L. N.: Lithospheric structure of Tasmania from a novel
1423 form of teleseismic tomography, *J. Geophys. Res.*, **111**, B02301, doi:10.1029/2005JB003803,
1424 2006.
1425
1426 Rosenberg, C. L.: Shear zones and magma ascent: A model based on a review of the Tertiary
1427 magmatism in the Alps, *Tectonics*, **23**, TC3002, doi:10.1029/2003TC001526, 2004.
1428
1429 Rosenberg, C.L., and Kissling, E.: Three-dimensional insight into Central-Alpine collision: Lower plate
1430 or upper-plate indentation?, *Geology*, **41**/12, 1219–122, doi:10.1130/G34584.1, 2013.
1431
1432 Rosenberg, C. L., Schneider, S., Scharf, A., Bertrand, A., Hammerschmidt, K., Rabaute, A., and Brun,
1433 J.-P.: Relating collisional kinematics to exhumation processes in the Eastern Alps, *Earth-Science*
1434 *Reviews*, **176**, 311–344, doi.org/10.1016/j.earscirev.2017.10.013, 2018.
1435
1436 Scharf, A., Handy, M.R., Favaro, S., Schmid, S.M., and Bertrand, A.: Modes of orogen-parallel
1437 stretching and extensional exhumation in response to microplate indentation and roll-back
1438 subduction (Tauern Window, Eastern Alps), *International Journal of Earth Sciences*, **102**, 1627-
1439 1654, doi.10.1007/s00531-013-0894-4, 2013.
1440
1441 Schefer, S., Cvetković, V., Fügenschuh, B., Kounov, A., Ovtcharova, M., Schaltegger, U., Schmid, S.
1442 M.: Cenozoic granitoids in the Dinarides of southern Serbia: age of intrusion, isotope
1443 geochemistry, exhumation history and significance for the geodynamic evolution of the Balkan
1444 Peninsula, *Int. J. Earth Sci.* **100**, 1181-1206, https://doi.org/10.1007/s00531-010-0599-x, 2011.
1445
1446 Schertl, H.-P., Schreyer, W., and Chopin, C.: The pyrope-coesite rocks and their country rocks at
1447 Parigi, Dora Maira Massif, Western Alps: detailed petrography, mineral chemistry and PT-path
1448 *Contrib. Mineral. Petrol.* **108**, 1-21, 1991
1449
1450 Schmid, S. M., Pfiffner, O. A., Froitzheim, N., Schönborn, G., and Kissling, E.: Geophysical-geological
1451 transect and tectonic evolution of the Swiss-Italian Alps, *Tectonics*, **15**, 1036-1064,
1452 doi.10.1029/96TC00433, 1996.
1453
1454 Schmid, S. M., Fügenschuh, B., Kissling, E., and Schuster, R.: Tectonic map and overall architecture of
1455 the Alpine orogen. *Eclogae geologicae Helvetiae* **97**, 93-117, doi.org/10.1007/s00015-004-1113-
1456 x, 2004.
1457
1458 Schmid, S. M., Bernoulli, D., Fügenschuh, B., Matenco, L., Schefer, S., Schuster, R., Tischler, M., and
1459 Ustaszewski, K.: The Alpine-Carpathian-Dinaridic orogenic system: correlation and evolution of
1460 tectonic units. *Swiss Journal of Geosciences*, **101**, 139-183, doi:10.1007/s00015-008-1247-3,
1461 2008.
1462
1463 Schmid, S. M., Scharf, A., Handy, M. R., and Rosenberg, C. L.: The Tauern Window (Eastern Alps,
1464 Austria): a new tectonic map, with cross-sections and a tectonometamorphic synthesis. *Swiss*
1465 *Journal of Geosciences*, **106**, 1-32, doi. 10.1007/s00015-013-0123-y, 2013.
1466
1467 Schmid, S. M., Kissling, E., Diehl, T., van Hinsbergen D. J. J., and Molli, G.: Ivrea mantle wedge, arc of



- 1468 the Western Alps, and kinematic evolution of the Alps–Apennines orogenic system, Swiss
1469 Journal of Geosciences, 110, 581–612, doi.10.1007/s00015-016-0237-0, 2017.
1470
- 1471 Schönborn, G.: Alpine tectonics and kinematic models of the central Southern Alps, Mem. Sci. Geol.
1472 Padova, 44, 229–393, 1992.
1473
- 1474 Schönborn, G.: Balancing cross sections with kinematic constraints: The Dolomites (northern Italy),
1475 Tectonics 18, 527–545, doi.org/10.1029/1998TC900018, 1999.
1476
- 1477 Schulmann, K., Lexa, O., Vojtech J., Lardeaux, J. M., and Edel, J. B.: Anatomy of a diffuse cryptic
1478 suture zone: An example from the Bohemian Massif, European Variscides, Geology, 42, 275–
1479 278, doi:10.1130/G35290.1, 2014.
1480
- 1481 Seghedi, I., and Downes, H.: Geochemistry and tectonic development of Cenozoic magmatism in the
1482 Carpathian–Pannonian region, Gondwana Research, 20, 655–672, doi:10.1016/j.gr.2011.06.009,
1483 2011.
1484
- 1485 Seghedi, I., Ersoy, Y.E., and Helvacı, C.: Miocene–Quaternary volcanism and geodynamic evolution in
1486 the Pannonian Basin and the Menderes Massif: A comparative study, Lithos 180–181, 25–42,
1487 doi.org/10.1016/j.lithos.2013.08.017, 2013.
1488
- 1489 Serpelloni, E., Vannucci, G., Anderlini, L., and Bennett, R. A.: Kinematics, seismotectonics and
1490 seismic potential of the eastern sector of the European Alps from GPS and seismic deformation
1491 data, Tectonophysics 688, 157–181, dx.doi.org/10.1016/j.tecto.2016.09.026, 2016.
1492
- 1493 Serretti, P., and Morelli, A.: Seismic rays and traveltimes tomography of strongly heterogeneous
1494 mantle structure: application to the Central Mediterranean, Geophys. J. Int., 187, 1708–1724,
1495 doi: 10.1111/j.1365-246X.2011.05242.x, 2011.
1496
- 1497 Shito, A., Karato, S., Matsukage, K., N., and Nishihara Y.: Towards Mapping the Three-Dimensional
1498 Distribution of Water in the Upper Mantle from Velocity and Attenuation Tomography,
1499 Geophysical Monograph, 168, 225–236, DOI: 10.1029/168GM17, 2006.
1500
- 1501 Singer, J., Diehl, T., Husen, S., Kissling, E., and Duretz, T.: Alpine lithosphere slab rollback causing
1502 lower crustal seismicity in northern foreland, Earth and Planetary Science Letters, 397, 42–56,
1503 doi.org/10.1016/j.epsl.2014.04.002, 2014.
1504
- 1505 Smye, A. J., Bickle, M. J., Holland, T. J. B., Parrish, R. R., and Condon, D. J.: Rapid formation and
1506 exhumation of the youngest Alpine eclogites: A thermal conundrum to Barrovian
1507 metamorphism, Earth and Planetary Science Letters, 306(3–4), 193–204, https://doi.
1508 org/10.1016/j.epsl.2011.03.037, 2011.
1509
- 1510 Spada, M., Bianchi, I., Kissling, E., Piana Agostinetti, N., and Wiemer, S.: Combining controlled-
1511 source seismology and receiver function information to derive 3-D Moho topography for Italy,
1512 Geophys. J. Int., 194, 1050–1068, doi: 10.1093/gji/ggt148, 2013.
1513



- 1514 Spakman, W., and Wortel, M.J.R.: Tomographic View on Western Mediterranean Geodynamics, in:
1515 The TRANSMED Atlas, The Mediterranean Region from Crust to Mantle, edited by: Cavazza, W.
1516 et al., Springer, Berlin, Heidelberg, 31-52, https://doi.org/10.1007/978-3-642-18919-7_2, 2004.
1517
- 1518 Speranza, F., Villa, I.M., Sagnotti, L., Florindo, F., Cosentino, D., Cipollari, P., and Mattei, M.: Age of
1519 the Corsica–Sardinia rotation and Liguro–Provençal Basin spreading: new paleomagnetic and
1520 Ar/Ar evidence, *Tectonophysics*, 231-251, [https://doi.org/10.1016/S0040-1951\(02\)00031-8](https://doi.org/10.1016/S0040-1951(02)00031-8),
1521 2002.
1522
- 1523 Stipčević, J., Tkalčić, H., Herak, M., Markušić, S., and Herak, D.: Crustal and uppermost mantle
1524 structure beneath the External Dinarides, Croatia, determined from teleseismic receiver
1525 functions, *Geophysical Journal International*, 185(3), 1103–1119. doi:10.1111/j.1365-
1526 246x.2011.05004.x, 2011.
1527
- 1528 Stipčević, J., Herak, M., Molinari, I., Dasović, I., Tkalčić, H., & Gosar, A.: Crustal thickness beneath the
1529 Dinarides and surrounding areas from receiver functions, *Tectonics*, 37,
1530 doi.org/10.1029/2019TC005872, 2020.
1531
- 1532 Tesauro, M., Kaban, M. K., and Cloetingh, S. A. P. L.: EuCRUST-07: A new reference model for the
1533 European crust, *Geophysical Research Letters*, 35(5), doi:10.1029/2007gl032244, 2008.
1534
- 1535 Ustaszewski, K., Schmid, S. M., Fügenschuh, B., Tischler, M., Kissling, E., and Spakman, W.: A map-
1536 view restoration of the Alpine–Carpathian–Dinaridic system for the Early Miocene, *Swiss J.*
1537 *Geosci.*, 101, 273–294, doi: 10.1007/s00015-008-1288-7, 2008.
1538
- 1539 Verwater, V. F., Le Breton, E., Handy, M. R., Picotti, V., Najafabadi, A.J., Haberland, C.: Neogene
1540 kinematics of the Giudicarie Belt and eastern Southern Alpine orogenic front (Northern Italy),
1541 *Solid Earth*, doi: [org/10.5194/se-2021-19](https://doi.org/10.5194/se-2021-19), 2021, this volume.
1542
- 1543 van der Meer, D. G., Spakman, W., van Hinsbergen, D. J. J., Amaru, M. L., and Torsvik, T. H.:
1544 Towards absolute plate motions constrained by lower-mantle slab remnants. *Nat. Geosci.*
1545 3, 36–40, 2010.
1546
- 1547 van der Meer, D. G., van Hinsbergen, D. J. J., and Spakman, W.: Atlas of the underworld: Slab
1548 remnants in the mantle, their sinking history, and a new outlook on lower mantle viscosity,
1549 *Tectonophysics*, 723, 309–448, doi.org/10.1016/j.tecto.2017.10.004, 2018.
1550
- 1551 van Hinsbergen, D. J. J., Torsvik, T. H., Schmid, S. M., Matenco, L. C., Maffione, M., Vissers, R. L. M.,
1552 Gürer, D., and Spakman, W.: Orogenic architecture of the Mediterranean region and kinematic
1553 reconstruction of its tectonic evolution since the Triassic. *Gondwana Research* 81, 79-229,
1554 <https://doi.org/10.1016/j.gr.2019.07.009>, 2020.
1555
- 1556 von Blanckenburg, F., and Davies, J. H.: Slab breakoff: A model for syncollisional magmatism and
1557 tectonics in the Alps, *Tectonics*, 14, 120-131, doi.org/10.1029/94TC0205, 1995.
1558



- 1559 Waldhauser, F., Lippitsch, R., Kissling, E., and Ansorge, J.: High-resolution teleseismic tomography of
1560 upper-mantle structure using an a priori three-dimensional crustal model, *Geophysical Journal*
1561 *International*, 150, 403–414, doi.org/10-1046/j.1365-246X.2002.01690.x, 2002.
1562
- 1563 Wortel, M., J. R., and Spakman, W.: Subduction and Slab Detachment in the Mediterranean-
1564 Carpathian Region: *Science*, 290, 1910-1917, doi: 10.1126/science.290.5498.1910, 2000.
1565
- 1566 Zhao, L., Paul, A., Malusà, M. G., Xu, X., et. al.: Continuity of the Alpine slab unraveled by high-
1567 resolution P wave tomography, *Journal of Geophysical Research, Solid Earth*, 121(12), 8720–
1568 8737, doi:10.1002/2016jb013310, 2016.
1569
1570